COLD ATOMS AND THE CONFORMAL BOOTSTRAP

A Dissertation

Presented to the Faculty of the Graduate School

of Cornell University

in Partial Fulfillment of the Requirements for the Degree of

Doctor of Philosophy

by

Joshua William Squires

August 2019

COLD ATOMS AND THE CONFORMAL BOOTSTRAP

Joshua William Squires, Ph.D.

Cornell University 2019

Statistical mechanics naturally lends itself to computational algorithms that use random sampling to leverage the law of large numbers. Though these methods have proven invaluable, in many cases yielding solutions to otherwise intractable problems, to an extent they also obscure the underlying physics. The two numerical methods studied in this thesis do not fit this description. The first, the conformal bootstrap, imposes symmetry constraints on the four-point correlation functions of a conformal field theory to restrict the spectrum of allowed scaling dimensions of a theory. A variation of the conformal bootstrap is implemented to treat two important non-unitary CFTs, percolation and the self-avoiding walk. The second involves a formalism which provides an integral equation with a kernel based on the two-body S-matrix. The solution of this integral equation represents a single particle's energy in the presence of interactions with the rest of a cold atom gas. The formalism is applied to Berezinskii-Kosterlitz-Thouless and upper branch phase transitions.

BIOGRAPHICAL SKETCH

Josh Squires was born on July 7, 1992. He grew up in Enfield, Connecticut and graduated from Enfield High School in 2010. After spending a few semesters studying molecular and cell biology at the University of Connecticut, he changed course and pursued physics. He graduated in May 2014 as a university scholar, the school's highest academic distinction, with B.S. degrees in physics and applied math. He enrolled in the physics Ph.D. program at Cornell the following fall, and a year later began working under André LeClair on problems in statistical mechanics.

ACKNOWLEDGEMENTS

First and foremost, I'd like to thank my advisor André LeClair for his continuous guidance over the last four years. I'd also like to thank Katja Nowack and Erich Mueller for their interesting A exam questions, and their generous help as I solved them. I thank Barry Wells and Vasili Kharchenko, my undergrad research advisors at the University of Connecticut. Finally, I'm thankful for my friends and family, and in particular my parents, for their endless support.

TABLE OF CONTENTS

LIST OF TABLES

LIST OF FIGURES

CHAPTER 1

INTRODUCTION

Interest in phase transitions has driven progress in physics since its inception. Countless experiments, theories, and numerical methods alike have been developed in order to better understand the way matter changes state. In this thesis, two distinct approaches to treating phase transitions are presented. First, the conformal bootstrap, a numerical method rooted in conformal field theory, is reviewed and applied to two prominent problems in statistical mechanics: percolation and the self avoiding walk. In the latter half, a theoretical framework for interacting gases at finite temperature, based on the S-matrix, is used to study exotic phase transitions in ultracold atomic gases.

Chapter 2 covers the conformal field theory preliminaries needed in subsequent chapters. CFT in arbitrary spatial dimensions is introduced before specifically considering the two dimensional case, where simplifications arise due to Virasoro symmetry. Theoretical challenges associated with logarithmic conformal field theories are described.

Chapter 3 introduces the conformal bootstrap for both unitary and non-unitary CFTs. Properties of conformal blocks and the advances in their representation that led to the contemporary bootstrap are discussed.

Chapter 4 presents the application of the conformal bootstrap to percolation and self-avoiding polymers, two logarithmic conformal field theories with many similarities. Adapted from:

"Conformal bootstrap for percolation and polymers" by André LeClair and Joshua Squires, published in J. Stat. Mech. 12, 123105 (2018).

Chapter 5 covers the basics of scattering theory, Feshbach resonances, and the S-matrix-based formalism used to treat phase transitions in interacting gases.

Chapter 6 studies the application of the formalism to two-dimensional Bose and Fermi gases. Approximate analytic expressions describing the Berezinskii-Kosterlitz-Thouless transition are derived. Adapted from:

"Two-dimensional Bose and Fermi gases beyond weak coupling" by Guilherme França, André LeClair, and Joshua Squires, published in J. Stat. Mech. 7 073103 (2017).

Chapter 7 studies the upper branch, a phase defined by the absence of bound states for a three-dimensional gas with repulsive interactions. Phase diagrams for both Bose and Fermi gases are determined. Adapted from:

" Metastability of Bose and Fermi gases on the upper branch" by André LeClair, Itzhak Roditi, and Joshua Squires, published in Phys. Rev. A 94, 063608 (2016).

1.1 Publication List

1. " Metastability of Bose and Fermi gases on the upper branch" by André LeClair, Itzhak Roditi, and Joshua Squires, published in Phys. Rev. A 94, 063608 (2016).
2. 'Two-dimensional Bose and Fermi gases beyond weak coupling" by Guilherme França, André LeClair, and Joshua Squires, published in J. Stat. Mech. 7 073103 (2017).
3. "Conformal bootstrap for percolation and polymers" by André LeClair and Joshua Squires, published in J. Stat. Mech. 12, 123105 (2018).

CHAPTER 2

CONFORMAL FIELD THEORY

The emergence of fluctuations at all length scales at a critical point implies a description in terms of a scale invariant quantum field theory. With rare exception such critical systems are also invariant under a larger class of transformations called conformal transformations, and therefore may be modeled by a conformal field theory This connection to critical phenomena has made conformal field theory (CFT) a pillar of contemporary theoretical physics.

In this chapter the basics of conformal symmetry in both $d = 2$ and $d \geq 3$ are reviewed. The conformal group in flat $d-$dimensional space is identified before discussing its action on operators and subsequently correlation functions. The radial quantization formalism is also introduced, primarily as a means of defining the operator product expansion. In higher dimensions, constraints from CFT form the backbone of the conformal bootstrap, a non-perturbative numerical technique for treating phase transitions. In two dimensions the infinite-dimensionality of the conformal algebra by itself leads to sufficient restrictions to exactly solve a wide array of models. Material for this chapter is largely based on the CFT texts [1, 2] and the notes by Ginsparg [3] and Rychkov [4].

2.1 CFT in any d

2.1.1 Conformal Group

Conformal transformations are transformations that preserve angles between lines. For a flat d dimensional space with metric $\eta_{\mu\nu} = diag(-1, \cdots +1, \dots)$, under a conformal transformation $x \to x'$ the metric is preserved up to a non-negative scale factor $\Omega(x)$

$$\eta_{\mu\nu} \to \eta_{\mu\nu}(x') = \Omega(x)\eta_{\mu\nu}(x). \tag{2.1}$$

Here the scale factor can be related to the Jacobian as $\Omega(x) = \left|\frac{\partial x'}{\partial x}\right|^{\frac{-2}{d}}$. In $d \geq 3$, the conformal group reduces to the Poincaré group consisting solely of translations and rotations, with the usual generators $P_\mu = -i\partial_\mu$ and $M_{\mu\nu} = i(x_\mu\partial_\nu - x_\nu\partial_\mu)$, when $\Omega(x) = 1$. More generally the conformal group also contains dilations $x^\mu \to x'^\mu = \lambda x^\mu$ with generator $D = -ix^\mu\partial\mu$ and special conformal transformations $x^\mu \to x'^\mu = \frac{x^\mu - (x\cdot x)b^\mu}{1-2(b\cdot x)+(b\cdot b)(x\cdot x)}$ with generator $K_\mu = -i(2x_\mu x^\nu\partial_\nu - (x\cdot x)\partial\mu)$ where b^μ is a constant vector.

2.1.2 Operators and Correlation Functions

In any d dimensional conformal field theory, a field $\phi_j(x)$ with scaling dimension Δ_j is called quasi-primary if it transforms as

$$\phi_j(x) \to \left|\frac{\partial x'}{\partial x}\right|^{\Delta_j/d} \phi_j(x') \tag{2.2}$$

under global conformal transformations. The above transformation implies N-point correlation functions of quasi-primaries obey the relation

$$\langle \phi_1(x_1) \dots \phi_n(x_n) \rangle = \left| \frac{\partial x'}{\partial x} \right|_{x=x_1}^{\Delta_1/d} \dots \left| \frac{\partial x'}{\partial x} \right|_{x=x_n}^{\Delta_n/d} \langle \phi_1(x'_1) \dots \phi_n(x'_n) \rangle. \tag{2.3}$$

More specifically, the action of the conformal group constrains the 2-point correlator to take the conventionally normalized form

$$\langle \phi_1(x_1)\phi_2(x_2) \rangle = \frac{1}{|x_{12}|^{\Delta_1+\Delta_2}} = \frac{1}{|x_1 - x_2|^{2\Delta}}. \tag{2.4}$$

Here the dependence on $x_{ij} \equiv x_i - x_j$ is required by translational and rotational symmetry, and invariance under special conformal transformations restricts $\Delta_1 = \Delta_2$ in all non-vanishing 2-point correlation functions. Similarly 3-point functions

$$\langle \phi_1(x_1)\phi_2(x_2)\phi_3(x_3) \rangle = \frac{\lambda_{123}}{|x_{12}|^{\Delta_1+\Delta_2-\Delta_3}|x_{23}|^{\Delta_2+\Delta_3-\Delta_1}|x_{13}|^{\Delta_3+\Delta_1-\Delta_2}}, \tag{2.5}$$

are fixed by conformal symmetry up to a constant λ_{123}.

N-point correlators of quasi-primaries with $N \geq 4$ have more freedom. Generally they are functions of conformally invariant cross ratios. For example, the four point function of identical scalar fields φ is a function of the ratios $u = \frac{x_{12}^2 x_{34}^2}{x_{13}^2 x_{24}^2}$ and $v = \frac{x_{14}^2 x_{23}^2}{x_{13}^2 x_{24}^2}$

$$\langle \varphi(x_1)\varphi(x_2)\varphi(x_3)\varphi(x_4) \rangle = \frac{g(u,v)}{|x_{12}|^{2\Delta_\varphi}|x_{34}|^{2\Delta_\varphi}}. \tag{2.6}$$

2.1.3 Radial Quantization

Correlation functions of local operators can also be interpreted as the scalar product of in states Ψ_{in} and out states Ψ_{out} created by operator insertions. In typical QFT, spacetime in d dimensions is quantized by constructing $d-1$ dimensional surfaces of equal time, each its own Hilbert space with states labeled

by their momenta $p = (E/c, p_1, p_2, \ldots p_{d-1})$. Calculating a correlation function between an out state on one surface and an in state on another, separated by Δt, requires the time evolution operator $U = e^{iH\Delta_t}$

$$\langle \Psi_{out} | U | \Psi_{in} \rangle. \tag{2.7}$$

In CFT, quantizing Euclidean spacetime with $d-1$ dimensional spheres centered at the origin is more useful. In radial quantization the dilation operator D acts as the Hamiltonian, and

$$U = e^{iD\Delta\tau} \tag{2.8}$$

evolves a state from one $(d-1)-$sphere to another. A state's good quantum numbers are then Δ and l, its scaling dimension and $SO(d)$ spin, respectively. The scaling dimension is the eigenvalue of the dilation operator

$$D|\Delta\rangle = i\Delta|\Delta\rangle \tag{2.9}$$

while the spin is relevant since $M_{\mu\nu}$ is the only conformal algebra generator that commutes with D.

The generators K_μ and P_μ meanwhile act as raising and lowering operators:

$$[D, P_\mu] = iP_\mu \tag{2.10}$$

$$[D, K_\mu] = -iK_\mu. \tag{2.11}$$

The allowed eigenvalues of the dilation operator are bounded from below, implying the existence of a state with lowest dimension such that applying K_μ to it yields the vacuum state $|0\rangle$. States with this property are called primary, and repeated application of P_μ to a primary state generates its descendant states, which correspond to the derivatives of a primary operator. This exemplifies the

state-operator correspondence, which states the existence of an isomorphism between states and local operators in a CFT. This isomorphism can be shown through radial quantization by considering a state living on a spherical surface centered at the origin. The state is created by the operators present inside the sphere. Without loss of generality suppose there are only two such operators $\mathcal{O}_1$ and $\mathcal{O}_2$ inserted at x_1 and the origin respectively.

$$|\Psi\rangle = \mathcal{O}_1(x_1)\mathcal{O}_2(0)|0\rangle. \tag{2.12}$$

After replacing $|\Psi\rangle$ by these operators and applying scale invariance to shrink the spherical surface to radius zero, it's clear $|\Psi\rangle$ can be expressed in terms of a basis of local operators at the origin.

2.1.4 Operator Product Expansion

Applying the state-operator correspondence argument above to two operators inserted at x_1 and x_2, separated from any other local operators by a sphere centered at y, immediately gives the operator product expansion (OPE)

$$\mathcal{O}_1(x_1)\mathcal{O}_2(x_2) = \sum_{\mathcal{O}} C_{\mathcal{O}}(x, \partial_y)\mathcal{O}(y). \tag{2.13}$$

Here the sum runs over all primary operators $\mathcal{O}$. The operator product expansion (OPE) states that the product of two local operators can be replaced by a sum of operators at a nearby third position. In typical QFT the OPE is valid only in the $x_1 \to x_2 \to y$ limit. In CFT, the OPE converges at a finite separation due to the state-operator correspondence [4]. Another significance of (2.13) is that conformal symmetry relates the OPE coefficients to the coefficients of the 3-point function

$$C_{\mathcal{O}}(x, \partial_y) = \lambda_{12\mathcal{O}}\widehat{C}_{\mathcal{O}}(x, \partial_y). \tag{2.14}$$

For this reason the coefficients of the 3-point function are often interchangeably referred to as OPE coefficients, since $\widehat{C}_O(x, \partial_y)$ is simply a fixed numerical factor.

2.2 CFT in 2d

In $2D$ the condition of invariance under the infinitesimal conformal transformation $x^\mu \to x^\mu + \epsilon^\mu$ reduces to the Cauchy-Riemann equations

$$\partial_0 \epsilon_0 = \partial_1 \epsilon_1 \qquad \partial_0 \epsilon_1 = -\partial_1 \epsilon_0. \tag{2.15}$$

Introducing the complex coordinates $z, \bar{z} = x^0 \pm i x^1$, conformal transformations in two dimensions are simply analytic holomorphic and antiholomorphic mappings

$$z \to z' = f(z) \qquad \bar{z} \to \bar{z}' = \bar{f}(\bar{z}) \tag{2.16}$$

where $f(z) = z + \epsilon(z)$, $f(\bar{z}) = \bar{z} + \bar{\epsilon}(\bar{z})$. Since (anti)holomorphic, the transformations can be Laurent expanded around $z = 0$

$$z' = z + \sum_{n \in \mathcal{Z}} \epsilon_n (-z^{n+1})$$
$$\bar{z}' = \bar{z} + \sum_{n \in \mathcal{Z}} \bar{\epsilon}_n (-\bar{z}^{n+1})$$

from which the infinite set of infinitesimal generators

$$l_n = -z^{n+1} \partial_z, \qquad \bar{l}_n = -\bar{z}^{n+1} \partial_{\bar{z}} \tag{2.17}$$

are obtained. The holomorphic generators obey a copy of the Witt algebra

$$[l_m, l_n] = (m - n) l_{m+n} \tag{2.18}$$

which commutes with a corresponding, antiholomorphic copy:

$$[\bar{l}_m, \bar{l}_n] = (m - n) \bar{l}_{m+n} \tag{2.19}$$

$$[l_m, \bar{l}_n] = 0. \tag{2.20}$$

There are a few notable characteristics of the Witt algebra. First, that two independent copies of the algebra are present indicates z and $\bar{z}$ are distinct complex variables rather than just complex conjugates [1]. Second, both copies contain a finite subalgebra, generated by l_{-1}, l_0, and l_1, describing the global conformal group. $l_{-1} = -\partial_z$ generates translations, $l_0 = -z\partial_z$ rotations and dilations, and $l_1 = -z^2\partial_z$ special conformal transformations. Finally, the Witt algebra permits a central extension, the Virasoro algebra, defined by

$$
\begin{aligned}
[L_m, L_n] &= (m-n)L_{m+n} + \frac{c}{12}(m^3 - m)\delta_{m+n,0} \\
[\overline{L}_m, \overline{L}_n] &= (m-n)\overline{L}_{m+n} + \frac{\overline{c}}{12}(m^3 - m)\delta_{m+n,0} \\
[L_m, \overline{L}_n] &= 0.
\end{aligned}
$$

2.2.1 Virasoro Representations

Consider the asymptotic state $|h, \overline{h}\rangle = \phi(0,0)|0\rangle$ created by acting on the vacuum with a primary operator ϕ. Suppressing antiholomorphic components for convenience, it can be shown $|h\rangle$ is the highest-weight state of a representation, with eigenvalue h,

$$
L_0|h\rangle = h|h\rangle \tag{2.21}
$$

as L_0 plays the role of the Hamiltonian in the radial quantization formalism. The generators L_m with $(m > 0)$ behave as lowering operators, annihilating $|h\rangle$, while L_{-m} $(m > 0)$ generate excited (descendant) states:

$$
\begin{aligned}
|h'\rangle &= L_{-m_1}^{r_1} L_{-m_2}^{r_2} \dots L_{-m_j}^{r_j} |h\rangle \\
h' &= h + (r_1 m_1 + r_2 m_2 + \dots r_j m_j) = h + N
\end{aligned}
$$

where conventionally $m_1 > m_2 > \dots m > k$ and N is the level of the descendant state. $|h\rangle$ and its infinite set of descendants together form a conformal family

and a subspace of the full Hilbert space. This subset is closed under the Virasoro generators, constituting a representation, the Verma module, of the Virasoro algebra. Every CFT can be characterized by its central charge c and Verma module $V(c,h)$.

2.2.2 Null States and Kac Determinant

If a subset of states in a given Verma module is itself closed under the Virasoro algebra the representation is reducible, and there exists a highest-weight state $|\chi\rangle$, which generates the closed submodule, such that $L_m|\chi\rangle = 0$ for $m > 0$. The so-called null state $|\chi\rangle$ is a vanishing linear combination of states of a given level N, and, along with its descendants, is orthogonal to $V(c,h)$. Null states must be removed to form an irreducible representation $M(c,h)$ of the Virasoro algebra, and can be calculated with the roots of the Kac determinant

$$\det M_N(c,h) = \alpha_N \prod_{\substack{rs\leq N \\ r,s\geq 1}} (h - h_{r,s}(c))^{P(N-rs)}. \tag{2.22}$$

Here

$$h_{r,s} = \frac{((p+1)r - ps)^2 - 1}{4p(p+1)} \tag{2.23}$$

$$c = 1 - \frac{6}{p(p+1)} \tag{2.24}$$

$$p = -\frac{1}{2} \pm \frac{1}{2}\sqrt{\frac{25-c}{1-c}} \tag{2.25}$$

and α_N is a constant. The lowest level null state is given by rs since $P(N-rs) = 0$ when $N-rs$ is negative. As an example which will prove useful in later chapters, consider null states at level 2. States with $N = 2$ are $L_{-2}|h\rangle$ and $L_{-1}^2|h\rangle$. If a

vanishing linear combination exists, the determinant of

$$\begin{pmatrix} \langle h|L_2L_{-2}|h\rangle & \langle h|L_1^2L_{-2}|h\rangle \\ \langle h|L_2L_{-1}^2|h\rangle & \langle h|L_1^2L_{-1}|h\rangle \end{pmatrix} = \begin{pmatrix} 4h + c/2 & 6h \\ 6h & 4h(1+2h) \end{pmatrix} \tag{2.26}$$

must be zero for some h, c pair. Taking the determinant gives the condition $2(16h^2 - 10h + (2h+1)c) = 0$, or equivalently $32(h - h_{1,1}(c))(h - h_{1,2}(c))(h - h_{2,1}(c))$, implying a level 2 null state occurs when

$$c = 2h(5 - 8h)/(2h + 1). \tag{2.27}$$

2.2.3 Unitary Representations and Minimal Models

The Kac determinant can be used to determine whether a given representation corresponds to a unitary CFT. It can be proven that unitary representations are guaranteed for $c \geq 1, h \geq 1$. Similarly, representations with negative central charge or negative conformal weight are assuredly nonunitary [2]. In between with $c < 1$, $h > 0$ and with r, s integers, only for the discrete set $p = 3, 4, \ldots$ constrained by $1 \leq r \leq p-1, 1 \leq s \leq r$ do (2.25) and (2.24) describe unitary representations of the Virasoro algebra. These are the minimal models of which the Ising model with $p = 3$, $c = \frac{1}{2}$ is the simplest. Since the highest weight $h_{r,s}$ has an $r \to (p - r)$, $s \to (p + 1 - s)$ symmetry the range of allowed (r, s) can be extended and graphically represented in a $(m-1) \times m$ grid, the Kac table. The Kac table for the $p = 3$ Ising model is shown in Table 2.1.

Continuing with the $2d$ Ising model for concreteness, each weight in the Kac table corresponds to a primary field $\Phi_{r,s}$ with scaling dimension $h + \overline{h} = 2h$ (since $L_0 + \overline{L}$ is the generator of dilations). These primary fields can be identified by their well-known relations to the critical exponents of the $2d$ Ising model. At the

Table 2.1: $2d$ Ising Kac table. s runs vertically from 1 to p, and r horizontally from 1 to $p-1$.

$\frac{1}{2}$	0
$\frac{1}{16}$	$\frac{1}{16}$
0	$\frac{1}{2}$

critical point $T \to T_c$, the spin and energy two-point functions,

$$\langle \sigma(x)\sigma(0)\rangle \propto \frac{1}{|x|^{d-2+\eta}} = \frac{1}{|x|^{2\Delta_\sigma}}, \tag{2.28}$$

$$\langle \epsilon(x)\epsilon(0)\rangle \propto \frac{1}{|x|^{2(d-1)/\nu}} = \frac{1}{|x|^{2\Delta_\epsilon}} \tag{2.29}$$

diverge as power laws, with $\eta = 1/4$ and $\nu = 1$. The exponent ν is of particular importance, as it describes the divergence of the correlation length

$$\xi \propto t^{-\nu} \tag{2.30}$$

as $t \equiv \frac{|T-T_c|}{T_c} \to 0$. The correlation length critical exponent relates to the energy operator scaling dimension as

$$\nu = \frac{1}{d-\Delta_\epsilon}. \tag{2.31}$$

From (2.29) it's clear $\Delta_\epsilon = 1$ and $\Delta_\sigma = 1/8$ suggesting the fields $\Phi_{2,1}$, $\Phi_{1,2}$ correspond to the energy and spin operators respectively. The remaining field $\Phi_{1,1}$ can be identified with the identity operator, and exhausts the conformal families present in the $2d$ Ising model.

2.2.4 Fusion Rules

Fusion rules dictate which conformal families are present in a given operator product expansion. In the case of the unitary minimal models, the conformal

families compose a closed algebra, the fusion algebra:

$$\left[\phi_{r_1,s_1}\right] \times \left[\phi_{r_2,s_2}\right] = \sum_{\substack{r_3=|r_1-r_2|+1 \\ r_1+r_2+r_3 \text{ odd}}}^{r_1+r_2-1} \sum_{\substack{s_3=|s_1-s_2|+1 \\ s_1+s_2+s_3 \text{ odd}}}^{s_1+s_2-1} \left[\phi_{r_3,s_3}\right]. \tag{2.32}$$

For the spin spin fusion rule of the Ising model ($r_1 = r_2 = 1, s_1 = s_2 = 2$), (2.32) reduces to

$$[\phi_{1,2}] \times [\phi_{1,2}] = \sum_{s_3=1,s_3=3} [\phi_{1,s_3}] = [\phi_{1,1}] + [\phi_{1,3}] \tag{2.33}$$

which can be written as

$$\implies [\sigma] \times [\sigma] = [1] + [\epsilon]. \tag{2.34}$$

2.3 Logarithmic Conformal Field Theory

In a logarithmic conformal field theory (LCFT), the scaling dimensions of two (or more) operators collide as some parameter n approaches a critical value n_c, resulting in logarithmic divergences in correlation functions. Consider the fields ϕ, ψ with scaling dimensions $\Delta_\phi(n), \Delta_\psi(n)$. If $\Delta_\psi(n) \to \Delta_\phi(n)$ as $n \to n_c$, acting with the dilation operator on

$$A \equiv \phi - \psi, \tag{2.35}$$

$$B \equiv (\Delta_\phi(n) - \Delta_\psi(n))\phi \tag{2.36}$$

results in

$$
\begin{aligned}
D|B\rangle &= \Delta_\phi |B\rangle, \\
D|A\rangle &= \Delta_\phi |\phi\rangle - \Delta_\psi |\psi\rangle \\
&= \Delta_\phi |\phi\rangle - \Delta_\psi |\psi\rangle + (\Delta_\psi |\phi\rangle - \Delta_\psi |\phi\rangle) \\
&= |B\rangle - \Delta_\psi |\psi\rangle + \Delta_\psi |\phi\rangle \\
&= |B\rangle + \Delta_\psi |A\rangle \\
&= |B\rangle + \Delta_\phi |A\rangle.
\end{aligned}
$$

Rather than acting diagonally as in a usual CFT, the dilation operator takes the form of a Jordan cell

$$
D \begin{pmatrix} A \\ B \end{pmatrix} = \begin{pmatrix} \Delta_\phi & 1 \\ 0 & \Delta_\phi \end{pmatrix} \begin{pmatrix} A \\ B \end{pmatrix} \tag{2.37}
$$

due to the degeneracy of Δ_ϕ and Δ_ψ as $n \to n_c$ [5, 6].

The non-diagonal action of D corresponds to the presence of an indecomposable representation of the conformal algebra, characteristic of LCFTs. The fields A and B form a logarithmic pair, with 2-point correlation functions

$$
\begin{aligned}
\langle A(x)A(0)\rangle &= -\frac{2a_1 \log x + a_0}{x^{2\Delta_\phi}}, \\
\langle B(x)A(0)\rangle &= \frac{a_1}{x^{2\Delta_\phi}}, \\
\langle B(x)B(0)\rangle &= 0.
\end{aligned}
$$

Here a_0 and a_1 are constants. The former can be scaled away, while the latter is an "indecompability parameter" characteristic of a given LCFT that behaves as a central charge [5].

2.3.1 Catastrophe at $c = 0$

Logarithms may also be present in higher order correlation functions if OPE coefficients diverge, as occurs for a large class of theories with $c = 0$. For example, both the $q = 1$ limit of the q-state Pott's model, describing percolation, and the $O(N)$ model as $N \to 0$, which corresponds to polymers or the self-avoiding walk (SAW), have logarithmic terms in their 4-point functions due to divergent OPE coefficients as $c \to 0$.

Generically, the OPE for the product of primary fields ϕ reads

$$\phi(x)\phi(0) = \frac{1}{x^{2\Delta_\phi}}\left(1 + \kappa\frac{\Delta_\phi}{c}x^d T(0) + \dots\right) \tag{2.38}$$

where $T(x)$ is the stress energy tensor, κ a constant, and the central charge c is defined as the coefficient of the leading order term of $\langle T(x)T(0)\rangle$. Clearly there's a problem at $c = 0$, which suggests the possible existence of another field with OPE contribution $\kappa'\frac{\Delta_\phi}{c}x^{d+\delta}T'(0)$ which cancels the divergence. Supposing $\kappa' \to \kappa$ and $\delta \to 0$ as $c \to 0$ and defining the operator $t(x) \equiv T' - T$, the OPE at $c = 0$ then states

$$\phi(x)\phi(0) = \frac{1}{x^{2\Delta_\phi}}\left(1 + \kappa\frac{\Delta_\phi}{b}x^d t(0) + \kappa\frac{\Delta_\phi}{b}\log(x)T(0) + \dots\right) \tag{2.39}$$

with $b \equiv -\lim_{c\to 0}\frac{c}{\delta}$ [6]. Thus fields T and T' collide in the limit, creating the logarithmic partner of the stress tensor $t(x)$ and averting the $c = 0$ catastrophe. The parameter b is Gurarie's indecomposability parameter a_1:

$$\begin{aligned}\langle t(x)t(0)\rangle &= -\frac{2b\log x + a_0}{x^{2\Delta_\phi}},\\ \langle T(x)t(0)\rangle &= \frac{b}{x^{2\Delta_\phi}},\\ \langle T(x)T(0)\rangle &= 0.\end{aligned}$$

Attempts to measure b through numerical simulation for percolation ($b = 5/6$) and the self-avoiding walk ($b = -5/8$) have been carried out in [7, 8].

CHAPTER 3

THE CONFORMAL BOOTSTRAP

The conformal bootstrap is the idea that a conformally invariant quantum field theory is completely characterized by its spectrum of anomalous dimensions and operator product expansion coefficients [9]. In $d = 2$ dimensions, implementation of the bootstrap is hardly necessary since the conformal symmetry becomes the infinite dimensional Virasoro symmetry, which leads to powerful methods such as Coulomb gas techniques, current algebra and their cosets, etc. [1]. Recently, after crucial advances in the study of conformal blocks [10, 11], it has been demonstrated that the conformal bootstrap can provide accurate results in higher dimensions [12]. The method has since been refined and applied most notabably to the $O(N)$ models [13–26], with particular success for the $d = 3$ Ising model, where the best results on anomalous dimensions is currently based on the bootstrap [19]. In this chapter, an overview of the conformal bootstrap and it's application to scalar fields in unitary and non-unitary CFTs will be provided. The material condensed here is presented with more detail in the reviews by Simmons-Duffin [27] and Rychkov [4].

3.1 Conformal Bootstrap

At the heart of the conformal bootstrap is the notion that constraints on the four-point functions of a CFT, namely conformal invariance, crossing symmetry, and unitarity, are sufficient to restrict, or even completely fix, the spectrum of allowed scaling dimensions of a theory. Conformal invariance constrains the

four-point function of a scalar field $\sigma(x)$ in a CFT to take the form

$$\langle\sigma(x_1)\sigma(x_2)\sigma(x_3)\sigma(x_4)\rangle = \frac{\sum_{\Delta,l} p_{\Delta,l} G_{\Delta,l}(u,v)}{|x_{12}|^{2\Delta_\sigma}|x_{34}|^{2\Delta_\sigma}}, \tag{3.1}$$

with $x_{ij} \equiv x_i - x_j$ and Δ_σ the scaling dimension of σ. The coefficients $p_{\Delta,l}$ are the square of the $\sigma(x_i)\sigma(x_j)$ OPE coefficients $\lambda_{\sigma\sigma\mathcal{O}}$, with $\mathcal{O}$ signifying a global primary operator of dimension Δ and conformal spin l. $G_{\Delta,l}(u,v)$ are global conformal blocks, which are functions of the conformally invariant cross ratios $u = \frac{x_{12}^2 x_{34}^2}{x_{13}^2 x_{24}^2}$ and $v = \frac{x_{14}^2 x_{23}^2}{x_{13}^2 x_{24}^2}$.

The correlation function (3.1) can be computed in multiple ways. For example, the OPE can be applied to the pairs $\sigma(x_1)\sigma(x_2)$ and $\sigma(x_3)\sigma(x_4)$ reducing the four-point function to a sum over two-point functions. Equivalently, the operators can be grouped as $\sigma(x_3)\sigma(x_2)$ and $\sigma(x_1)\sigma(x_4)$ resulting in a different series. Asserting the equivalence of both results gives a crossing relation. Formally, crossing symmetry is imposed on (3.1) by considering the transformation of (3.1) under $x_1 \leftrightarrow x_3$. Defining

$$F_{\Delta_\sigma,\Delta,l} \equiv v^{\Delta_\sigma} G_{\Delta,l}(u,v) - u^{\Delta_\sigma} G_{\Delta,l}(v,u) \tag{3.2}$$

crossing symmetry is respected if

$$\sum_{\Delta,l} p_{\Delta,l} F_{\Delta_\sigma,\Delta,l}(u,v) = 0. \tag{3.3}$$

This constraint, which should hold in any consistent CFT, depends solely on the CFT data: the OPE coefficients $\lambda_{\sigma\sigma\mathcal{O}}$ and the spectrum, the scaling dimensions and spins, of the operators appearing in the sum. Extracting the CFT data allows the calculation of any local observable or correlation function, higher-order or otherwise. Doing so, however, is non-trivial as (3.3) is formally an infinite set of constraints depending on an infinite set of parameters.

3.1.1 Bootstrapping Unitary Theories

The infinite set of constraints is handled by Taylor expanding around the symmetric point $u = v = \frac{1}{4}$ to order Λ. Choosing this symmetric point is primarily a convention, although it's been argued [28] that picking $u = v = 1/4$ makes the conformal block expansions present in the $x_1 \leftrightarrow x_3$ exchange converge quickest. Under the change of variables

$$u = \frac{a^2 - b}{4}, \qquad v = \frac{4 - 4a + a^2 - b}{4} \tag{3.4}$$

the Taylor expanded crossing relation takes the form

$$\sum_{\Delta,l} p_{\Delta,l} F^{(m,n)}_{\Delta_\sigma,\Delta,l}(a,b) = 0 \qquad (m,n \in \mathbb{N}, m \,\text{odd}). \tag{3.5}$$

with $F^{(m,n)}$ a vector with components

$$\left(F^{(m,n)}_{\Delta_\sigma,\Delta,l}(a,b)\right)^{mn} = \partial_a^m \partial_b^n F_{\Delta_\sigma,\Delta,l}(a,b)|_{a=1,b=0} \tag{3.6}$$

and $m + n \leq \Lambda$. Note the exclusion of even m is owed to the two terms of (3.6) contributing oppositely in such cases.

Restricting the infinite set of operators present in the crossing relation in part requires an appeal to unitarity. In a unitary theory, allowed scaling dimensions are bounded from below as a result of imposing that all of a primary operator's descendants have positive norm. The unitary bounds

$$\Delta \geq \frac{(d-2)}{2} \qquad l = 0 \tag{3.7}$$

$$\Delta \geq l + d - 2 \qquad l \geq 1 \tag{3.8}$$

hold in arbitrary spatial dimension. Since no similar upper bound exists, an artificial cutoff N must be introduced to truncate the crossing relation. In practice this is not problematic as the OPE is shown to converge exponentially fast; for

computable constant $a > 0$, operators above a given cutoff scaling dimension Δ_N have maximal contribution $\exp(-a\Delta_N)$ [28].

In unitary theories, the coefficients $p_{\Delta,l}$ are strictly positive due to reality of $\lambda_{\sigma\sigma O}$. This is an essential ingredient in determining whether or not the crossing relation has a consistent solution. With $p_{\Delta,l} \geq 0$, (3.5) can be viewed as a vector sum which adds to zero. Since the coefficients of the sum are necessarily positive, if a separating plane through the origin can be found such that all of the vectors point to one side of the plane, a solution that respects crossing symmetry is impossible. Note the identity OPE coefficient is conventionally normalized to unity, eliminating the trivial solution. Alternately, the problem can be viewed as searching for a functional $\alpha = \sum_{mn} \alpha_{mn} \partial_a^m \partial_b^n [\cdot]|_{a=1,b=0}$ such that $\alpha F^{(m,n)}_{\Delta_\sigma,\Delta,l}, \geq 0$. In this manner parameter space can be searched, regions where physical CFTs cannot exist can be ruled out, and bounds can be placed on allowed scaling dimensions.

Numerically, this takes the form of a linear programming problem

$$\sum_i a_i \mathbf{v}_i = 0, \qquad \forall_{i\neq 0} a_i \geq 0 \qquad a_0 = 1, \tag{3.9}$$

which can be solved with standard algorithms, such as Dantzig's simplex algorithm as implemented in JuliBootS [29]. While simplex algorithms are successful in handling four-point correlators of identical fields, in instances where bootstrapping mixed correlators is important [20] the problem is no longer linear in the coefficients $p_{\Delta,l}$. In such cases, semidefinite progrmaming approaches are more appropriate, most notably implemented in Simmons-Duffin's SDPB solver [30].

3.1.2 Non-Unitary Bootstrap

The power of the conformal bootstrap largely lies in its generality. The scaling dimensions of low lying operators of a theory can be accurately bounded without knowing anything about its description as a field theory; at no point is information specific to a particular CFT entered into the bootstrap. But if this generality isn't desired, is the full machinery of the bootstrap required? Can any of its main assumptions be relaxed? The answer to both questions is a resounding yes, as demonstrated in [31, 32].

In the determinant or "Gliozzi" conformal bootstrap method, rather than searching the space of all possible CFTs for bounds which are independent of a specific theory, a particular CFT is chosen by explicitly specifying the dimensions and spins of the first N operators that contribute to a given four-point function. Truncating the sum in (3.5) to the first N operators appearing in the OPE and taking $M \geq N$ derivatives, where each M signifies a distinct $(m, n) = \partial_a^m \partial_b^n$ pair, gives a system of $\binom{M}{N}$ equations which has a solution only if all minors of order N vanish

$$\det \mathbf{F}_i = 0, \qquad \mathbf{F}_i \subset \mathbf{F} = \left[F^{(m,n)}_{\Delta_\sigma, \Delta, l} \right]_{N \times M} . \tag{3.10}$$

Bootstrapping with his method has two key advantages over the more general approach outlined in the previous section. First, the convex optimization problem has been recast as a straightforward, homogeneous system of equations. Second, and more importantly, the coefficients $p_{\Delta,l}$ need not be strictly positive, opening the bootstrap to non-unitary theories which may have imaginary OPE coefficients. As such, this method has been leveraged to study two important non-unitary theories: the Yang-Lee edge singularity [31–33] and poly-

mers [34]. The increased applicability of the Gliozzi bootstrap also comes with a cost. Truncating the crossing equation (3.3), which is only strictly satisfied when the sum runs over an infinite number of operators, introduces an error which has not yet been systematically analyzed, though a recent study [35] has taken steps to formalize an error estimation procedure. In extreme cases, the error may not converge at all as the number of retained operators is increased, in which case the CFT is deemed not truncable and the Gliozzi method cannot be applied.

Note this type of truncation is not the same as the truncation discussed in the previous section for unitary theories. There, a large scaling dimension cutoff is chosen, and *all* operators (potentially an infinite number, as the space of operators itself is continuously infinite) below this value are "included". Here, for nonunitary theories particularly in $d \geq 3$, typically $N \leq 10$, either because information on the desired CFT is limited, or because raising N limits the interpretability of the solution. The latter arises because the uncontrolled truncation error means any solution of (3.10) is approximate, and in general vanishing minors do not perfectly coincide and are instead clustered about a solution, requiring visual interpretation. Potential subjectivity arising from interpreting plots of vanishing minors can be avoided to an extent by using the equivalent condition [36] that the $M \times N$ matrix $\mathbf{F}$, with elements $F^{(m,n)}_{\Delta_\sigma,\Delta,l}$, must have at least one vanishing singular value. With this condition, an approximate solution is represented by a singular value that tends to zero. Minimizing the smallest singular value as a function of desired scaling dimensions is in some cases more precise than interpreting non-coincident vanishing minors.

As more operators are kept in the truncation of (3.5), additional derivatives

must be added. For smaller matrices the set of derivatives chosen can greatly influence the bootstrapped scaling dimensions, as explored in the appendix of the next chapter. This appears to be an inherent ambiguity in the determinant conformal bootstrap method (hereafter referred to simply as the conformal bootstrap), and a method of objectively choosing derivatives should be decided. In the next chapter, only longitudinal derivatives $(m, 0)$ are used, both for numerical efficiency, since the ∂_a^m derivates are quicker to calculate, and because doing so is more effective for the theories considered. Calculation of $F^{(m,n)}_{\Delta_\sigma,\Delta,l}$ is performed with the numerical bootstrap package JuliBootS [29], which implements a partial fraction representation of conformal blocks [16] and recursively calculates their derivatives [37].

3.2 Conformal Blocks

The component of four point correlation functions fixed by conformal symmetry are called conformal blocks. A conformal block represents the contribution of a particular primary operator and its descendants to the operator product expansion. Advances in the efficient calculation of conformal blocks direclty led to the resurgence in the conformal bootstrap over the last decade. In this section a few of the advances made in the way scalar conformal blocks are represented and calculated, that are of particular use in our work, are presented. An introduction of greater scope can be found in the review [38].

Historically, conformal blocks have been treated by power series expansion since closed-form expressions were not known. In the early 2000's, Dolan and Osborn [39] found simple formulas for conformal blocks in even spatial dimen-

sions in terms of hypergeometric functions. For example, in two and four dimensions, in terms of the variables $u = z\bar{z}, v = (1-z)(1-\bar{z})$:

$$G_{\Delta,l}(u,v)^{d=2} = \frac{1}{2}\left[k_{\Delta+l}(z)k_{\Delta-l}(\bar{z}) - (z \leftrightarrow \bar{z})\right] \tag{3.11}$$

$$G_{\Delta,l}(u,v)^{d=4} = \frac{(-1)^l}{2^l}\frac{z\bar{z}}{z-\bar{z}}\left[k_{\Delta+l}(z)k_{\Delta-l-2}(\bar{z}) - (z \leftrightarrow \bar{z})\right] \tag{3.12}$$

$$k_\beta(x) = x^{\beta/2}{}_2F_1(\beta/2, \beta/2, \beta; x) \tag{3.13}$$

These results directly led to the modern conformal bootstrap [12], though analogous closed form results for general d remain elusive. Progress continued in [15], where conformal blocks in arbitrary spatial dimension for the case of four identical scalar fields are computed. Specifically, conformal blocks are computed along the diagonal $z = \bar{z}$ using recursion relations that arise as a result of the blocks being eigenfunctions of the quadratic Casimir operator $\mathcal{D}$:

$$\mathcal{D}\, G_{\Delta,l}(z,\bar{z}) = \frac{1}{2}C_{\Delta,l}G_{\Delta,l}(z,\bar{z}). \tag{3.14}$$

Here the eigenvalue $C_{\Delta,l} \equiv \Delta(\Delta-d) + l(l+d-2)$ and the operator is

$$\mathcal{D} \equiv (1-z)z^2\partial_z^2 - \left(z^2 - (d-2)\frac{z\bar{z}(1-z)}{z-\bar{z}}\right)\partial_z + (z \leftrightarrow \bar{z}). \tag{3.15}$$

The aforementioned recursion relation [15] reads

$$\begin{aligned}(l+d-3)(2\Delta+2-d)G_{\Delta,l}(z) \\ = (d-2)(\Delta+l-1)G_{\Delta,l-2}(z) \\ + \frac{2-z}{2z}(2l+d-4)(\Delta-d+2)G_{\Delta+1,l-1}(z) \\ - \frac{\Delta(2l+d-4)(\Delta+2-d)(\Delta+3-d)(\Delta-l-d+4)^2 G_{\Delta+2,l-2}(z)}{16(\Delta+1-d/2)(\Delta-d/2+2)(l-\Delta+d-5)(l-\Delta+d+4)}\end{aligned} \tag{3.16}$$

and allows computation of any conformal block on the diagonal in terms of spin 0 and spin 1 conformal blocks

$$G_{\Delta,0} = \left(\frac{z^2}{1-z}\right)^{\Delta/2}{}_3F_2\left(\Delta/2, \Delta/2, \Delta/2-d/2+1; \frac{\Delta+1}{2}, \Delta-d/2+1; \frac{z^2}{4(z-1)}\right) \tag{3.17}$$

$$G_{\Delta,1} = \frac{2-z}{2z}\left(\frac{z^2}{1-z}\right)^{(\Delta+1)/2}{}_3F_2\left(\frac{\Delta+1}{2}, \frac{\Delta+1}{2}, \frac{\Delta+1}{2}-d/2+1; \frac{\Delta}{2}+1, \Delta-d/2+1; \frac{z^2}{4(z-1)}\right).$$

In the conformal bootstrap, the crossing relation is Taylor expanded around the point $z = \bar{z} = \frac{1}{2}$, thus efficient calculation of the derivatives of the conformal blocks, both along and transverse to the diagonal, is essential. Properties of hypergeometric functions and the relation (3.17) can be used to recursively calculate derivatives along the diagonal [40]. Working in the a, b basis and defining $h_{m,n} = \partial_a^m \partial_b^n$, applying the Frobenius method to the Casimir equation gives a recursion relation [15] for transverse derivatives:

$$\begin{aligned}
2(d+2n-3)h_{m,n} = & \\
& + 2m(d+2n=3)[-h_{m-1,n} + (m+1)h_{m-2,n} + (m-1)(m-2)h_{m-3,n}] \\
& -h_{m+2,n-1} + (d-m+4n+4)h_{m+1,n-1} \\
& +[2C_{\Delta,l} + 2d(m+n-1) + m^2 + 8mn - 9m + 4n^2 - 6n + 2]h_{m,n-1} \\
& +m[d(m-2n+1) + m^2 + 12mn - 15m + 12n^2 - 30n + 20]h_{m-1,n-1} \\
& +(n-1)[h_{m+2,n-2} - (d-3m-4n+4)h_{m+1,n-2}].
\end{aligned} \tag{3.18}$$

In principle, the above recursion relations for conformal blocks and their derivatives are all that are needed to implement the bootstrap for the case of identical external scalars fields. However, further improvements are possible. It was argued in [28, 29, 40] that optimal convergence of the conformal block expansions is achieved by working in the radial coordinates

$$\rho = re^{i\theta} = \frac{z}{(1-\sqrt{1-z})^2}, \qquad \cos\theta = \eta \tag{3.19}$$

rather than $z, \bar{z}$. Conformal blocks may be approximated in terms of rational functions of Δ [18] by expanding in terms of r about $r = r_* = 3 - 2\sqrt{2}$ ($z = \bar{z} = 1/2$) and applying constraints from the Casimir equation, giving the partial fraction representation [16]

$$\partial_r^m \partial_\eta^n G_{\Delta,l}(r,\eta)|_{r=r_*,\eta=1} = r_*^\Delta \left(p_l^{m,n}(\Delta) + \sum_i \frac{a_{l,i}^{m,n}}{\Delta - \Delta_i} \right). \tag{3.20}$$

Here $a_{l,i}^{m,n}$ are coefficients, $p_l^{m,n}$ polynomials in Δ, and Δ_i poles of the conformal blocks. The primary advantage of using the rational approximation is that the poles, coefficients, and $p_l^{m,n}$ can all be tabulated, allowing for rapid computation of the blocks at various Δ values. Current state of the art numerical bootstrap packages utilize (3.20) to calculate conformal blocks and their derivatives along the diagonal, before converting to $z, \bar{z}$ coordinates and applying (3.18) to obtain transverse derivatives.

CHAPTER 4

CONFORMAL BOOTSTRAP FOR PERCOLATION AND POLYMERS

This chapter was adapted from "Conformal bootstrap for percolation and polymers" by André LeClair and Joshua Squires, published in J. Stat. Mech. 12, 123105 (2018).

4.1 Abstract

The conformal bootstrap is applied to percolation and dilute self-avoiding polymers in arbitrary dimension d. In both cases we propose a spectrum of operators motivated by Virasoro symmetry in $d = 2$ which is devoid of a stress energy tensor as an approximate means of enforcing $c = 0$. Percolation is treated in $2 \leq d \leq 6$ dimensions, and the self-avoiding walk in $2 \leq d \leq 4$.

4.2 Introduction

The conformal bootstrap has proven wildly successful in treating the Ising model. In this chapter, the power, or possible limitations, of the bootstrap is explored for two conformal theories that are connected to and as important as the Ising model, namely percolation and polymers. The latter is commonly referred to as the self-avoiding walk (SAW). These theories present several interesting challenges in the context of the conformal bootstrap. First of all, they are not unitary. Furthermore, they are very closely related in that they share some anomalous dimensions, and in $d = 2$ they have the same Virasoro central charge $c = 0$. It should be mentioned that some important problems in Anderson local-

ization, such as the critical point in quantum Hall transitions for non-interacting fermions, are also expected to be described by $d = 2$, $c = 0$ conformal field theories, many of whose description remains unknown. In contrast, the Ising model is essentially a unique theory: in $d = 2$ it is the only unitary theory with central charge $c = 1/2$, which makes it easier to locate.

Percolation and the SAW can be viewed as continuous limits of other models that pass through the Ising model. The SAW is known to correspond to the $O(N)$ model as $N \to 0$, where the Ising model is $N = 1$. Similarly percolation is the $q \to 1$ limit of the q-state Potts model, where $q = 2$ corresponds to the Ising model. Due to these limits, both these theories have an energy operator and spin field, and fusion rule

$$[\sigma] \times [\sigma] = [1] + [\epsilon]. \tag{4.1}$$

In two dimensions these theories have been extensively studied, for instance in [41–46]. Extending (2.24) to allow half interger r, s, the spin field of both percolation and the SAW corresponds to $(r, s) = (3/2, 3/2)$ with $\Delta_\sigma = 5/48$. Thus, percolation and the SAW must differ in the energy sector, particularly in which descendants are included in the fusion rule. For the SAW, the energy operator corresponds to $(r, s) = (1, 3)$ with $\Delta_\epsilon = 2/3$, which gives $\nu = 3/4$. On the other hand, for percolation it is $(r, s) = (2, 1)$ with dimension $\Delta_\epsilon = 5/4$ which leads to $\nu = 4/3$.

The above discussion leads to some interesting questions. First of all, both percolation and the SAW have the same fusion rule (2.32) and same central charge $c = 0$. Can the bootstrap distinguish between the two? How well does the bootstrap work in higher dimensions, in the absence of the added Virasoro symmetry? In attempting to answer these questions, some subtleties associated

with logarithmic CFTs must be handled.

First, the OPE (2.39) proposed in the detailed study [5] by Gurarie and Ludwig

$$\sigma(x)\sigma(0) = \frac{1}{x^{2\Delta_\sigma}}\left(1 + \kappa\frac{\Delta_\phi}{b}x^d t(0) + \kappa\frac{\Delta_\phi}{b}\log(x)T(0) + \dots\right) \tag{4.2}$$

requires logarithmic conformal blocks, rather than the usual scalar blocks, to account for the logarithmic divergence [47]. Second, for both theories in $d = 2$, the identity decouples exactly when $q = 1$ or $N = 0$ [6, 46, 48], altering the fusion rule (2.32) to

$$[\sigma] \times [\sigma] = [\epsilon]. \tag{4.3}$$

This is not surprising, since when $q = 1$ or $N = 0$, the spin field does not formally exist, which is consistent with the fact that the fusion rule (4.3) implies that the two point function of spin fields vanishes. Taking percolation for example, this can be understood by noting that the probability P that two sites are both contained in the same connected cluster is given by

$$P = \lim_{q\to 1}(q-1)^{-1}\langle\sigma(z_1)\sigma(z_2)\rangle \tag{4.4}$$

[6, 48]. Since P must be finite the two-point function must be proportional to $(q-1)$ and therefore go to zero at $q = 1$. Furthermore, the vanishing of the identity channel is demonstrated by the more sophisticated calculation of Dotsenko [46], through a careful renormalization procedure within the Coulomb gas formalism. In particular, Dotsenko had to introduce a small parameter ϵ, where $c \propto \epsilon$. Only after he renormalized the 4-point function in a particular manner did the identity channel vanish as $\epsilon \to 0$.

These two issues, the theoretical decoupling of the identity and the logarithmic nature of the percolation and SAW OPE are treated in the same way.

Rather than throwing out the identity, rigorously imposing $c = 0$, and including logarithmic OPE terms by utilizing the more complicated logarithmic conformal blocks in the bootstrap, one can instead simply retain the identity operator and view it as a numerical tool rather than a physical operator. The added free parameter approximately incorporates all of excluded logarithmic features. The justification and consequences of this decision are explored in detail in Appendix A.

4.3 Percolation

Consider a rectangular lattice of sites between which nearest neighbor bonds can be drawn with probability p, or left open with probability $(1 - p)$ as shown in Figure 4.1. Connected bonds form clusters which increase in size with p. Given a particular value of p, percolation theory seeks to answer whether or not the lattice can be traversed while moving only on closed, connected bonds. In the thermodynamic limit (lattice dimensions tend to infinity), there exists a critical probability p_c such that for $p > p_c$, an infinite cluster always exists, and the lattice can always be crossed. For $p < p_c$, an infinite spanning cluster never exists. Analogously, the crossing probability

$$\pi(p) = \begin{cases} 1, & p > p_c \\ 0, & p < p_c \end{cases} \tag{4.5}$$

is discontinuous at the critical probability. The order parameter of the transition between states with or without an infinite spanning cluster is typically taken to be the probability a given site is part of an infinite spanning cluster, $P(p)$. Above

p_c, $P(p)$ transitions from 0 to

$$P(p) \propto |p - p_c|^{\beta}, \tag{4.6}$$

with β the associated critical exponent. Another relevant exponent is the correlation length critical exponent ν. The correlation length ξ measures the size of the largest finite cluster. Near p_c,

$$\xi \sim |p - p_c|^{-\nu}. \tag{4.7}$$

4.3.1 Potts Model

Percolation as a CFT is often formulated as the $q \to 1$ limit of the $q-$state Potts model. The Potts model consists of nearest neighbor spins interacting on a lattice. Each spin σ_i takes one of q possible values, with the energy of a given configuration being

$$H = K \sum_{(i,j)} \delta_{\sigma_i,\sigma_j}. \tag{4.8}$$

Here $\delta_{\sigma_i,\sigma_j}$ is the usual Kroenecker-delta symbol, signifying an interaction energy K only if there is a bond between adjacent, identical spins. The partition function of the Potts model is given by tracing over the product of bonds [41]

$$Z = \sum_{\sigma} \prod_{(i,j)} (1 + x\delta_{\sigma_j\sigma_j}) \tag{4.9}$$

with $x = p/(1-p)$. Specifically for percolation (4.9) can be rewritten

$$Z = \sum_{R} p^{B(r)}(1-p)^{B-B(R)} \tag{4.10}$$

where B is the total possible number of bonds, $B(R)$ the number of occupied bonds, and R the set of occupied bonds [1]. Writing the partition function in this manner makes it obvious that $Z = 1$, which implies percolation is a logarithmic CFT with vanishing central charge [5, 6].

4.3.2 Selection Rules

Low lying perators must be selected in order to treat percolation with the conformal bootstrap. It is not difficult to show that there is a null state at level 2 for a primary field with conformal weights $h, \overline{h}$ if the following equation is satisfied

$$c = \frac{2h(5-8h)}{(2h+1)} \tag{4.11}$$

(See section 2.2.2). For $c = 0$, this null state occurs at $h = 5/8$ and $h = 0$. Since $h = 5/8$ corresponds to the energy operator, this suggests we discard its level 2 descendant, $[\Delta_\epsilon + 2, 2]$. Here we introduce the notation $[\Delta, l]$ to represent an operator with dimension $\Delta = h + \overline{h}$ and conformal spin $l = h - \overline{h}$. The $c = 0$ catastrophe discussed in relation to equation (2.38) also suggests we discard $[D, 2]$ and its descendants, based on the null state at $h = 0$. One can also interpret this as effectively setting $T = 0$ in (2.38) to avoid the $c = 0$ catastrophe. This motivates a fusion rule consisting of the identity operator and Virasoro descendants of ϵ:

$$[\Delta_\sigma, 0] \times [\Delta_\sigma, 0] = [0,0] + [\Delta_\epsilon, 0] + [\Delta_\epsilon + 4, 4] + [\Delta_\epsilon + 6, 6] + [\Delta_\epsilon + 8, 8] + \dots \tag{4.12}$$

Curiously, when constructing $\mathbf{F}$ with the above operators we observe a noticeable increase in the accuracy of the bootstrapped $2d$ percolation scaling dimensions if the $(m, n) = (1, 0)$ constraint is avoided. For consistency we also omit the $(1, 0)$ derivative constraint in higher dimensions, as well as in our treatment of the self-avoiding walk. In all dimensions considered for percolation, the M rows of $\mathbf{F}$ are labeled by the M lowest order longitudinal derivatives with $m \geq 3$, and the N columns are labeled by the first N operators present in the trial spectrum (4.12). A discussion of the decision to use only longitudinal derivatives with $m \geq 3$ is provided in Appendix B.

4.3.3 Results

Bootstrapping in $d = 2$ dimensions with the above operators for fixed $\Delta_\sigma = 5/48$ gives a vanishing singular value at $\Delta_\epsilon = 1.255$, in agreement with the exact $\Delta_\epsilon = 5/4$. Varying the spin field scaling dimension and minimizing z, the smallest singular value of $\mathbf{F}$, as a function of both Δ_ϵ and Δ_σ finds $\Delta_\sigma = 0.101, \Delta_\epsilon = 1.235$, as shown in Figure 4.2. In $d = 4$ the presence of the free field theory with scaling dimensions $\Delta_\sigma = 1$ and $\Delta_\epsilon = 2$ makes it difficult to minimize in Δ_σ, and the omission of the $(1, 0)$ derivative constraint only compounds the problem. All higher order derivatives of the convolved vacuum conformal block $F_{\Delta_\sigma,0,0}$ quickly tend to zero as the free field Δ_σ is reached, since $F^{(1,0)}_{\Delta_\sigma,0,0}$ becomes linear as $\Delta_\sigma \to 1$. Thus with our approach a trivial vanishing singular value near $\Delta_\sigma = 1$ is unavoidable in four dimensions. Nevertheless, minimizing the smallest singular value of $\mathbf{F}$ gives $\Delta_\sigma = 0.997, \Delta_\epsilon = 2.557$. This solution is depicted in Figure 4.3, where we actually work with the scaled matrix $\mathbf{F}/F^{(3,0)}_{\Delta_\sigma,0,0}$. This is purely for visual convenience; it smooths the precipitous dip in z near $\Delta_\sigma = 1$ but has no bearing on the bootstrapped scaling dimensions. Our bootstrapped Δ_ϵ corresponds to a correlation length critical exponent $\nu = 0.693$ which compares favorably with $\nu = 0.6920$, obtained by four-loop calculation [49].

Applying the bootstrap to percolation's upper critical dimension $d = 6$ with the same OPE truncation as in two and four dimensions is unsuccessful. No vanishing singular values of $\mathbf{F}$ are found when $M > N$, which for our minimal set of operators appears to be necessary in order to restrict both Δ_σ and Δ_ϵ. In some sense it's surprising this problem does not arise in three or four dimensions. Our postulated fusion rule, which is clearly reliant on Virasoro symmetry, is likely not more than a very rough approximation to the true spectrum of

low-lying percolation operators in $d > 2$. Even without finding a solution to (3.5) in $6d$, there's still a signature of the free field result. In Figure 4.4, $\log(z)$ curves flatten as $\Delta_\sigma = 2, \Delta_\epsilon = 4$ is approached. The diminishing peaks can be viewed as a lesser violation of crossing symmetry, with the smallest such violation (peak) occurring when $\Delta_\sigma = 2.002$ (red curve in Figure 4.4). A plot of z at fixed $\Delta_\sigma = 2.002$ exhibits a slight but well-defined dip at $\Delta_\epsilon = 4.003$, as shown in Figure 4.5.

Unlike in even spatial dimensions, in $d = 3$ and $d = 5$ the fusion rule (4.12) is not adequate to distinguish both the spin and energy field scaling dimensions. In $3d$, for any given Δ_σ a vanishing singular value is present, but no clear minimal z is found as a function of Δ_σ and Δ_ϵ. This may be due to the similarity in operator content and close proximity of percolation, SAW, and the Ising model, as all three theories have spin field scaling dimensions clustered near $\Delta_\sigma = 0.5$ in three dimensions. In $5d$ no vanishing singular values are present when $M > N$. In both cases we can still bootstrap one of the scaling dimensions given the other is held fixed. Taking $\Delta_{\sigma,3d} = 0.4765$ and $\Delta_{\sigma,5d} = 1.4718$ [49], $\Delta_{\epsilon,3d} = 1.615$ and $\Delta_{\epsilon,5d} = 3.416$ are obtained using $N = 5, M = 6$ and $N = M = 7$, respectively. Compiled in Table 4.1 are all of our bootstrapped scaling dimensions for percolation.

As a final note before moving on to the SAW, we mention the work of [50] which argues many of the relevant observables of $2d$ percolation can be obtained within a conformal field theory with $c = -24$. Without restating their argument, they find all the weights in the Kac table shift by -1, implying

$$\begin{aligned} \Delta_\sigma &= 5/48 \quad \to -91/48 \\ \Delta_\epsilon &= 5/4 \quad \to -3/4. \end{aligned}$$

Table 4.1: Percolation scaling dimensions. Bold values are calculated with the bootstrap, and adjacent values in parenthesis are either exact results ($d = 2, d = 6$) or calculated by Padé approximant at four loops ($d = 3, d = 4, d = 5$) [49]. In odd spatial dimensions we're unable to determine both Δ_σ and Δ_ϵ, and instead bootstrap with the referenced value of Δ_σ.

d	Δ_σ	Δ_ϵ
2	**0.101** (5/48)	**1.235** (5/4)
3	- (0.4765)	**1.615** (1.8849)
4	**0.997** (0.9523)	**2.557** (2.5549)
5	- (1.4718)	**3.416** (3.2597)
6	**2.002** (2)	**4.003** (4)

Bootstrapping with longitudinal derivatives and (4.12) with scaling dimensions shifted accordingly, for fixed $\Delta_\sigma = -91/48$ we obtain a clear solution at $\Delta_\epsilon = -0.728$ with $N = M = 6$. The general agreement with $\Delta_\epsilon = -3/4$ lends further evidence that our fusion rule is not just coincidentally successful.

4.4 Polymers

Polymers are long, flexible chains of repeating subunits called monomers. Since only a single monomer can occupy a given space, polymers in solution are modeled well by self-avoiding walks. Formally an $n-$step SAW on a d-dimensional lattice $\mathbb{Z}^d$ is an ordered set

$$\omega = (\omega(0), \omega(1), \ldots, \omega(n)), \tag{4.13}$$

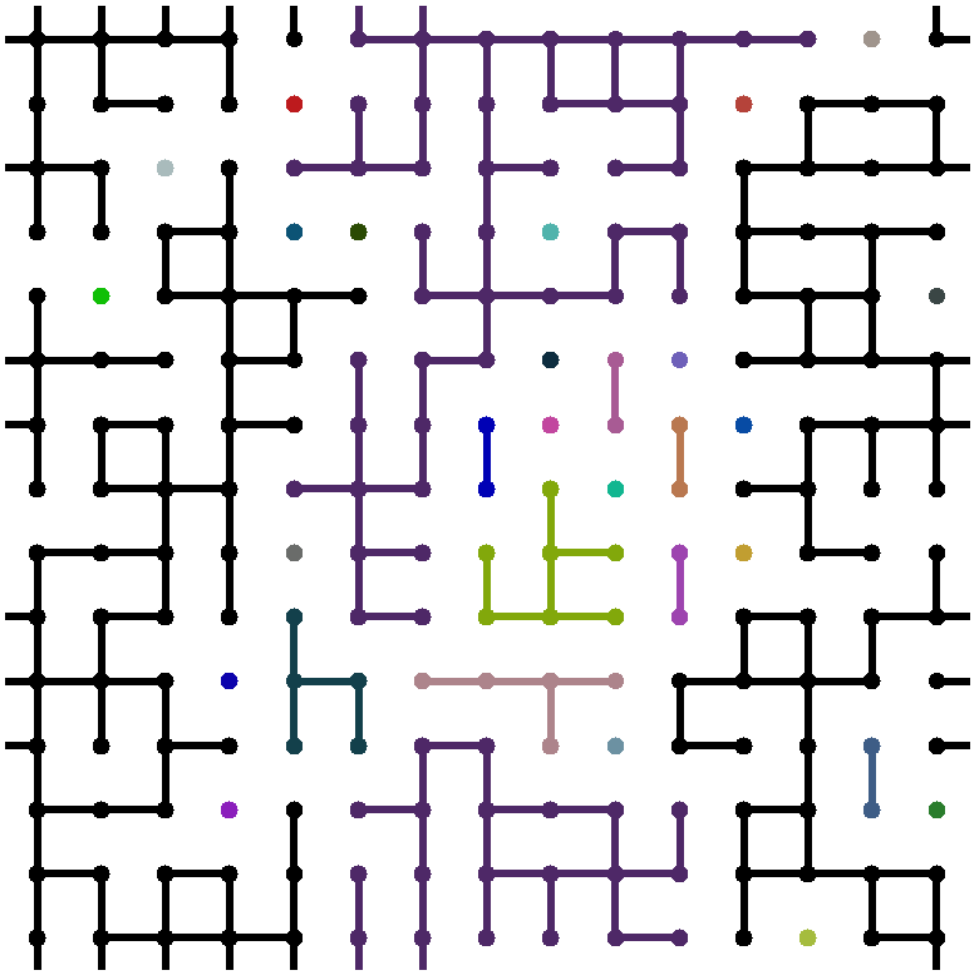

Figure 4.1: **2d Percolation.** Percolation on a square 15 by 15 site grid with $p = 0.51$. For this random instance, no horizontal or vertical crossing exists though both are assured in the thermodynamic limit. Clusters are plotted in different colors for clarity.

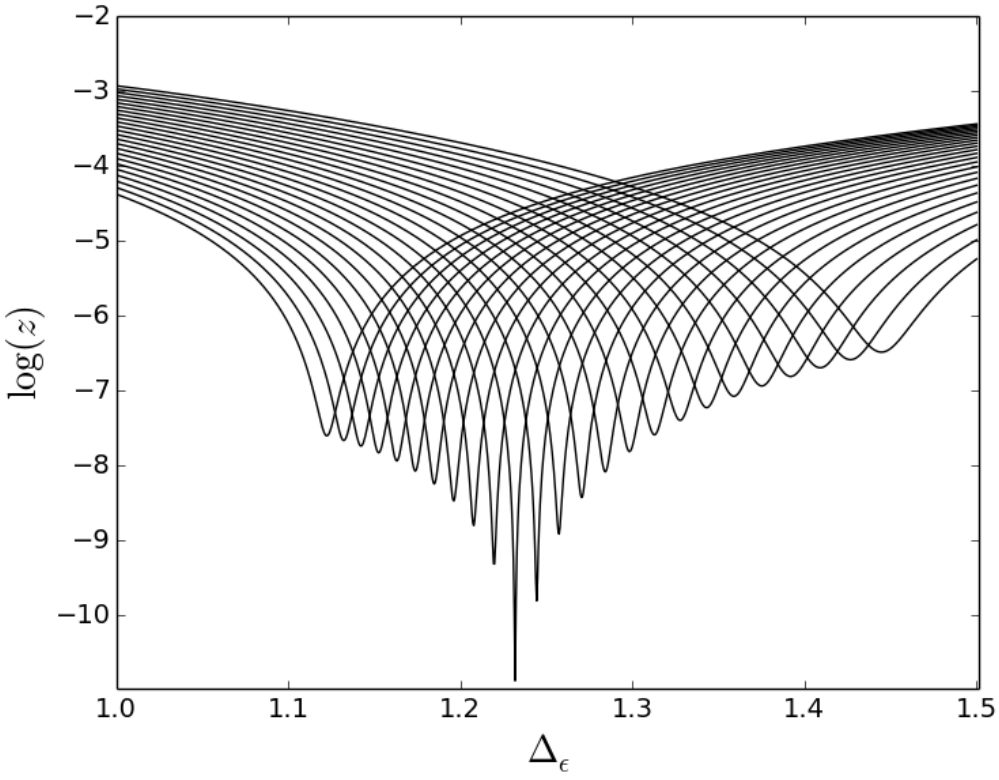

Figure 4.2: **2d Percolation.** Logarithm of the smallest singular value z of $\mathbf{F}$ with $N = 5, M = 6$ as a function of Δ_σ and Δ_ϵ. Each curve corresponds to a distinct value of Δ_σ, linearly spaced from $\Delta_\sigma = 4/48$ (left-most dip) to $\Delta_\sigma = 6/48$ (right-most dip). The minimal $\log(z)$ occurs at $\Delta_\sigma = 0.101, \Delta_\epsilon = 1.235$.

with $\omega(j) \in \mathbb{Z}^d, |\omega(j) - \omega(j-1)| = 1$, and $\omega(i) \neq \omega(j) \, \forall i \neq j$. Two questions of primary interest regarding the SAW are: What's the mean square displacement $\langle R_n^2 \rangle$ of an $n-$step SAW, and what's its asymptotic behavior as $n \to \infty$? The proposed answer to the latter [51, 52] is

$$\langle R_n^2 \rangle \propto \begin{cases} Dn^{2\nu}, & d \neq 4 \\ Dn^{2\nu} (\log n)^{1/4}, & d = 4 \end{cases} \tag{4.14}$$

with D a positive constant depending on spatial dimension and ν the critical exponent.

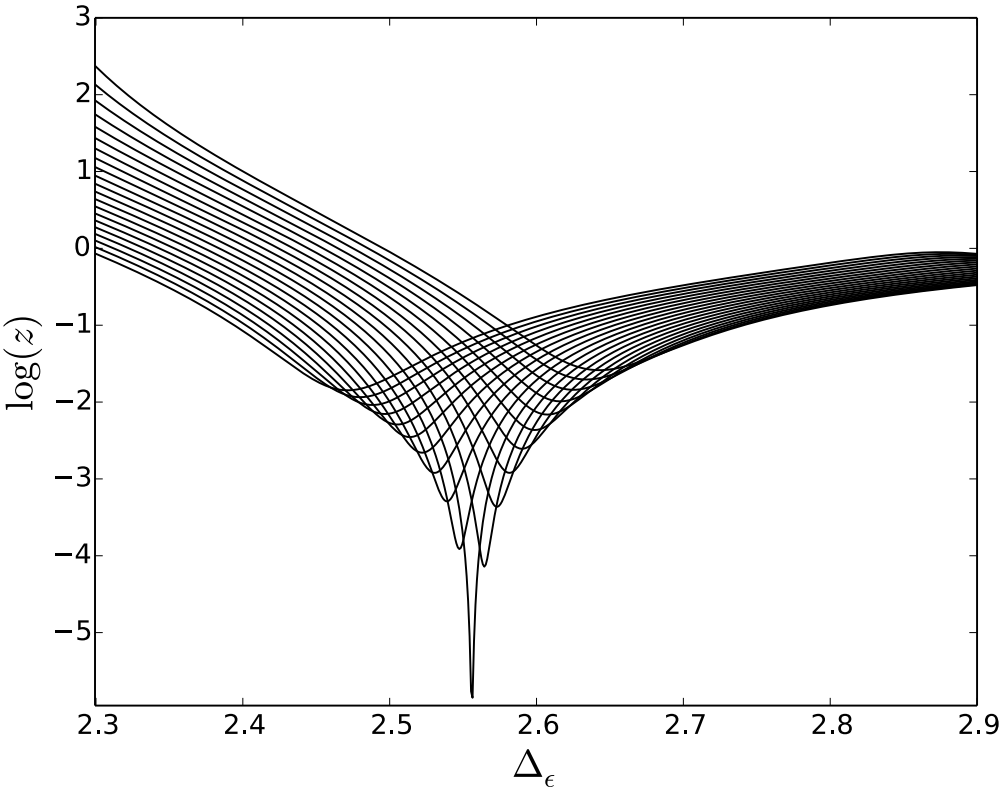

Figure 4.3: **4d Percolation.** Logarithm of the smallest singular value z of the matrix $\mathbf{F}/F^{(3,0)}_{\Delta_\sigma,0,0}$ with $N = 5, M = 6$ as a function of Δ_σ and Δ_ϵ. Each curve corresponds to a distinct value of Δ_σ, linearly spaced from $\Delta_\sigma = 0.98$ (left-most dip) to $\Delta_\sigma = 1.02$ (right-most dip). The minimal $\log(z)$ occurs at $\Delta_\sigma = 0.997, \Delta_\epsilon = 2.557$.

4.4.1 $O(N)$ Model

The SAW can be considered as the $N \to 0$ limit of the $O(N)$ vector model. The $O(N)$ model describes interacting, $N-$component spins on a lattice with Hamiltonian

$$H = -J \sum_{(i,j)} \mathbf{s}_i \mathbf{s}_j. \tag{4.15}$$

In addition to the spin field σ and energy operator

$$\epsilon = \sum_{a=1}^{N} : \sigma_a^2 :, \tag{4.16}$$

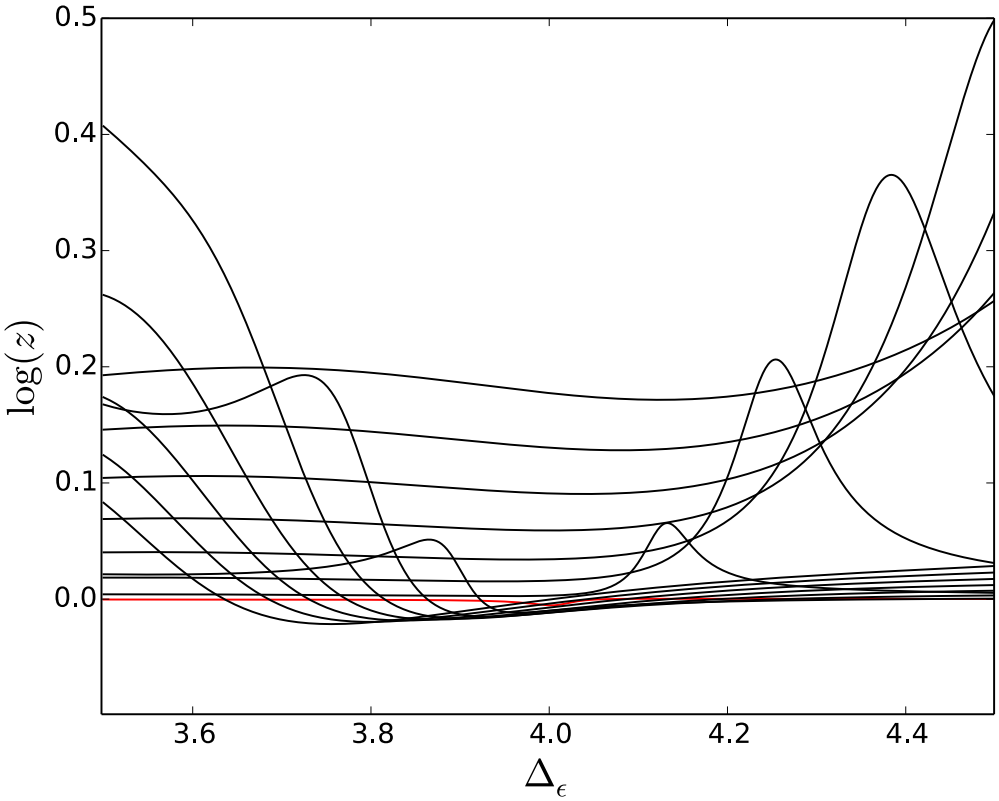

Figure 4.4: **6d Percolation.** Logarithm of the smallest singular value z of the matrix $\mathbf{F}/F^{(3,0)}_{\Delta_\sigma,0,0}$ with $N = 6, M = 8$ as a function of Δ_σ and Δ_ϵ. Each curve corresponds to a distinct value of Δ_σ, linearly spaced from $\Delta_\sigma = 1.8$ (left) to $\Delta_\sigma = 2.2$ (right). Near $\Delta_\epsilon = 4$ the curves flatten. The red curve corresponding to $\Delta_\sigma = 2.002$ has the smallest peak and a minimum at $\Delta_\epsilon = 4.003$. As in $4d$, using $\mathbf{F}/F^{(3,0)}_{\Delta_\sigma,0,0}$ rather than $\mathbf{F}$ has no bearing on the determination of the spin and energy operator scaling dimensions.

the $O(N)-$symmetric tensor

$$\varphi_{ab}(x) =: \sigma_a\sigma_b : -(1/N)\delta_{ab}\sum_{c=1}^{N} : \sigma_c^2 : \tag{4.17}$$

is of critical importance. The scaling dimensions Δ_ϵ and Δ_φ collide as $N \to 0$, leading to logarithmic behavior [6].

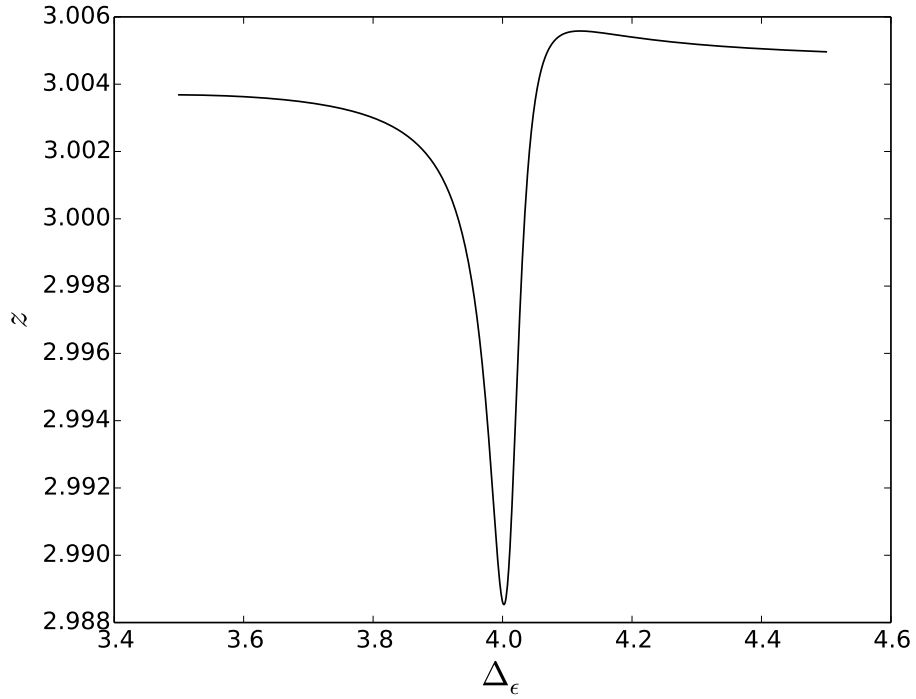

Figure 4.5: **6d Percolation.** Smallest singular value z of $\mathbf{F}$ at fixed $\Delta_\sigma = 2.002$ (red curve from Figure 4.4) achieves its minimal value at $\Delta_\epsilon = 4.003$.

4.4.2 Selection Rules

The energy operator for the $2d$ SAW corresponds to the primary field $\Phi_{1,3}$ with $h_{1,3} = 1/3$, and it has a null state at level 3 rather than level 2 as in percolation. Therefore one difference in operator content which may distinguish the two $c = 0$ theories is the inclusion of the $[\Delta_\epsilon + 2, 2]$ descendant. Another is the inclusion of the lowest lying $O(N)$ symmetric tensor $[\Delta_\varphi, 2]$, whose dimension $\Delta_\varphi \to \Delta_\epsilon$ as $N \to 0$ [14]. We find φ essential in applying the bootstrap to the SAW. The primary purpose of this operator is to input $O(N)$ symmetry. Secondarily it fulfills the role the identity operator did for percolation: it introduces an OPE coefficient independent of the energy sector, which can roughly account

for the ignorance of logarithmic features. Retaining the identity operator in the presence of φ is therefore redundant; we find $2d$ scaling dimensions change by less than 5% if the identity operator is also included. As in percolation $[D, 2]$ and other descendants of the identity are discarded to avoid the $c = 0$ catastrophe. For SAW in $2 \leq d \leq 4$ we thus create $\mathbf{F}$ with the operators

$$[\Delta_\sigma, 0] \times [\Delta_\sigma, 0] = [\Delta_\epsilon, 0] + [\Delta_\varphi, 2] + [\Delta_\epsilon + 2, 2] + [\Delta_\varphi + 2, 4] + [\Delta_\epsilon + 4, 4] + [\Delta_\epsilon + 6, 6] + \ldots \tag{4.18}$$

and the M lowest order longitudinal derivatives of $F_{\Delta_\sigma, \Delta, l}$ with $m \geq 3$.

4.4.3 Results

Bootstrapping in $2d$ with the above spectrum we're unable to distinguish a solution with $\Delta_\varphi, \Delta_\epsilon$, and Δ_σ all left arbitrary. The SAW is more difficult to isolate than percolation due to the collision of Δ_ϵ and Δ_φ. Taking $N = M = 6$, fixing both $\Delta_\varphi = 0.667$ and $\Delta_\sigma = 5/48$ finds $\Delta_\epsilon = 0.666$. With just a single scaling dimension fixed, the minimization procedure is not as reliable as in the percolation case, often getting caught in a local rather than a global minima. Fixing only $\Delta_\varphi = 0.667$ tentatively finds $\Delta_\epsilon = 0.666$, $\Delta_\sigma = 0.101$.

In three and four dimensions the free theory obscures the SAW solution, due to the $[\Delta_\epsilon, 0]$ and $[\Delta_\varphi, 2]$ operators. $\mathbf{F}$ always has a vanishing singular value as $\Delta_\varphi \to \Delta_\epsilon$ because $G_{\Delta,2} \simeq G_{\Delta,0}$ near $\Delta = d - 2$ where the scalar and spin two conformal blocks become degenerate. For the $3d$ SAW again there is difficulty in determining all three scaling dimensions using our proposed fusion rule (4.18). As we did for $3d$ percolation we fix $\Delta_\sigma = 0.514$ [14] and bootstrap the remaining scaling dimensions using $N = 5, M = 6$, finding $\Delta_\varphi = 1.326$ and $\Delta_\epsilon = 1.326$

Table 4.2: Polymer scaling dimensions. Bold values are calculated with the bootstrap, and adjacent values in parenthesis are either exact results ($d = 2, d = 4$), computed by ϵ-expansion (Δ_ϵ in $d = 3$) [53], or Borel summation (Δ_σ in $d = 3$) [54].

d	Δ_σ	Δ_φ	Δ_ϵ
2	**0.101** (5/48)	- (2/3)	**0.666** (2/3)
3	- (0.514)	**1.326** (1.336)	**1.326** (1.336)
4	**0.999** (1)	**1.999** (2)	**1.999** (2)

(Fig. 4.6). In $4d$, with $\Delta_\varphi, \Delta_\epsilon, \Delta_\sigma$ all arbitrary two solutions are present. One corresponds to $\Delta_\epsilon = \Delta_\varphi$ and is independent of Δ_σ. The second varies with Δ_σ. Minimizing the smallest singular value of $\mathbf{F}$ as a function of $\Delta_\varphi, \Delta_\epsilon$, and Δ_σ finds $\Delta_\varphi = 1.999, \Delta_\epsilon = 1.999, \Delta_\sigma = 0.999$ where the two solutions converge, as shown in Figure 4.7. This is expected, since the upper critical dimension for the self-avoiding walk is $d = 4$. All bootstrapped SAW scaling dimensions are collected in Table 4.2.

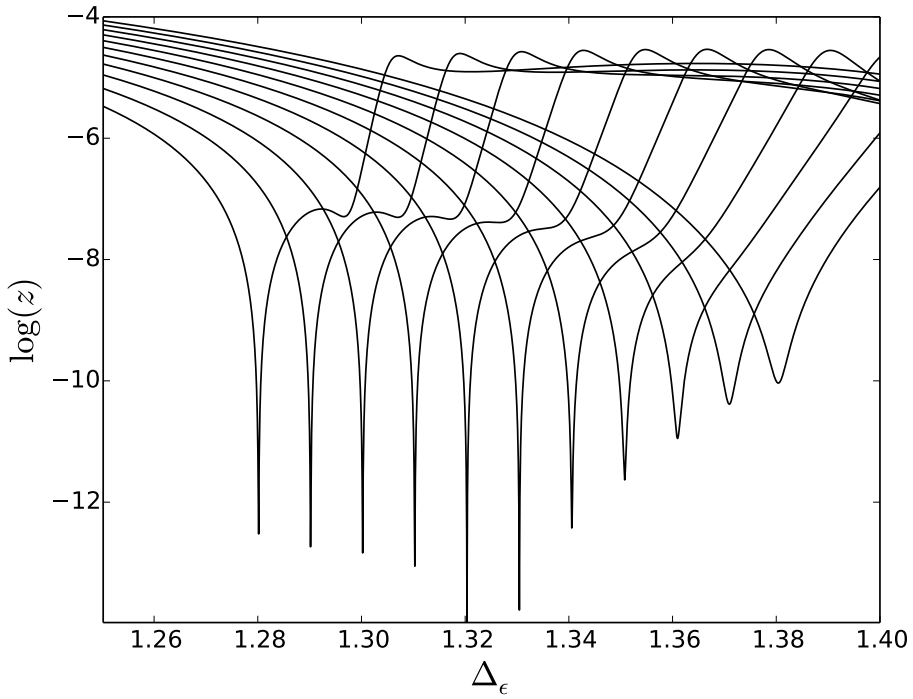

Figure 4.6: **3d SAW.** Logarithm of the smallest singular value z of $\mathbf{F}$ with $N = 5, M = 6$ as a function of Δ_σ and Δ_ϵ for fixed $\Delta_\sigma = 0.514$. Each curve corresponds to a distinct value of Δ_φ, linearly spaced from $\Delta_\varphi = 1.28$ (left) to $\Delta_\varphi = 1.38$ (right). $\log(z)$ has a minimum at $\Delta_\varphi = 1.326, \Delta_\epsilon = 1.326$.

4.5 Conlusion

The primary purpose of this work was to determine whether or not percolation and the self-avoiding walk could be distinguished with the conformal bootstrap. Though both theories share the same fusion algebra, central charge, and spin field scaling dimension in $d = 2$, we've shown they can be isolated. Using a simplistic spectrum of operators based on Virasoro symmetry, and excluding descendants of the identity to indirectly specify $c = 0$, the identity operator and a pair of spin 2 operators – a descendant of ϵ at level 2 and an $O(N)$ symmetric

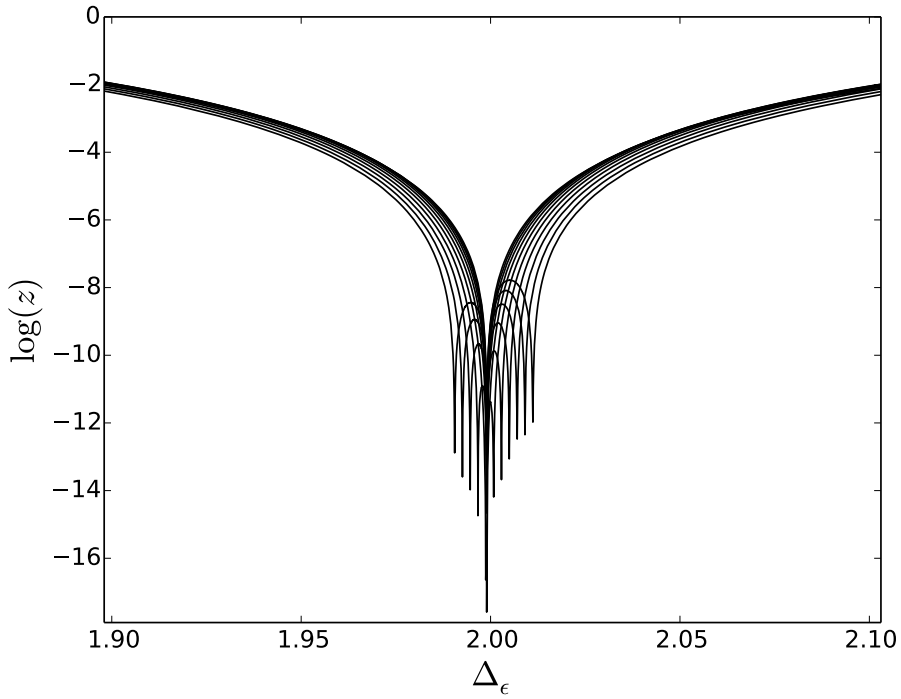

Figure 4.7: **4d SAW.** Logarithm of the smallest singular value z of $\mathbf{F}$ with $N = 6, M = 8$ as a function of Δ_σ and Δ_ϵ at $\Delta_\varphi = 1.999$. Each curve undergoes two dips in $\log(z)$, with one fixed at $\Delta_\epsilon = \Delta_\varphi$ and the second shifting with Δ_σ, which varies linearly from $\Delta_\sigma = 0.95$ (left) to $\Delta_\sigma = 1.05$ (right). The two solutions coincide and achieve a minimal $\log(z)$ at $\Delta_\varphi = 1.999, \Delta_\epsilon = 1.999, \Delta_\sigma = 0.999$.

tensor operator whose scaling dimension becomes degenerate with that of ϵ as $N \to 0$ – can be used to discriminate between percolation and the SAW in any d.

For percolation in two and four spatial dimensions, our bootstrapped scaling dimensions agree relatively well with established results. In particular in $4d$ our determination of the correlation length critical exponent ν, obtained with only $N = 5$ operators, is within about 0.1% of the value obtained by an involved four-loop calculation [49]. For the upper critical dimension in $6d$, while no rigorous bootstrapped solution is found we do see evidence of the anticipated free

field solution. Bootstrapping percolation in odd d is not as robust; to obtain a solution with our particular set of selection rules Δ_σ must be used as input. We point out that while this is the first treatment of percolation in $d > 2$ with the conformal bootstrap, a similar implementation has been used to extract the structure constants of $2d$ percolation [55]. Applying the bootstrap to the SAW, for the upper critical dimension $4d$ we easily recover the expected scaling dimensions of the free theory. However, in $d = 2$ and $d = 3$ additional input is required to find solutions. Namely at least one of the three independent scaling dimensions appearing in the truncated spectrum must be held fixed. To conclude, while more accurate results are surely possible by using larger, more complicated spectrums, percolation and the self-avoiding walk are clearly distinguishable with the conformal bootstrap.

Encouraged by these results, it would be interesting to use the conformal bootstrap to explore the space of $c = 0$ theories in a systematic manner, since many such theories are expected to have important physical applications. In particular very interesting problems in Anderson localization, such as the elusive critical point for transitions in the integer quantum Hall effect, are expected to be described by a $c = 0$ CFT in $2d$ [56].

4.6 Appendix

4.6.1 A. Percolation Fusion Rule

A potential criticism of our work is that to be in accordance with the exact fusion rule $[\sigma] \times [\sigma] = [\epsilon]$, the identity operator's contribution should vanish at a solution if that solution is to truly represent percolation. In practice we instead find that the OPE coefficient of the identity, though minimized at a solution, is larger than that of the energy operator. In this appendix we posit that, while physically the identity operator should decouple, its inclusion is a) a numerical necessity in treating percolation with global conformal blocks in the Gliozzi bootstrap, and b) does not alter the bootstrapped scaling dimensions.

To show this, we'll consider $2d$ percolation. In $2d$ the four-point function can be written in terms of the Virasoro conformal blocks

$$\langle \mathcal{O}(\infty)\mathcal{O}(1)\mathcal{O}(z)\mathcal{O}(0)\rangle = \sum_p a_p |\mathcal{F}(c, h, h_p, z)|^2. \tag{4.19}$$

Here a_p are the OPE coefficients squared (note in general $a_p \neq p_{\Delta,l}$ [57]), $\mathcal{F}$ the Virasoro conformal blocks, and the sum runs over Virasoro primaries. The utility of the Virasoro blocks for our purposes is twofold. First, each block contains all contributions to the four point function from a given conformal family, leading to simplification of the bootstrap equations for fusion rules containing just one Virasoro primary. Second, they're a function of c and thus $c = 0$ can be implemented directly.

To bootstrap with the Virasoro blocks, the analogues of the formulas provided in section 3.1 are required. These are provided in [36], for example, and

restated here. Crossing symmetry is respected if

$$\sum_p a_p^2 \left[\mathcal{F}(c,h,h_p,z)\overline{\mathcal{F}}(c,h,\overline{h}_p,\overline{z}) - \mathcal{F}(c,h,h_p,1-z)\overline{\mathcal{F}}(c,h,\overline{h}_p,1-\overline{z})\right] = 0. \tag{4.20}$$

Expanding around $z = \overline{z} = 1/2$ generates the homogeneous system

$$\sum_p a_p^2 \, g_{h,h_p}^{(m,n)} = 0 \tag{4.21}$$

with

$$g_{h,h_p}^{(m,n)} = \partial_z^m \partial_{\overline{z}}^n \left[\mathcal{F}(c,h,h_p,z)\overline{\mathcal{F}}(c,h,\overline{h}_p,\overline{z}) - \mathcal{F}(c,h,h_p,1-z)\overline{\mathcal{F}}(c,h,\overline{h}_p,1-\overline{z})\right]|_{z=\overline{z}=1/2}. \tag{4.22}$$

Note $m+n$ must be odd or else $g_{h,h_p}^{(m,n)}$ is trivially zero. For the fusion rule $[\sigma]\times[\sigma] = [\epsilon]$ the homogeneous system becomes

$$\partial_z^m \mathcal{F}(c,h_\sigma,h_\epsilon,z)|_{z=1/2} = 0 \quad \text{or} \quad \partial_z^n \mathcal{F}(c,h_\sigma,h_\epsilon,z)|_{z=1/2} = 0. \tag{4.23}$$

As argued in [36], since $m+n$ is odd, either all even or all odd derivatives vanish at a solution to the crossing equation.

The argument above implies a simple way to determine whether or not it's even possible to use the Gliozzi bootstrap to find a solution with the correct OPE coefficients for 2d percolation: since either all odd derivatives or all even derivatives must vanish at a solution, if $\partial_z^1 \mathcal{F}(c,h_\sigma,h_\epsilon,z)|_{z=1/2} \neq 0$ and $\partial_z^2 \mathcal{F}(c,h_\sigma,h_\epsilon,z)|_{z=1/2} \neq 0$ as $c \to 0$ near $(h_\sigma = 5/96, h_\epsilon = 5/8)$, then percolation can't be correctly found by the conformal bootstrap without treating the logarithmic CFT aspects more carefully.

The results (Fig 4.8) are unfortunately not so clear. With $h_\epsilon = 5/8$ fixed, for $c > 0$, no solution is found regardless of how close c is to zero. For $c < 0$, both even and odd derivatives vanish at two points equidistant from $h_\sigma = 5/96$. The two solutions converge as $c \to 0$, as shown in Fig. 4.9 for $\partial_z^1 \mathcal{F}(c,h_\sigma,5/8,z)$. This

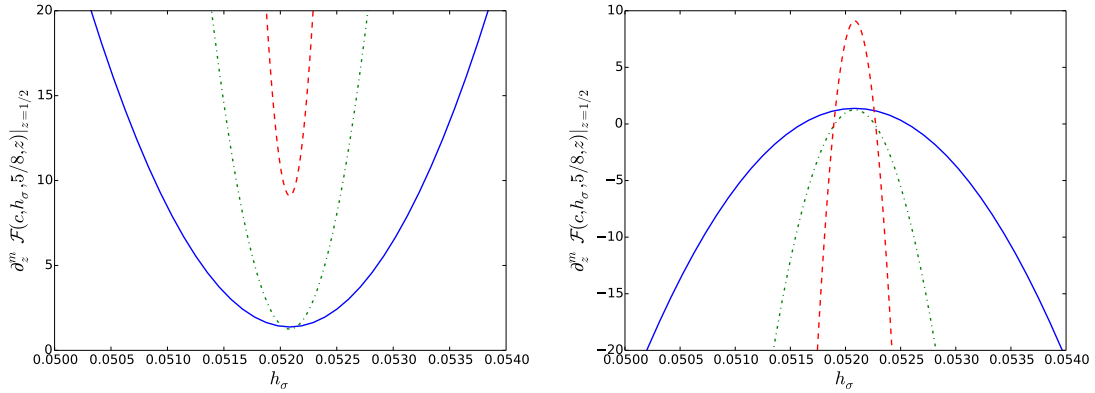

(a) $c = 10^{-6}$ (b) $c = -10^{-6}$

Figure 4.8: $\partial_z^m \mathcal{F}(c, h_\sigma, 5/8, z)|_{z=1/2}$ for $m = 1, 2, 3$ (solid blue, green dash-dot, dashed red)

structure is present only very near to $h_\epsilon = 5/8$. This is expected; away from $q = 1$ the fusion rule becomes $[\sigma] \times [\sigma] = [1] + [\epsilon]$.

The minima (maxima) of the $c > 0$ ($c < 0$) curves in Fig. 4.8 all occur exactly at $h_\sigma = 5/96$, and clearly should correspond to $\partial_z^m \mathcal{F}(c, h_\sigma, h_\epsilon, z)|_{z=1/2} = 0$ since percolation should be a solution. The shift above 0 (which does not change as $|c| \to 0$) might represent the error in ignoring logarithmic terms in the OPE, which would be compounded in higher order derivatives. Including the identity operator in the fusion rule appears to correct the shift shown in Fig. 4.8 at the cost of obtaining the correct OPE coefficients. In this case the sum in (4.21) contains $N = 2$ terms: the ϵ block and the identity block. The latter is given by the Virasoro vacuum block, truncated to include only the lowest order contribution

$$\mathcal{F}(c, h, 0, z) = 1/z^{2h}. \tag{4.24}$$

Since now two blocks are included in the fusion rule, the bootstrap must be

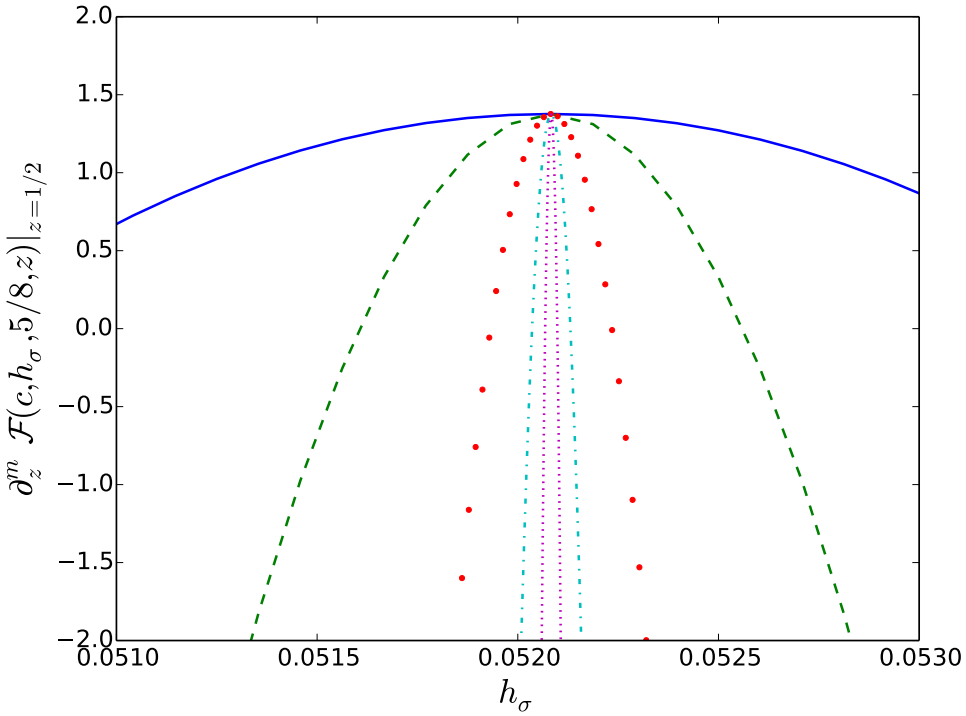

Figure 4.9: h_σ vs $\partial_z^1 \mathcal{F}(c,h,5/8,z)|_{z=1/2}$. The two solutions converge towards $h_\sigma = 5/96$ as $c \to 0$. c values:-10^{-5} (solid blue),-10^{-6} (dashed green),-10^{-7}(red circles),-10^{-8} (cyan dash-dot),-10^{-9} (magenta dots).

performed with (4.22) rather than (4.23). With $m+n$ necessarily odd, we take $M = 2$ derivatives and

$$d_{23} = \begin{pmatrix} g^{(2,1)}_{h,0} & g^{(2,1)}_{h,5/8} \\ g^{(3,0)}_{h,0} & g^{(3,0)}_{h,5/8} \end{pmatrix} \tag{4.25}$$

with $c = -10^{-6}$ in order to make the closest possible comparison to the green and red curves of Fig. 4.8b. The smallest vanishing singular value of d_{23} is found to occur at $h_\sigma = 0.0519 \approx 5/96$. Thus the two solutions equidistant from $h_\sigma = 5/96$ found with the exact fusion rule are replaced with a single solution at the proper value solely by including the identity operator. The exact fusion rule is sufficient to find percolation only if $c \to 0^-$, which is unenforceable when bootstrapping

with global blocks as in the main text. Keeping the identity operator in our fusion rule is essentially a numerical crutch; a method of correcting for using scalar rather than logarithmic conformal blocks.

The drawback of retaining the identity operator in our fusion rule comes in the form of inaccurate OPE coefficients. For a_ϵ normalized to unity, inserting our solution ($h_\sigma = 0.0519, h_\epsilon = 5/8$) into the linear system associated with d_{23} finds $a_{\mathbb{1}} = 0.453$. As the magnitude of c is further decreased this OPE coefficient grows, becoming larger than a_ϵ. For example generating d_{23} with $c = -10^{-7}$ instead leads to an approximate solution at $h_\sigma = 0.0521$ and $a_{\mathbb{1}} \approx 4.3$. It's encouraging that even as $a_{\mathbb{1}}$ increases h_σ remains relatively unperturbed. Including the identity operator here, and in the main text, does not drive the solution away from the percolation critical point. In this case its non-vanishing contribution, and more specifically $a_{\mathbb{1}} > a_\epsilon$, appears to be a signature of bootstrapping very close to $c = 0$. This analysis suggests deviation from the known exact h_σ, h_ϵ values of $2d$ percolation has more to do with the truncation of the ϵ block than the presence of the identity operator. Also playing a role is the choice of derivative constraints used to construct the homogeneous system of equations in the bootstrap, which is the subject of Appendix B.

4.6.2 B. Derivatives

If a theory is easily truncable, which Taylor expansion terms are chosen to create **F** shouldn't strongly influence the outcome of the bootstrap. With the small number of operators kept in this work, a significant volatility in convergence is observed as the chosen set of derivatives is changed. This also arises in [34]

where for the $3d$ self-avoiding walk $\Delta_\epsilon = 1.325$ is found with just one of the four 3×3 minors considered.

To illustrate consider the spectrum

$$[\Delta_\sigma, 0] \times [\Delta_\sigma, 0] = [0,0] + [\Delta_\epsilon, 0] + [\Delta_\epsilon + 4, 4] + [\Delta_\epsilon + 6, 6] + [\Delta_\epsilon + 8, 8] + \dots \quad (4.26)$$

in $2d$. Aside from the identity these operators are all present in both the SAW and percolation. With this fusion rule and fixed $\Delta_\sigma = 5/48$, we report in Table 4.3 the bootstrapped value of Δ_ϵ, located by minimizing the smallest singular value of the crossing matrix as a function of Δ_ϵ for three different methods of choosing derivative constraints. For the natural choice $m \geq n$ (i.e. the (m, n) sequence $(1,0), (1,1), (3,0), (3,1) \dots$) a solution which converges to the $2d$ self-avoiding walk $\Delta_\epsilon = 2/3$ is found. On the other hand employing only longitudinal derivatives and excluding $M = (1,0)$ (i.e. the sequence $(3,0), (5,0), (7,0) \dots$) finds a Δ_ϵ consistent with percolation, as shown in Figure 4.10.

Thus there is evidence polymers and percolation can be distinguished without appealing to the $O(N)$ symmetry of the self-avoiding walk as done in the main text, but instead by being selective with the Taylor expansion terms used to construct $\mathbf{F}$. While this may appear to be just a trivial tuning of the system of equations to achieve a known result, using the same set of operators (4.26) and the derivatives from column 2 (column 3) of Table 4.3 also picks out percolation (SAW) in 4d, as shown in Figure 4.3 (Figure 4.11).

The decision to exclude transverse derivatives in the main text was initially made out of convenience; evaluating longitudinal derivatives of conformal blocks is less computationally intensive than evaluating their transverse counterparts. However, it's clear setting $n = 0$ and using only longitudinal derivatives is more successful at bootstrapping $2d$ percolation. Presumably this

Table 4.3: Comparison of possible truncations of the crossing equation in two dimensions with fixed $\Delta_\sigma = 5/48$ and square matrices ($N = M$). In each successive row of the table, the lowest dimension operator from (4.26) and lowest order derivative available is added, and the bootstrapped Δ_ϵ is reported. Three possible methods of choosing derivatives are considered.

	$m \geq 1$	$m \geq 3$	$m \geq n$
N	$(m, 0)$	$(m, 0)$	(m, n)
2	1.221	1.321	-
3	1.216	1.250	0.705
4	1.216	1.260	0.681
5	1.216	1.255	0.672
6	1.215	1.255	0.667

variance in outcome, as shown in Table III, is evidence our spectrum of operators (4.12) is not comprehensive. With an exact, complete set of operators one would anticipate the results of the bootstrap being more robust. Indeed, when the fusion rule (4.26) is expanded to include all descendants of the energy operator, which are inherently present in the ϵ Virasoro blocks making up d_{23} in the previous appendix, utilizing the $(m, n) = (2, 1)$ constraint is not a problem. Appendix A also sheds some light on why accuracy is improved if the $(m, n) = (1, 0)$ term is avoided. In Fig. 4.8b the curves corresponding to $m = 2$ and $m = 3$ have solutions which exactly coincide while those of $m = 1$ deviate further from $h_\sigma = 5/96$. This discrepancy is eliminated as $c \to 0^-$, but this isn't enforceable with global conformal blocks. In theory, implementing logarithmic conformal blocks [47] along with increasing the number of retained operators should eliminate any need to worry about which derivative constraints are chosen.

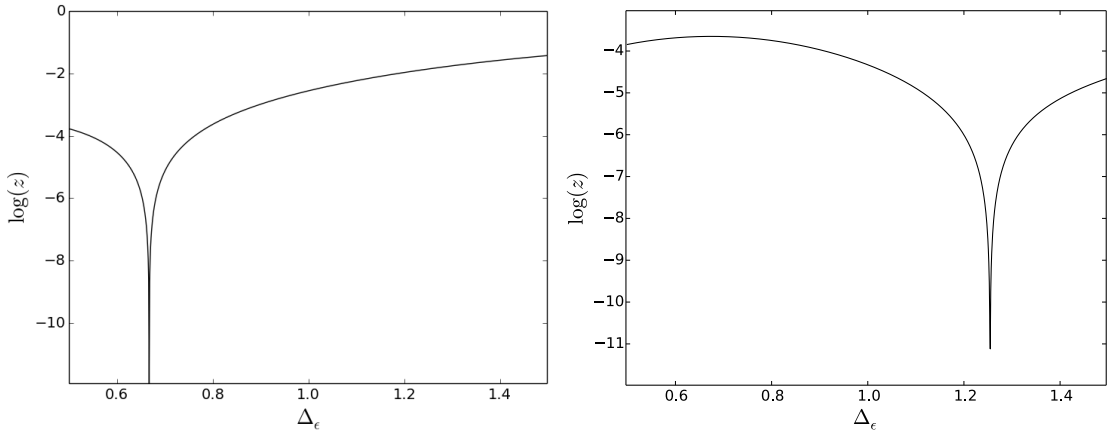

(a) $m \geq n$ derivative prescription finds a solution at $\Delta_\epsilon = 0.667$, consistent with $2d$ SAW.

(b) $m \geq 3$ derivative prescription finds a solution at $\Delta_\epsilon = 1.255$, consistent with $2d$ percolation.

Figure 4.10: Logarithm of the smallest singular value z of $\mathbf{F}$ for $N = M = 6$ and fixed $\Delta_\sigma = 5/48$.

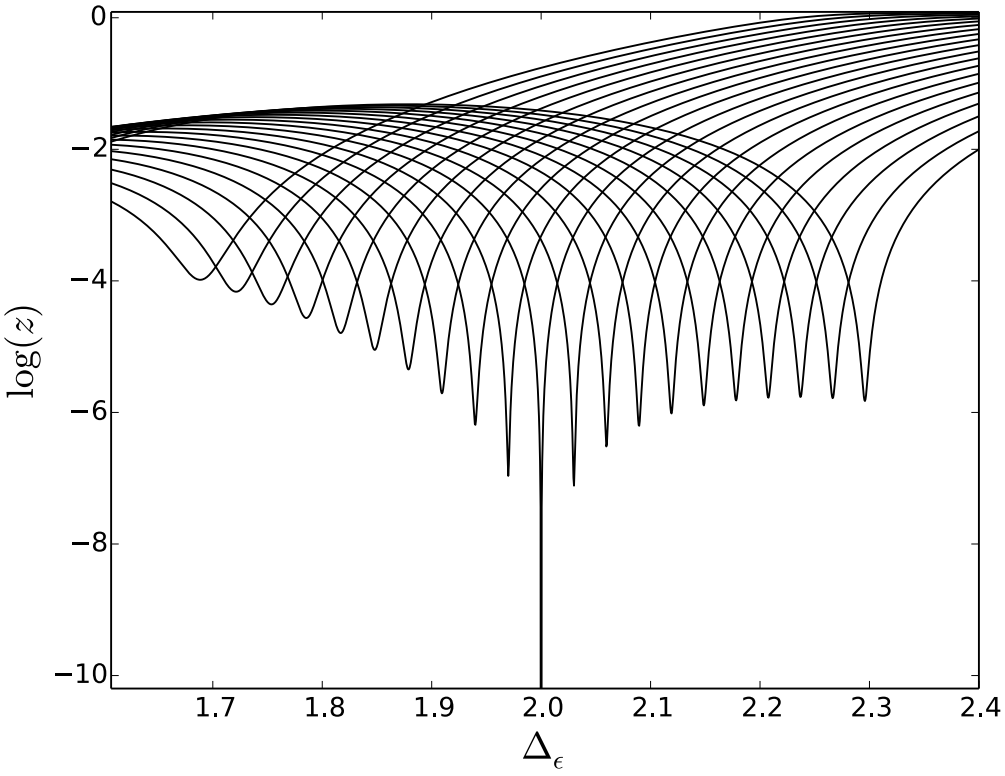

Figure 4.11: Logarithm of the smallest singular value z of $\mathbf{F}$ with $N = 6, M = 7$ as a function of Δ_σ and Δ_ϵ, with the derivative prescription for 2d SAW. Each curve corresponds to a distinct value of Δ_σ, linearly spaced from $\Delta_\sigma = 0.9$ (left) to $\Delta_\sigma = 1.1$ (right). Minimizing $\log(z)$ finds the solution $\Delta_\sigma = 1.000, \Delta_\epsilon = 2.000$ as anticipated for the $4d$ SAW.

CHAPTER 5

SCATTERING AND FORMALISM

Ultracold atoms are valuable in part because of their tunability, which leads to a close correspondence between theory and experiment. Simple theoretical frameworks can be constructed to model complex physical phenomena, such as exotic phase transitions. Precise experiments, with controlled interatomic interactions, may be devised to evaluate their validity.

In the following chapters, a formalism based on the zero temperature S-matrix is used to study Berezinskii-Kosterlitz-Thouless and upper branch phase transitions. The basics of this formalism and atomic scattering theory are presented below.

5.1 Scattering Theory and Feshbach Resonances

For an ultracold atomic gas, two-body interactions can be fully described by the s-wave scattering length, a_s. This parameter can be tuned over many orders of magnitude with a Feshbach resonance, a phenomenon in which open and closed scattering channels are coupled when the total energy of the states in the open channel is equal to the total energy of the bound state in the closed channel [58, 59]. One can think of the process as the atoms occupying an open channel briefly scattering into a state in a closed channel before returning to the open channel.

Schematically, this is a second order process and therefore the scattering

length should be proportional to the energy difference between channels

$$a_s \propto \frac{1}{E_{\text{open}} - E_{\text{res}}}. \tag{5.1}$$

In the above equation E_{open} is the energy of the atoms in the open channel, and E_{res} the energy of the bound state in the closed channel. Crucially, the bound state has a magnetic moment that differs from the magnetic moment of the atoms partaking in the two-body scattering process due to the hyperfine interaction. Thus an external magnetic field affects the bound and scattering states differently, allowing the energy difference, and subsequently the scattering length, to be experimentally controlled. Feshbach resonances allow the interaction strength of an atomic gas to be controlled with great precision across many orders of magnitude. In the remainder of this section, the details of scattering theory necessary to derive this important result are presented.

5.1.1 Scattering Theory

The wavefunction describing scattering of an incident plane wave off a particle of size r_0, in the large r limit, can be written as the sum of incoming and scattered waves

$$\psi(r) = e^{ikz} + f(\theta)\frac{e^{ikr}}{r} \tag{5.2}$$

with $f(\theta)$ the scattering amplitude. This wavefunction can also be found directly by solving the Schrödinger equation in a central potential $V(r)$. Spherical symmetry suggests solutions may be expanded in terms of the Legendre polynomials $P_l(\cos\theta)$

$$\psi(r) = \sum_{l=0}^{\infty} R(r) C_l P_l(\cos\theta) \tag{5.3}$$

where $R(r)$ are the solutions to the radial Schrödinger equation, which in the $r \to \infty$ limit take the form

$$R(r) = \frac{1}{kr} \sin(kr - \frac{l\pi}{2} + \delta_l). \tag{5.4}$$

Here, δ_l are the phase shifts of the scattered wave due to the scatterer. Similarly expanding (5.2)'s plane wave in terms of Legendre polynomials and comparing to (5.3) leads to the well-known result for the scattering amplitude

$$f(\theta) = \frac{1}{k} \sum_{l=0}^{\infty} (2l + 1) e^{i\delta_l} \sin \delta_l P_l(\cos \theta). \tag{5.5}$$

In the low energy, or s-wave, limit where $kr_0 << 1$ the scattering amplitude becomes constant, as the structure of the particle is invisible to the incident wave. The $l = 0$ term dominates the sum and (5.5) becomes a constant

$$f(\theta) = \lim_{k \to 0} \left(\frac{e^{i\delta_0}}{k} \sin \delta_0 \right) \approx \frac{\delta_0}{k}. \tag{5.6}$$

Conventionally, this constant is written $-a_s$, with a_s the scattering length:

$$a_s = \frac{-\delta_0}{k}. \tag{5.7}$$

The s-wave scattering cross section is thus completely determined by the scattering length:

$$\sigma = \int \frac{d\sigma}{d\Omega} d\Omega \tag{5.8}$$

$$= \int |f(\theta)|^2 d\Omega \tag{5.9}$$

$$= \lim_{k \to 0} \int \frac{\sin(\delta_0)^2}{k^2} \tag{5.10}$$

$$= 4\pi a_s^2 \tag{5.11}$$

5.1.2 Feshbach Resonances

Following the argument in [58], consider splitting the Hilbert space into two subspaces P and Q, with P containing the open channels and Q the closed channels. Any given state can then be written

$$|\psi\rangle = |\psi_P\rangle + |\psi_Q\rangle \tag{5.12}$$

with $|\psi_P\rangle = \mathcal{P}|\psi\rangle$, $|\psi_Q\rangle = \mathcal{Q}|\psi\rangle$ and $\mathcal{P}$, $\mathcal{Q}$ the respective projection operators of the subspaces. Applying $\mathcal{P}$ to the Schrödiner equation on the left gives

$$(E - H_{PP})|\psi_P\rangle = H_{PQ}|\psi_Q\rangle, \tag{5.13}$$

where $H_{IJ} = \mathcal{I}H\mathcal{J}$. Repeating with $\mathcal{Q}$ and inserting into (5.13) results in

$$(E - H_0 - U)||\psi_P\rangle = 0, \tag{5.14}$$

with $U = U_P + U_{FR}$, and

$$U_{FR} \equiv H_{PQ}(E - H_{QQ} + i\epsilon)^{-1}H_{QP}. \tag{5.15}$$

Above, H_{PP} has been broken into interacting and non-interacting pieces, and U_{FR} is the interaction term responsible for Feshbach resonances. As evidenced by the form of (5.15), it may be thought of as an interaction in the P subspace due to a transition from $P \to Q \to P$.

To interpret (5.14) and relate to experiment, we can use the T-matrix. The Lippmann-Schwinger equation with propagator $G_0 \equiv (E - H_0 + i\epsilon)^{-1}$ reads

$$T = U + UG_0T \tag{5.16}$$

and can be solved with the given interaction potential:

$$T = T_P + (1 - U_PG_0)^{-1}U_{FR}(1 - G_0U)^{-1}. \tag{5.17}$$

Above, T_P is the T-matrix for the subspace of open channel states in the absence of transitions to Q.

Calculating the matrix elements of (5.17) for plane waves with momenta $\mathbf{k}, \mathbf{k}'$ to first order in U_{FR} and utilizing the T-matrix's relation to the s-wave scattering length at zero energy [58]

$$T = \frac{4\pi\hbar^2 a_s}{m} \tag{5.18}$$

yields

$$\frac{4\pi\hbar^2}{m}a = \frac{4\pi\hbar^2}{m}a_P + \sum_n \frac{\langle\psi_n|H_{QP}|\psi_0\rangle|^2}{E_{th} - E_n} \tag{5.19}$$

with a_p the scattering length in the absence of interactions between open and closed channels, E_{th} is the energy of the scattering atoms at large separation $r >> r_0$, and the sum runs over all states in Q. If E_{th} lies near the energy of a particular bound state n = res then the energy dependence of all other E_n contributing to the sum may be neglected. Their contribution can be rolled together with a_p into a non-resonant term

$$\frac{4\pi\hbar^2}{m}a_s = \frac{4\pi\hbar^2}{m}a_{nr} + \frac{\langle\psi_{res}|H_{QP}|\psi_0\rangle|^2}{E_{th} - E_{res}}. \tag{5.20}$$

Expanding the denominator and supposing it vanishes at some particular value of external B field, we can expand $E_{th} - E_{res} \sim (\mu_{res} - \mu_1 - \mu_2)(B - B_0)$ with and $\mu_i = -\frac{\partial E_i}{\partial B}$ the magnetic moment of the individual atoms and bound state. Substituting into (5.20) gives

$$a_s = a_{nr}\left(1 - \frac{\Delta B}{B - B_0}\right) \tag{5.21}$$

with

$$\Delta B = \frac{m}{4\pi\hbar^2 a_{nr}} \frac{|\langle\psi_{res}|H_{QP}|\psi_0\rangle|^2}{\mu_{res} - \mu_\alpha - \mu_\beta}, \tag{5.22}$$

which are the main results describing Feshbach resonances and their importance. By controlling B, the scattering length can be adjusted, allowing one to

tune the gas from effective repulsive to attractive interactions. This is of particular value near resonance $B = B_0$, where slight adjustments to B may cause large changes to a_s.

5.2 Formalism

In this section, an overview of the formalism developed in [60] is given. The formalism is inspired by the thermodynamic Bethe ansatz (TBA) in that both involve expressing the free energy in terms of a pseudo-energy which satisfies an integral equation. The Bethe ansatz is a technique for finding exact solutions to integrable interacting quantum systems in one spatial dimension. Models which can be solved by the Bethe ansatz have an exact zero-temperature S-matrix that factorizes into products of two-body S-matrices. The Bethe ansatz results in expressions that characterize the momenta of particles of a given state of a system, which can subsequently be used to calculate quantities in the thermodynamic limit. The TBA, first applied by Yang and Yang to the Bose gas [61] formalizes this idea by providing a framework for summing up contributions from many states to incorporate finite temperatures.

The formalism described below extends the TBA approach to thermodynamics to higher dimensional systems where exact solutions are generally not possible, as the S-matrix does not factorize into products of two-body interactions. Nevertheless these two-body interactions may be summed to all orders in the coupling, effectively capturing some non-perturbative behavior. Consequentially, for some models, solutions of the resulting integral equation are valid beyond typical weak-coupling regimes [62].

5.2.1 Partition Function in terms of the S-matrix

We begin by expressing the partition function

$$Z(\beta,\mu) = \mathrm{tr}\, e^{-\beta(H-\mu N)} \tag{5.23}$$

in terms of the S-matrix operator

$$\widehat{S}(E) = 1 + 2\pi i\delta(E - H_0)\widehat{T}(E) \tag{5.24}$$

as

$$Z = Z_0 + \frac{1}{2\pi}\int dE e^{-\beta E}\,\mathrm{tr}\,\mathrm{Im}\partial_E \log\widehat{S}(E). \tag{5.25}$$

Here, $\beta = 1/T$, μ is the chemical potential, H_0 and Z_0 are the free parts of the Hamiltonian and partition function, respectively, and $\widehat{T}(E)$ has on shell matrix elements $T = (2\pi)^d\delta_{\mathbf{k},\mathbf{k}'}\mathcal{M}_{\{k\}\to\{\mathbf{k}'\}}$ with $\mathcal{M}$ the scattering amplitudes. The integral over E can be put in a more useful form by observing $\log\widehat{S}(E) \propto \delta(E - H_0)$, and defining the operator W

$$\mathrm{Im}\log\widehat{S}(E) \equiv 2\pi\delta(E - H_0)W(E). \tag{5.26}$$

Substitution this relation into (5.25) and integrating by parts results in

$$Z = \int dE e^{-\beta E}\,\mathrm{tr}(\delta(E - H_0)\widehat{W} \tag{5.27}$$

with

$$\widehat{W} \equiv W\beta + 1. \tag{5.28}$$

The above expression for Z takes the form of a configuration integral, and reduces to unity in the absence of interactions as expected. In analogy with Mayer's cluster expansion for classical gases, a decomposition of Z in terms of clusters can be developed. The cluster decomposition of $\widehat{W}$ for state $|\Psi\rangle$ reads

$$\langle\Psi'|\widehat{W}|\Psi\rangle = \sum_{\text{partitions}} s^P\langle\Psi'_1|\widehat{W}|\Psi_1\rangle_c\langle\Psi'_2|\widehat{W}|\Psi_2\rangle_c\langle\Psi'_3|\widehat{W}|\Psi_3\rangle_c\ldots \tag{5.29}$$

Above s is 1 for bosons, -1 for fermions, and the sum is over all possible partitions of $|\Psi\rangle$ into i-particle clusters $|\Psi_i\rangle$. $\widehat{W}$'s dependence on the S-matrix implies only connected clusters will contribute. Defining $\widehat{w}_N(\mathbf{k}_1, \ldots, \mathbf{k}_N)$ as the sum of terms composed of connected N-particle matrix elements of $\widehat{W}$, i.e.

$$\widehat{w}_1(\mathbf{k}_1) = \langle \mathbf{k}_1 | \widehat{W} | \mathbf{k}_1 \rangle_c \tag{5.30}$$

$$\widehat{w}_2(\mathbf{k}_1, \mathbf{k}_2) = \langle \mathbf{k}_1 \mathbf{k}_2 | \widehat{W} | \mathbf{k}_1 \mathbf{k}_2 \rangle_c + s \langle \mathbf{k}_2 | \widehat{W} | \mathbf{k}_2 \rangle_c \langle \mathbf{k}_1 | \widehat{W} | \mathbf{k}_2 \rangle_c, \tag{5.31}$$

leads to the simplification

$$\log Z = \sum_N \frac{z^N}{N!} \int d\mathbf{k}_1 \ldots d\mathbf{k}_N e^{-\beta \sum_{i=1}^N \omega_{\mathbf{k}_i}} \widehat{w}_N(\mathbf{k}_1, \ldots \mathbf{k}_N), \tag{5.32}$$

where $z = e^{\beta\mu}$ is the fugacity and $\omega_{\mathbf{k}_i} = \mathbf{k}_i^2/2m$ is the energy of the free, non-relativistic single particle state $|\mathbf{k}_i\rangle$ with mass m. Pulling out a factor of volume $\widehat{w}_N(\mathbf{k}_1, \ldots \mathbf{k}_N) \equiv V w_N(\mathbf{k}_1, \ldots, \mathbf{k}_N)$ gives the free energy density in terms of connected matrix elements

$$\mathcal{F} = -\frac{1}{\beta} \sum_N \frac{z^N}{N!} \int d\mathbf{k}_1 \ldots d\mathbf{k}_N e^{-\beta \sum_{i=1}^N \omega_{\mathbf{k}_i}} w_N(\mathbf{k}_1, \ldots \mathbf{k}_N). \tag{5.33}$$

Contributions to (5.33) due to 1 particle factors yield delta functions

$$\widehat{w}_1(\mathbf{k}, \mathbf{k}') = \langle \mathbf{k}' | \widehat{W} | \mathbf{k} \rangle_c = (2\pi)^d \delta_{\mathbf{k},\mathbf{k}'} \tag{5.34}$$

and thus are easily integrated over. Considering their contributions to all orders yields

$$\mathcal{F} = \mathcal{F}_0 - \frac{1}{\beta} \sum_{N \geq 2} \frac{1}{N!} \int \left(\prod_{i=i}^N d\mathbf{k}_i f_0(\mathbf{k}_i) \right) w_N(\mathbf{k}_1, \ldots, \mathbf{k}_N), \tag{5.35}$$

where $\mathcal{F}_0$ is the free-particle contribution

$$\mathcal{F}_0 = \frac{s}{\beta} \int \frac{d^d\mathbf{k}}{(2\pi)^d} \log(1 - sze^{-\beta\omega_{\mathbf{k}}}) \tag{5.36}$$

and

$$f_0(\mathbf{k}) \equiv \frac{z}{e^{\beta\omega_{\mathbf{k}}} - sz} \tag{5.37}$$

is the free filling fraction. In the diagrammatic description of the formalism, each line in a diagram is associated with a factor of $f_0(\mathbf{k})$. Each vertex is assigned a factor of $(2\pi)^d \beta \mathcal{V}_n(\mathbf{k}'_1, \ldots, \mathbf{k}'_n; \mathbf{k}_1, \ldots, \mathbf{k}_n)$ where $\mathcal{V}_n$ is the n-particle vertex function, defined in terms of $\widehat{W}$ as

$$\langle \mathbf{k}'_1, \ldots, \mathbf{k}'_m | \widehat{W} | \mathbf{k}_1, \ldots, \mathbf{k}_n \rangle_c = (2\pi)^d \beta \delta_{\mathbf{k},\mathbf{k}'} \mathcal{V}_n(\mathbf{k}'_1, \ldots, \mathbf{k}'_n; \mathbf{k}_1, \ldots, \mathbf{k}_n). \tag{5.38}$$

$\mathcal{F} - \mathcal{F}_0$ from (5.35) may be viewed as a sum of diagrams. A full description of the diagrammatic interpretation of the formalism is provided in [60].

5.2.2 Integral Equation

In this section, an integral equation satisfied by the single particle pseudo-energy $\epsilon(\mathbf{k})$, defined in terms of the physical filling fraction

$$f(\mathbf{k}) = \frac{1}{e^{\beta\epsilon(\mathbf{k})} - s}, \tag{5.39}$$

is derived. The density can be expressed in terms of the filling fraction by

$$n = \int \frac{d^d\mathbf{k}}{(2\pi)^d} f(\mathbf{k}). \tag{5.40}$$

The pseudo-energy represents a single particle's energy in the presence of interactions with the rest of the gas, that takes into account multiple scatterings. Differentiating (5.35) with respect to μ gives

$$f(\mathbf{k}) = f_0(\mathbf{k}) + f_0(\mathbf{k})(s f_0(\mathbf{k}) + 1) \sum_{N=1}^{\infty} \frac{1}{N!} \int \left[\prod_{i=1}^{N} d\mathbf{k}_i \, f_0(\mathbf{k}_i) \right] w_{N+1}(\mathbf{k}, \mathbf{k}_1, \ldots \mathbf{k}_N). \tag{5.41}$$

In the diagrammatic description $\widetilde{f}(\mathbf{k}) = e^{\beta(\epsilon(\mathbf{k}) - \omega_{\mathbf{k}} + \mu)} f(\mathbf{k})$ plays the role of the full propagator, and satisfies an analog of the Dyson equation which may be written

$$\widetilde{f}(\mathbf{k}) - f_0(\mathbf{k}) = -\beta \widetilde{f}(\mathbf{k})(1 + s f_0(\mathbf{k})) \frac{\delta F_1}{\delta f(\mathbf{k})}. \tag{5.42}$$

Here, F_1 is a functional related to the physical corrections to $\mathcal{F} - \mathcal{F}_0$ by replacing f_0 with $\widetilde{f}$.

At low density and high temperatures two body interactions dominate. The two-body approximation is enforced in the formalism by including only the four-vertex $G_2(\mathbf{k}, \mathbf{k}') \equiv \mathcal{V}_2(\mathbf{k}', \mathbf{k})$ and considering only "foam diagrams" (diagrams of all orders in the $\mathcal{F} - \mathcal{F}_0$ expansion with the smallest possible number of vertices). Excluding higher order interactions, (5.42) becomes

$$\widetilde{f}(\mathbf{k}) - f_0(\mathbf{k}) = \widetilde{f}(\mathbf{k}) \left(s\beta f_0(\mathbf{k}) \int d\mathbf{k}' G_2(\mathbf{k}, \mathbf{k}') \widetilde{f}(\mathbf{k}') \right), \tag{5.43}$$

or equivalently,

$$\epsilon(\mathbf{k}) = \omega_{\mathbf{k}} - \mu - \frac{1}{\beta} \log \left(1 + \beta \int d\mathbf{k}' G_2(\mathbf{k}, \mathbf{k}') \frac{e^{\beta(\epsilon(\mathbf{k}') - \omega_{\mathbf{k}'} + \mu)}}{e^{\beta\epsilon(\mathbf{k}')} - s} \right). \tag{5.44}$$

In summary, consistent resummation of two-body scattering has led to an integral equation for the pseudo-energy $\epsilon(\mathbf{k})$, whose solution can be used to calculate thermodynamic quantities of interest. Defining

$$y(\mathbf{k}) = e^{-(\varepsilon(\mathbf{k}) - \omega_{\mathbf{k}} + \mu)/T}, \tag{5.45}$$

which becomes unity in the absence of interactions, the integral equation can be written

$$y(\mathbf{k}) = 1 + \beta \int \frac{d^d\mathbf{k}'}{(2\pi)^d} G_2(\mathbf{k}, \mathbf{k}') \frac{z}{e^{\beta\omega_{\mathbf{k}'}} - szy(\mathbf{k}')} \tag{5.46}$$

5.2.3 Kernel in Two and Three Dimensions

The kernel $G_2(\mathbf{k}, \mathbf{k}')$ is based on the logarithm of the two-body S-matrix at zero temperature. To be exact, it's the connected part of the diagonal matrix element

of Im $\log \widehat{S}(E)$. For the non-relativistic theories we will consider, the two body S-matrix can be calculated exactly, i.e. to all orders in the coupling. Therefore although contributions from many-body ($n > 2$) interactions are difficult to calculate, and thus not considered, some non-perturbative aspects are included within this framework. In two dimensions, the two-body S-matrix and kernel are given by

$$S(|\mathbf{k}-\mathbf{k}'|) = \frac{4\pi/mg + \log(2\Lambda/|\mathbf{k}-\mathbf{k}'|) - i\pi/2}{4\pi/mg + \log(2\Lambda/|\mathbf{k}-\mathbf{k}'|) + i\pi/2} \tag{5.47}$$

$$= \frac{\log(2\Lambda_*/|\mathbf{k}-\mathbf{k}'|) - i\pi/2}{\log(2\Lambda_*/|\mathbf{k}-\mathbf{k}'|) + i\pi/2}, \tag{5.48}$$

and

$$G(\mathbf{k}-\mathbf{k}') = -\sigma\frac{4i}{m}\log S(\mathbf{k}-\mathbf{k}')$$

$$= \frac{8}{m}\text{arccot}\left[\frac{2}{\pi}\log\left(a_s|\mathbf{k}-\mathbf{k}'|/2\right)\right]. \tag{5.49}$$

Here, $\sigma = 1$ for bosons and $1/2$ for fermions, and Λ_* is a UV cutoff. In the following chapter, for convenience the notation $G_\pm$ will be used to distinguish between the bosonic ($G+ = G$) and fermionic ($G_- = G/2$) kernels. Note also the generic $\mathbf{k}, \mathbf{k}'$ dependence has been replaced with $\mathbf{k} - \mathbf{k}'$, which is required by rotational invariance. In three dimensions, the two-body S-matrix and kernel become

$$S_{\text{matrix}}(|\mathbf{k}-\mathbf{k}'|) = \frac{2/a_s - i|\mathbf{k}-\mathbf{k}'|}{2/a_s + i|\mathbf{k}-\mathbf{k}'|}. \tag{5.50}$$

and

$$G(\mathbf{k},\mathbf{k}') = -\frac{16\pi\sigma}{m|\mathbf{k}-\mathbf{k}'|}\arctan\left(\frac{a_s.|\mathbf{k}-\mathbf{k}'|}{2}\right). \tag{5.51}$$

CHAPTER 6

TWO DIMENSIONAL BOSE AND FERMI GASES BEYOND WEAK COUPLING

This chapter was adapted from"Two-dimensional Bose and Fermi gases beyond weak coupling" by Guilherme França, André LeClair, and Joshua Squires, published in J. Stat. Mech. 7 073103 (2017).

6.1 Abstract

Using a formalism based on the two-body S-matrix we study two-dimensional Bose and Fermi gases with both attractive and repulsive interactions. Approximate analytic expressions, valid at weak coupling and beyond, are developed and applied to the Berezinskii-Kosterlitz-Thouless (BKT) transition. We successfully recover the correct logarithmic functional form of the critical chemical potential and density for the Bose gas. For fermions, the BKT critical temperature is calculated in BCS and BEC regimes through consideration of Tan's contact.

6.2 Introduction

The absence of conventional long range order in two-dimensional systems is well known to be a consequence of low energy fluctuations [63, 64]. Phase transitions at finite temperature in 2d are instead marked by a topolgical order as described by Berezinskii, Kosterlitz, and Thouless (BKT) [65, 66]. Quasi long range order is exhibited below the BKT transition temperature, where spatial

correlations of the order parameter decay algebraically rather than exponentially. The destruction of this ordering, due to the unpairing of vortices, has been observed experimentally using atomic gases [67].

Ultracold atomic gases are well suited for the exploration of BKT theory, as they can be effectively constrained to 2d [68–75] using an optical lattice or harmonic trap, and because their interactions are highly tunable through the use of Feshbach resonances. Theoretical studies of BKT physics in two dimensions using quantum gases are numerous. Fermi gases have been used to explore Cooper pairing and superconductivity in 2d [76, 77], as well as the normal Fermi liquid phase [78–80]. The superfluid transition and critical point of the 2d Fermi gas have also been treated [81–83]. Bose Einstein condensation in 2d, particularly at weak coupling, has been widely studied [84, 85]. The critical point of the 2d Bose gas has been obtained in this limit through classical ϕ^4 theory [86–88], and with a renormalization group (RG) approach [89]. An RG analysis has also been used to examine the ground state of the Bose gas in arbitrary dimension [90].

In this paper we apply the formalism developed in [60] to study two-dimensional Bose and Fermi gases with both attractive and repulsive interactions. Inspired by the Yang-Yang equations of the Thermodynamical Bethe Ansatz [61], the formalism is centered around an integral equation with a kernel based on the logarithm of the two-body S-matrix. The main advantage of our approach is that the two-dimensional integral equation admits approximate analytic solutions in terms of the Lambert W function. Furthermore these approximate solutions remain useful beyond weak coupling, and as detailed in section III, they can be used to calculate any thermodynamic quantity of inter-

est. In this work we primarily use this correspondence to calculate the critical points of the BKT transition for both Bose and Fermi gases. Below we summarize our chosen models, couplings, and formalism before describing our main results in sections 6.5 and 6.6.

6.3 Physical Couplings, Scaling functions

Both non-relativistic bosons and fermions are treated in this chapter. The Bose gas will be defined by the action

$$S = \int d^2\mathbf{x}\, dt \left(i\phi^\dagger \partial_t \phi - \frac{|\vec{\nabla}\phi|^2}{2m} - \frac{g}{4}(\phi^\dagger\phi)^2 \right). \tag{6.1}$$

with ϕ a complex scalar field. A two component field $\psi_{\uparrow,\downarrow}$ is needed for the Fermi gas, due to fermionic statistics:

$$S = \int d^2\mathbf{x}\, dt \left(\sum_{\alpha=\uparrow,\downarrow} i\psi_\alpha^\dagger \partial_t \psi_\alpha - \frac{|\vec{\nabla}\psi_\alpha|^2}{2m} - \frac{g}{2}\psi_\uparrow^\dagger \psi_\uparrow \psi_\downarrow^\dagger \psi_\downarrow \right). \tag{6.2}$$

In both models, the parameter g characterizes the strength of the quartic interactions, with positive (negative) g describing repulsive (attractive) interactions. The coupling g has a renormalization group (RG) flow, described by the beta function

$$\frac{dg}{d\log\Lambda} = \frac{mg^2}{4\pi}. \tag{6.3}$$

This beta function, with momentum cutoff Λ introduced to regularize ultraviolet divergences, is calculated from the exact 2-body S-matrix [60] and is a signature of BKT phase transitions. The coupling g is marginally irrelevant when positive, maginally relevant when negative, and related the RG invariant physical coupling Λ_* by

$$\Lambda_* = \Lambda\, e^{4\pi/mg}. \tag{6.4}$$

We define the physical scattering length a_s as

$$a_s = \frac{1}{\Lambda_*} = \frac{1}{\Lambda} e^{-4\pi/mg}, \tag{6.5}$$

though in two-dimensions this is merely one possible convention. Another, used in [89], is $a_s = e^{-\gamma_E}/\Lambda_*$, where γ_E is the Euler-Mascheroni constant. In contrast to three dimensions, a negative scattering length is not physically possible. Note quantities are best expressed in terms of the scattering length rather than the coupling g since the latter isn't an RG invariant. At finite temperature and density, it is convenient to define the dimensionless variables:

$$\alpha = \frac{\lambda_T}{a_s}, \quad \widetilde{\mu} = \frac{\mu}{T} \tag{6.6}$$

where $\lambda_T = \sqrt{2\pi/mT}$ is the thermal de Broglie wavelength and μ the chemical potential. Relations between the parameters discussed above, and their strong/weak coupling limits are summarized in Table 6.1.

Table 6.1: The parameter α is defined below in (6.6). The weak coupling limit is obtained with $\alpha \to \infty$ for repulsive interactions and $\alpha \to 0$ for attractive interactions. The strong coupling limit corresponds to finite α in both cases. $\widetilde{g}$, defined in (6.10), is also finite at strong coupling.

	weak coupling			strong coupling		
	g	a_s	α	g	a_s	α
repulsive	0^+	0	∞	$+\infty$	$1/\Lambda^*$	$\mathcal{O}(1)$
attractive	0^-	∞	0^+	$-\infty$	$1/\Lambda^*$	$\mathcal{O}(1)$

In terms of the dimensionless $\widetilde{\mu}$ and α we can define the scaled density

$$\widetilde{n} = n\lambda_T^2 \tag{6.7}$$

and free energy density

$$\mathcal{F} = -\frac{\pi^2}{6} T \lambda_T^{-2}\, c(\widetilde{\mu}, \alpha), \tag{6.8}$$

where the scaling function c is to be defined below. In two dimensions the Fermi wave-vector is $k_F = \sqrt{2\pi n} = \lambda_T^{-1}\sqrt{2\pi\widetilde{n}}$ and the Fermi temperature $T_F = \pi n/m$, which implies $T/T_F = 2/\widetilde{n}$. In units of the Fermi energy, the energy per particle takes the form

$$\frac{E}{N} = \frac{\pi^2}{12}\left(\frac{T}{T_F}\right)^2 c(\widetilde{\mu}, \alpha). \tag{6.9}$$

For comparison with other calculations and experiments, it is also useful to define a physical coupling $\widetilde{g}$ as

$$\widetilde{g} = \frac{8\pi}{|\log(n a_s^2)|} = \frac{8\pi}{|\log(\widetilde{n}/\alpha^2)|} = \frac{4\pi}{\left|\log\left(\frac{k_F a_s}{\sqrt{2\pi}}\right)\right|} \tag{6.10}$$

The above definition is such that at weak coupling $\widetilde{g} \approx g$.

6.4 Integral Equation

Rescaling $\mathbf{k} \to \sqrt{2mT}\,\mathbf{k}$, the $2D$ integral equation (5.46) and scaling functions are given by ($k = |\mathbf{k}|$):

$$\widetilde{n} = 2\int_0^\infty dk\, k \frac{y(k) z}{e^{k^2} - s y(k) z}, \tag{6.11}$$

$$c = -\frac{12}{\pi^2}\int_0^\infty dk\, k \left[s \log\left(1 - s z y(k) e^{-k^2}\right) + \frac{1}{2}\frac{z(y(k)-1)}{e^{k^2} - s z y(k)}\right] \tag{6.12}$$

and

$$y(k) = 1 + \frac{m}{2\pi^2}\int d^2\mathbf{k}'\, G(\mathbf{k} - \mathbf{k}')\, \frac{z}{e^{\mathbf{k}'^2} - s z y(\mathbf{k}')}, \tag{6.13}$$

where the kernel is

$$G(\mathbf{k} - \mathbf{k}') = \frac{8}{m}\operatorname{arccot}\left[\frac{2}{\pi}\log\left(\frac{\sqrt{\pi}|\mathbf{k} - \mathbf{k}'|}{\alpha}\right)\right]. \tag{6.14}$$

Note $c = 1$ for a free boson at zero chemical potential.

The free theory limit corresponds to *both* $\alpha \to \infty$ ($g \to 0^+$) and $\alpha \to 0$ ($g \to 0^-$). It will be convenient to write the integral equation (6.13) as

$$y(k) = 1 + \int_0^\infty dk'\, k'\, H(k,k')\, \frac{z}{e^{k'^2} - sz\, y(k')}, \tag{6.15}$$

where

$$H(k,k') = \frac{4}{\pi^2} \int_0^{2\pi} d\theta\, \mathrm{arccot}\left[\frac{1}{\pi} \log\left(\frac{\pi(k^2 + k'^2 - 2kk'\cos\theta)}{\alpha^2}\right)\right]. \tag{6.16}$$

In theory the integral equation (5.46) is valid for all interaction strengths and temperatures, including $T = 0$. However, as our formalism only includes a pseudo-energy for single particles, the integral equation is only solvable in the absence of bound states, limiting its applicability at zero temperature. Low temperature results are accurate only if the gas remains in the normal phase. As a concrete example, we calculated Tan's contact for the attractive Fermi gas in the normal phase for temperatures as low as $T/T_F = 0.001$ (see Figure 5 and the discussion in Section V).

We also expect solutions of the integral equation to become less reliable if the coupling is large enough to result in appreciable many-body interactions, as only two-body effects are considered. If we take the coupling constant $\widetilde{g}$ as a measure of strong versus weak coupling, then because of the logarithm, $\widetilde{g} \approx 1$ requires (for repulsive interactions) a very large α, on the order of 10^6 (see below). For such large α we can disregard the momentum dependence of the kernel. Thus, henceforth

$$H \approx \frac{8}{\pi}\mathrm{arccot}\left[-\frac{2}{\pi}\log\alpha\right] \approx -\frac{4}{\log\alpha} \to 0^{\pm}. \tag{6.17}$$

is a constant that differs in sign depending on whether the interaction is attractive or repulsive. Keeping the momentum dependence of the kernel does not

significantly alter the results presented in the following sections.

6.5 Bosons

Since the kernel is a constant, y is also a constant. The integral over k can be performed and the integral equation (6.15) becomes the transcendental equation

$$y(y-1) = \frac{2\log(1-yz)}{\log\alpha}. \tag{6.18}$$

The equation of state is then

$$\widetilde{n} = -\log(1-yz). \tag{6.19}$$

Given the solution to (6.18) for y as a function of z, the above equation determines how the density depends on the chemical potential and temperature.

For very weak coupling, $y \approx 1$, and (6.18) can be approximated as

$$y = 1 + \frac{2\log(1-yz)}{\log\alpha} \tag{6.20}$$

which can be expressed in terms of the Lambert W-function. The W function by definition satisfies

$$W(u)e^{W(u)} = u. \tag{6.21}$$

One then has the following solution of the transcendental equation:

$$y = 1 - a\log(1-y/b) \quad \Rightarrow \quad y = b + aW\left(-\frac{b}{a}e^{(1-b)/a}\right). \tag{6.22}$$

Thus

$$y = \frac{1}{z} - \frac{2}{\log\alpha}\,W\left(\frac{\log\alpha}{2z}e^{(1/z-1)\log\sqrt{\alpha}}\right). \tag{6.23}$$

For real u, $W(u)$ has two real valued branches, as shown in Figure 6.1 below. If $u \geq 0$ there is only the principal branch denoted by $W_0(u)$, and if $-1/e \leq u <$

0 we have the secondary branch $W_{-1}(u)$ in addition. The two branches only coincide when $u = -1/e$, where $W_0(-1/e) = W_{-1}(-1/e) = -1$.

6.5.1 Repulsive Bosons

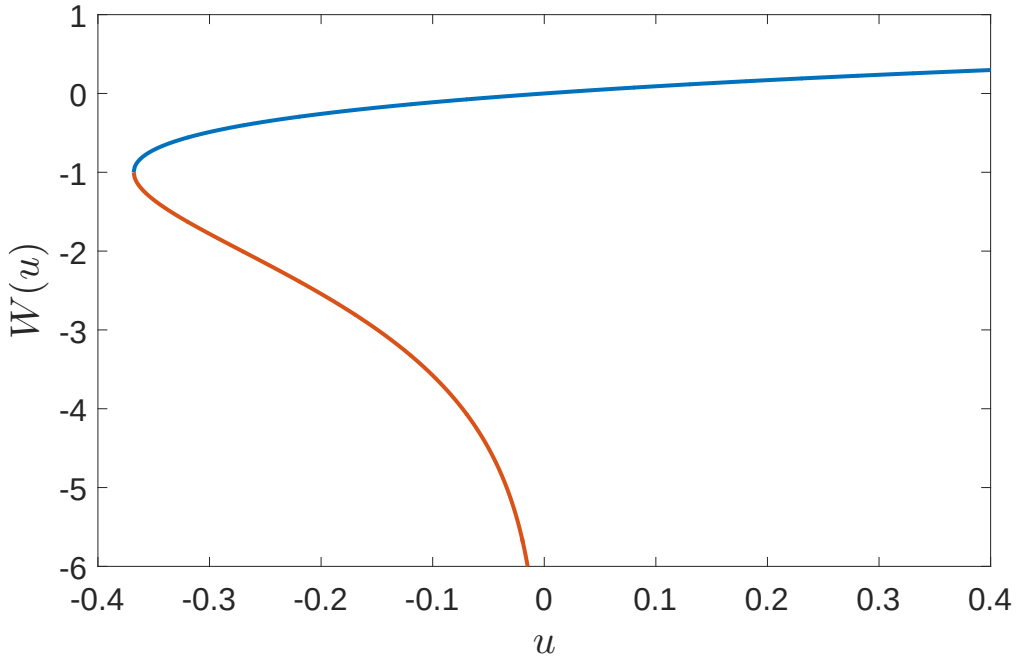

Figure 6.1: (color online) The two real branches of the Lambert W-function. The top blue part is the principal branch $W_0(u)$, whereas the lower orange part is $W_{-1}(u)$. The branches meet at $u = -1/e$.

For repulsive bosons the argument of W is positive and one should chose the principle branch, henceforth simply denoted as W. In order to compare with other theories and experiments, we wish to plot $\widetilde{n}$ as a function of $\widetilde{\mu}$ for various $\widetilde{g}$. Though $\widetilde{g}$ depends on chemical potential through $\widetilde{n}$, the primary variation of $\widetilde{g}$ comes from α. Therefore we plot $\widetilde{n}$ as a function $\widetilde{\mu}$ for a fixed α. Along such a curve $\widetilde{g}$ is nearly constant, and we can meaningfully associate each fixed-α curve with value $\widetilde{g}_0 = \widetilde{g}(\widetilde{\mu} = 0^-, \alpha)$.

Our results, which use the approximation (6.23), compare reasonably well to experimental data [73], as shown in Figure 6.2 for $\widetilde{g}_0$ ranging between 0.05 and 0.66. This requires a very large range of α due to the logarithm in the definition of $\widetilde{g}$. For instance $\widetilde{g}_0 = 0.05$ corresponds to $\alpha \approx 10^{110}$ whereas $\widetilde{g}_0 = 0.66$ coincides with $\alpha \approx 10^8$. As $\widetilde{\mu} \to -\infty$ the behavior is of a free gas $\widetilde{n} \approx -\log(1-z)$. For finite $\widetilde{\mu}$, our predictions increasingly underestimate the experimental results as $\widetilde{g}$ increases.

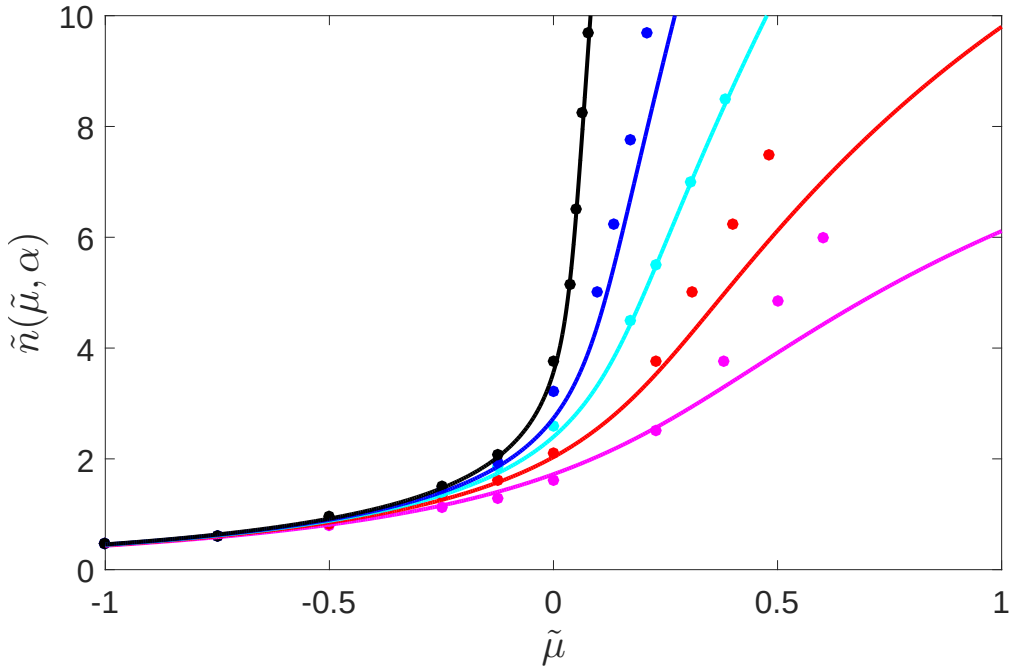

Figure 6.2: (color online) The scaled density $\widetilde{n}$ as a function of the scaled chemical potential $\widetilde{\mu}$ for various $\widetilde{g}_0$. From top to bottom, the solid colored lines correspond to $\widetilde{g}_0 = 0.05, 0.15, 0.24, 0.41, 0.66$ respectively. The colored points, which have the same ordering from top to bottom, are experimental data estimated from [73].

The bose gas undergoes a phase transition to a superfluid at some critical density $\widetilde{n}_c$. For a two dimensional interacting gas, as in the 3d non-interacting case, at the critical point the scaled density $\widetilde{n}$ develops an imaginary part. This occurs for $y \approx 1/z$ where the RHS of (6.18) has a branch cut. In order to study this

critical point analytically using known functions, we consider the approximate solution of (6.18) given by (6.23). Taking $y = 1/z_c$ implies

$$W\left(\frac{\log\sqrt{\alpha}}{z_c}e^{(1/z_c-1)\log\sqrt{\alpha}}\right) = 0. \tag{6.24}$$

Since the argument of W is arbitrarily large and positive for weakly coupled repulsive interactions, the approximation $W_0(u) \approx \log u$ can be used, giving

$$\log\left(\frac{\log\sqrt{\alpha}}{z_c}\right) + \log\sqrt{\alpha}\left(\frac{1}{z_c} - 1\right) = 0. \tag{6.25}$$

The solution z_c to the above equation can again be expressed in terms of the Lambert W function

$$z_c = \frac{\log\sqrt{\alpha}}{W\left(\sqrt{\alpha}\right)}. \tag{6.26}$$

Noting to second order, for large u, $W_0(u) \approx \log u - \log\log u$, one can use the above equation and (6.19) to compute the critical chemical potential and density:

$$\begin{aligned} \widetilde{\mu}_c &\approx \frac{\log\log\sqrt{\alpha}}{\log\sqrt{\alpha}} \\ \widetilde{n}_c &\approx \log\log\sqrt{\alpha}. \end{aligned} \tag{6.27}$$

We now compare (6.27) with known results and experiments. From the scattering length definition given by (6.5) we see $\log\sqrt{\alpha} \approx 2\pi/mg$. This leads to

$$\begin{aligned} \widetilde{\mu}_c &\approx \frac{mg}{2\pi}\log\left(\frac{2\xi_\mu}{mg}\right) \\ \widetilde{n}_c &\approx \log\left(\frac{2\xi}{mg}\right) \end{aligned} \tag{6.28}$$

with $\xi = \xi_\mu = \pi$. The above functional dependence on g agrees with [73, 87] except for the constants inside the logarithm, where it was found that $\xi_\mu \approx 13.2$ and $\xi \approx 380$. The simplest explanation for this discrepancy is that we are neglecting intrinsic 3-body interactions and higher; however it is hard to see how these would lead to the same functional form as in (6.28). Though we found

no numerical evidence this was the case, it's more likely a consequence of neglected momentum dependence in the integral equation's kernel, in the large α limit.

6.5.2 Attractive Bosons

For attractive interactions in the weak coupling limit, (6.17) is positive, and $\alpha \to 0^+$. In this regime there exists only very small regions of parameter space where there is a solution to (6.18). This instability is reflected in the equation of state, as shown in Figure 6.3.

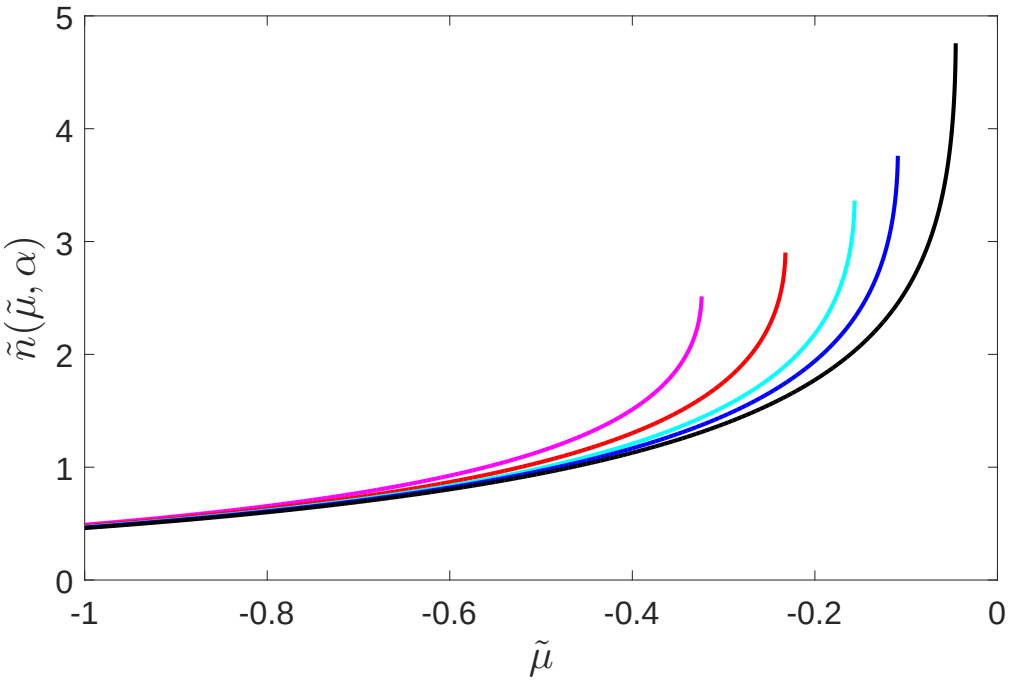

Figure 6.3: (color online) The scaled density $\widetilde{n}$ as a function of the scaled chemical potential $\widetilde{\mu}$ for various $\widetilde{g}_0$. From bottom to top, the solid colored lines correspond to $\widetilde{g}_0 = 0.05, 0.15, 0.24, 0.41$, and 0.66 respectively. Each $\widetilde{n}$ curve terminates at a specific chemical potential, after which no solution to (6.20) exists for larger values of $\widetilde{\mu}$.

At the critical point, $\widetilde{n}$ again becomes complex. The main difference in repeating the analysis of the previous section is now, for attractive interactions, the argument of W in (6.23) is arbitrarily small and negative and one must choose the secondary branch rather than the principle branch. After setting $y = 1/z_c$ we find

$$W_{-1}\left(\frac{\log\sqrt{\alpha}}{z_c}e^{(1/z_c-1)\log\sqrt{\alpha}}\right) = 0. \tag{6.29}$$

Utilizing the asymptotic expansion of the secondary branch $W_{-1}(-\frac{1}{u}) \approx -\log u - \log\log u$ gives

$$\log\left(\frac{|\log\sqrt{\alpha}|}{z_c}\right) - \left(\frac{1}{z_c} - 1\right)|\log\sqrt{\alpha}| = 0, \tag{6.30}$$

from which it follows

$$z_c = \frac{\log\sqrt{\alpha}}{W_{-1}\left(-\sqrt{\alpha}\right)}. \tag{6.31}$$

As in the repulsive case the critical density can be computed by inserting the above expression into (6.19). Using the asymptotic expansion of W_{-1} a second time results in

$$\begin{aligned} \widetilde{\mu}_c &\approx \frac{-\log|\log\sqrt{\alpha}|}{|\log\sqrt{\alpha}|} \\ \widetilde{n}_c &\approx \log|\log\sqrt{\alpha}|. \end{aligned} \tag{6.32}$$

6.6 Fermions

In the fermionic case the kernel $G_- = G_+/2$. The analogs of (6.18) and (6.19) for fermions at weak coupling are then

$$y(y-1) = -\frac{\log(1+yz)}{\log\alpha} \tag{6.33}$$

and

$$\widetilde{n} = \log(1+yz). \tag{6.34}$$

Mirroring our treatment of bosons, we find approximate solutions for y in the attractive ($\alpha \to 0$)

$$y = -\frac{1}{z} + \frac{1}{\log \alpha} W_{-1}\left(\frac{\log \alpha}{z} e^{(1/z-1)\log \sqrt{\alpha}}\right) \tag{6.35}$$

and repulsive ($\alpha \to \infty$)

$$y = -\frac{1}{z} + \frac{1}{\log \alpha} W_{0}\left(\frac{\log \alpha}{z} e^{(1/z-1)\log \sqrt{\alpha}}\right) \tag{6.36}$$

regimes in terms of the Lambert function.

Attractive Fermions

A useful quantity to calculate is the contact parameter, C, which is set by the antiparallel spin pair correlation function $g_{\uparrow\downarrow}(r)$ at short distances ($r \ll 1/k_F$). Tan's relations provide a connection between C, and thus the short range interactions of the system, and macroscopic quantities such as the pressure of the gas [91]. One can define a dimensionless contact in terms of a derivative of the energy with respect to the interaction parameter

$$C' = C/k_F^2 = \pi \frac{d\frac{E}{E_F}}{d\log(k_F a_s)}. \tag{6.37}$$

Note since $T/T_F = 2/\widetilde{n}$ this derivative can be calculated explicitly with our formalism. Using the approximations given by (6.34) and (6.35):

$$C' = \frac{2\pi\left[\log \alpha^{(1+1/z)} - W_{-1}(v)\right]}{\log\left(\frac{zW_{-1}(v)}{\log \alpha}\right)^2\left[\log \alpha\,(W_{-1}(v)+1)\right]} \tag{6.38}$$

where $v = \alpha^{(1+1/z)} \log \alpha^{1/z}$.

For the 2d attractive fermi gas, the contact was recently measured experimentally at $T/T_F = 0.27$ [69]. In Figure 6.4 below we compare C' as calculated

with our approximations to experiment, as well as to a $T = 0$ Fermi liquid theory result [79]. Our C' compares favorably with the experimental measurements until diverging abruptly as $\alpha \to 1$.

Since C' is proportional to the number of atomic pairs, which follows from the relation between the contact and $g_{\uparrow\downarrow}(r)$ [92], a divergence in C' may signal a phase transition. Identifying the critical point of the BKT transition with a diverging C' yields the phase diagram shown in Figure 6.5.

In the 2d BCS limit $\log(k_F a_s) \gg 1$, the critical temperature of the superfluid transition has been calculated using mean field theory [81, 83]

$$\frac{T_c}{T_F} = \frac{2e^{\gamma-1}}{\pi k_F a_s} = \frac{c_{MF}}{k_F a_s}. \tag{6.39}$$

Fitting our phase boundary to a second order model

$$\frac{T_c}{T_F} = \frac{c_1}{k_F a_s} + \frac{c_2}{(k_F a_s)^2} \tag{6.40}$$

gives $c_1 = 0.865 = 2.08 c_{MF}$ and $c_2 = 6.07$. Our results begin to significantly depart from those of mean field theory around $\log(k_F a_s) = 3$ which corresponds to $\widetilde{g} \approx 6$. This is well into the regime of strong interactions, so it's unsurprising we deviate from a mean field theory prediction.

Before considering repulsive interactions, we note that Monte Carlo simulations have been used to calculate both the contact and energy per particle at $T = 0$ on both sides of the BEC-BCS crossover. For example, in [93] for $\log(k_F a_s) = 5.18$, the normalized energy per particle is reported as $E/N = 0.821$. To compare to this data we calculate E/N using (6.9) at low temperature. For convenience we take $T/T_F = 0.01$, which fixes the density $\widetilde{n}$. Since the interaction parameter $\log(k_F a_s)$ only depends on $\widetilde{n}(\widetilde{\mu}, \alpha)$ and α, setting $\log(k_F a_s) = 5.18$ uniquely determines α. With α and $\widetilde{n}(\widetilde{\mu}, \alpha)$ known, a corresponding $\widetilde{\mu}$ can be

found numerically, and used to calculate the energy per particle. Utilizing the approximations (6.34) and (6.35) throughout, we obtain $E/N = 0.995$. Although E/N is provided for a range of interaction strengths, most of the data presented in [93] occurs in the presence of a bound state, which our formalism is not suited to handle.

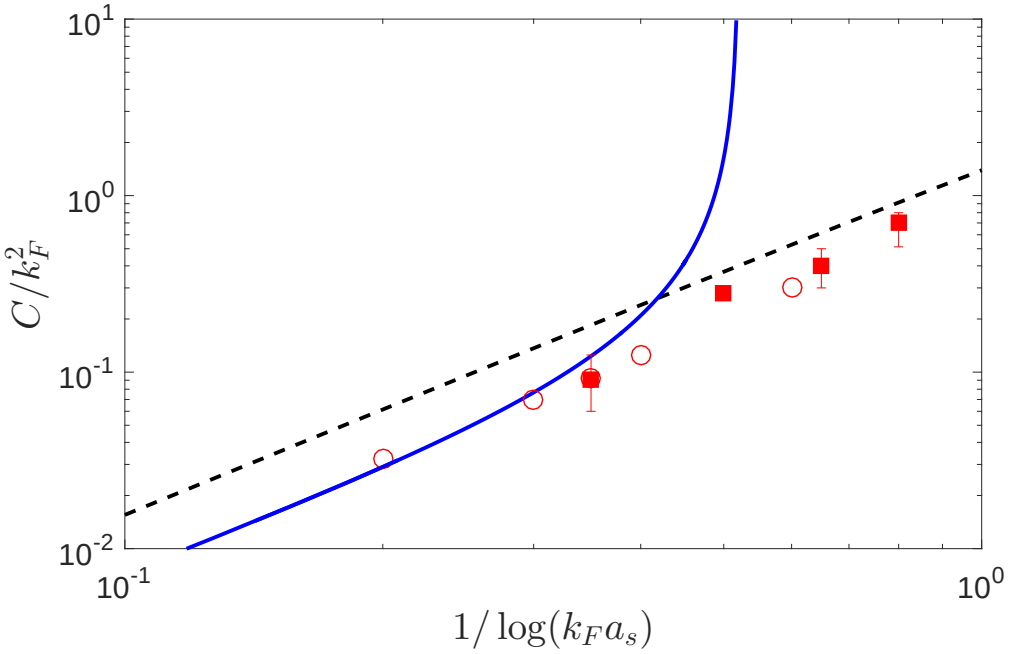

Figure 6.4: Dimensionless contact C' vs. $1/\log(k_F a_s)$ at $T/T_F = 0.27$. The red squares and error bars are experimental data estimated from [69]. The red open circles are from the same group, but calculated from a model which accounts for their specific experimental configuration. The dashed black line is a 2nd order $T = 0$ homogenous Fermi liquid theory result, and the solid blue curve uses the Lambert approximation (6.35) to calculate C'.

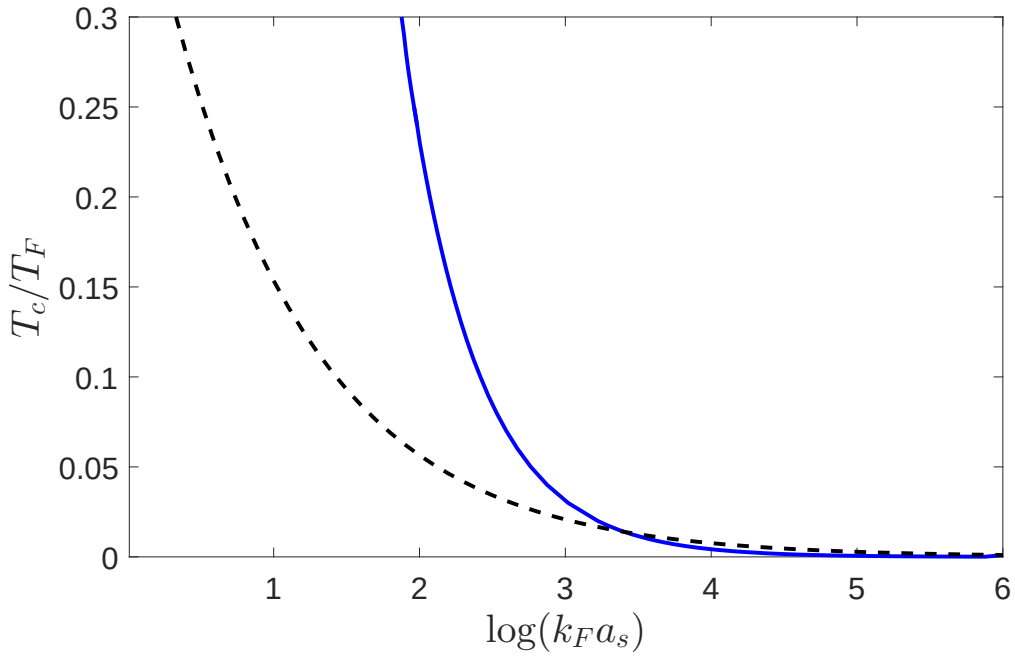

Figure 6.5: T_c/T_F as a function of the interaction parameter $\log(k_F a_s)$. The dashed black line is the mean field theory result (6.39) and the blue is obtained through the method described in the text. Up to $\log(k_F a_s) \approx 3$ our T_c/T_F closely matches the mean field theory prediction.

Repulsive Fermions

While we don't have experimental data to compare to on the BEC side, the contact is equivalent to (6.38) with $W(v)$ in place of $W_{-1}(v)$. As in the attractive case, a sharp increase in C' is observed (see Figure 6) which we take as indication of a phase transition. In the BEC limit of $\log(k_F a_s) \ll -1$, the predicted critical temperature is

$$\frac{T_c}{T_F} = \frac{1}{2}\left(\log\left(\frac{\xi}{2\pi}\log\left(\frac{2\sqrt{\pi}}{k_F a_s}\right)\right)\right)^{-1} \tag{6.41}$$

with $\xi = 380$ [81, 87]. We instead find T_c/T_F to be more consistent with the value $\xi = \pi$ from (6.28), as shown in Figure 7. The return of this discrepancy is expected based on the analysis in section IV, as in this limit the system behaves

as a weak Bose gas.

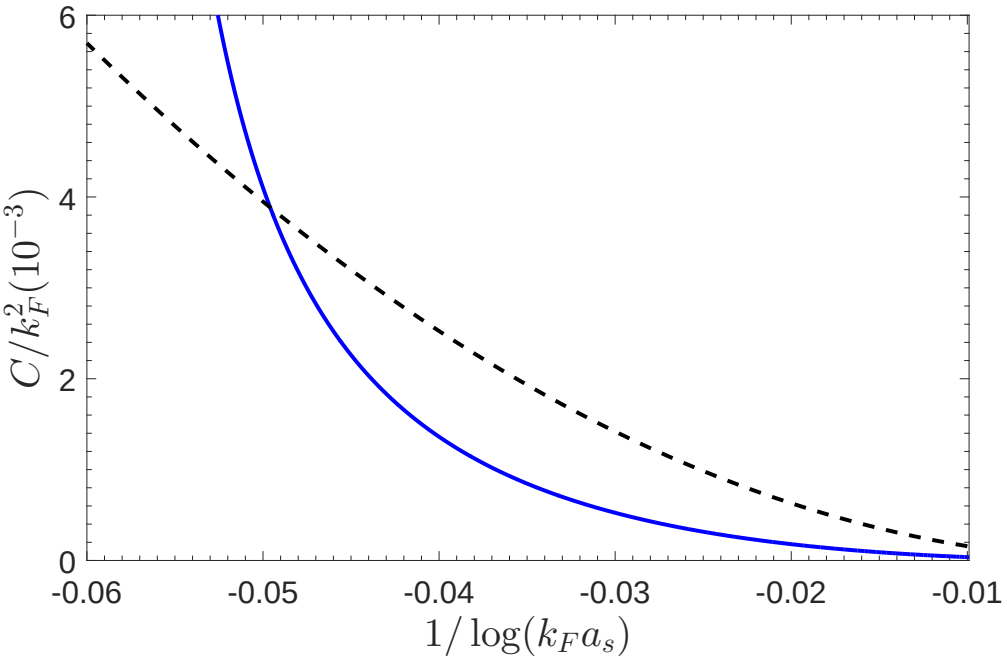

Figure 6.6: Dimensionless contact C' vs. $1/\log(k_F a_s)$ at $T/T_F = 0.1$. The dashed black line is the 2nd order $T = 0$ homogenous Fermi liquid theory prediction, and the blue uses the Lambert approximation (6.36) to calculate C'.

6.7 Conclusion

The S-matrix-based formalism developed in [60] has been applied to two-dimensional Bose and Fermi gases. The main obstacle in utilizing this method to extract measurable thermodynamic functions is solving an integral equation whose kernel takes a particularly complicated form in two dimensions. This makes exact solution of the integral equation an impossible task, and numerical treatments computationally intensive. Fortunately, in the limits $\alpha \ll 1$ and $\alpha \gg 1$ the momentum dependence of the kernel becomes irrelevant, and ele-

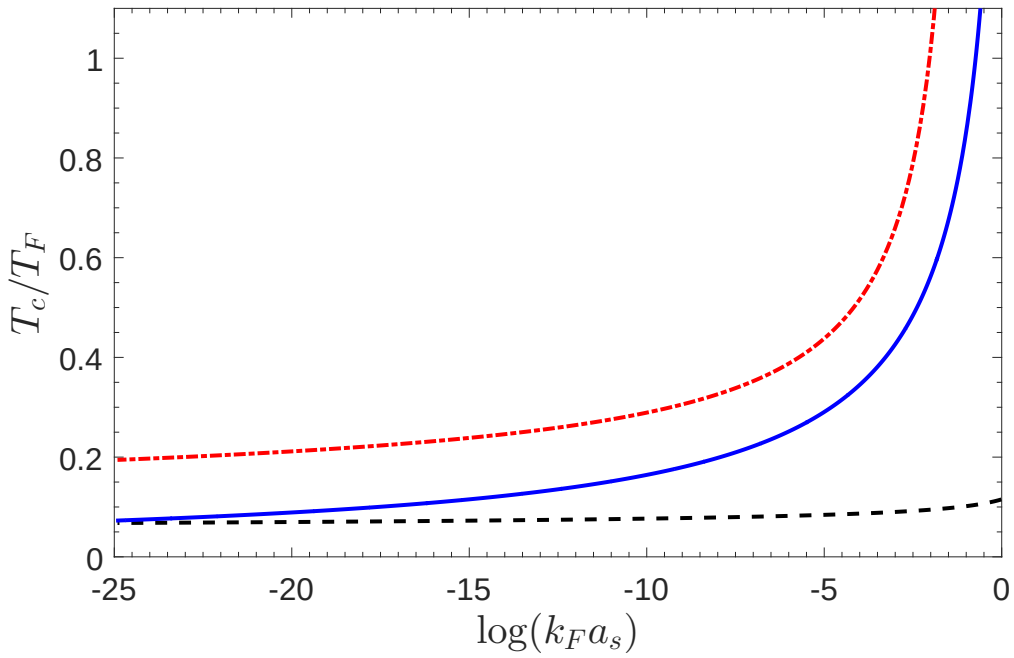

Figure 6.7: T_c/T_F as a function of the interaction parameter $\log(k_F a_s)$.The dashed black line is the mean field theory result given by (6.41). The red dash-dot line uses the same model except with our previously calculated $\xi = \pi$ instead of $\xi = 380$. The solid blue curve is determined by the behavior of C', as described in the text.

gant solutions of the integral equation can be written in terms of the Lambert W function.

While we initially anticipated these approximate solutions would only remain valid in the limit of extremely weak coupling, it turns out $\widetilde{g}$ is a more appropriate measure of coupling strength than α, due to its explicit density dependence. For strong coupling, $\widetilde{g} \gtrsim 1$ which is reached in the $\alpha \ll 1$ or $\alpha \gg 1$ limit depending on the sign of the interaction.

For bosons, we were able to recover the well-established logarithmic functional form of the critical density and chemical potential with the Lambert approximation, up to a constant obtained with Monte Carlo methods [87]. For

fermions our approximations result in an explicit expression for the contact parameter, from which the critical temperature of the BKT transition has been deduced. This novel approach agrees with known weak coupling mean field theory calculations [81, 83].

As two-dimensional gases are poised to garner even greater attention in the near future, we hope our explicit analytic results are found to be useful.

6.8 Appendix

6.8.1 Virial Expansion

We thank John Stout for collaboration in the early stages of this work which led to this Appendix. The following results were not used in the main body of the chapter, but are presented in the hope that they may have future utility.

The virial expansion is formally defined as a series expansion of $\mathcal{F}$ in powers of the fugacity z:

$$\begin{aligned} -\mathcal{F}\lambda_T^2/T &= \sum_{n=1}^{\infty} b_n z^n \\ n\lambda_T^2 &= \sum_{n=1}^{\infty} n\, b_n z^n \end{aligned} \tag{6.42}$$

where the second relation follows from $n = -\partial\mathcal{F}/\partial\mu$. In the free theory, the series expansion of the poly-logarithm $s\mathrm{Li}_2(sz)$ gives $b_n = s^{n+1}/n^2$.

As explained in [94] our formalism gives the corrections to b_2 and b_3:

$$\begin{aligned} b_2 = \frac{s}{4} + \frac{\lambda_T^2}{2T}\int \frac{d^2\mathbf{k}}{(2\pi)^2}\frac{d^2\mathbf{k}'}{(2\pi)^2} \\ \times\left(e^{-\omega_{\mathbf{k}}/T}e^{-\omega_{\mathbf{k}'}/T}G_{\pm}(\mathbf{k}-\mathbf{k}')\right), \end{aligned} \tag{6.43}$$

$$\begin{aligned} b_3 = \frac{1}{9} + \frac{s\lambda_T^2}{2T}\int \frac{d^2\mathbf{k}}{(2\pi)^2}\frac{d^2\mathbf{k}'}{(2\pi)^2} e^{-\omega_{\mathbf{k}}/T}e^{-\omega'_{\mathbf{k}}/T}G_{\pm}(\mathbf{k}-\mathbf{k}') \\ \times\left(e^{-\omega_{\mathbf{k}}/T} + e^{-\omega_{\mathbf{k}'}/T}\right). \end{aligned}$$

The second virial coefficient b_2 is exact, whereas b_3 is not since it does not contain the intrinsic 3-body physics. Hence we only consider b_2. Rescaling $\mathbf{k} \to$

$\sqrt{2mT}\,\mathbf{k}$, and making the change of variables $\mathbf{k}_1 = \mathbf{k} - \mathbf{k}'$, $\mathbf{k}_2 = \mathbf{k} + \mathbf{k}'$, the integral factorizes and the integral over $\mathbf{k}_2$ is simply a gaussian. The result is

$$b_2 = \frac{s}{4} + \frac{2\sigma}{\pi} \int_0^\infty dk\, k\, e^{\frac{-k^2}{2}} \operatorname{arccot}\left[\frac{2}{\pi} \log\left(\frac{\sqrt{\pi}\,k}{\alpha}\right)\right] \tag{6.44}$$

where $k = |\mathbf{k}|$ and $\sigma = 1$ for bosons and $1/2$ for fermions. To a good approximation,

$$\begin{aligned} b_2(\alpha) \approx \frac{s}{4} + \sigma\Bigg(&-1 + 2e^{-\alpha^2/2\pi} + \dots \\ &\dots - \frac{2}{\pi} \arctan\left[\frac{1}{\pi} \log\left(\frac{2\pi \log 2}{\alpha^2}\right)\right]\Bigg). \end{aligned} \tag{6.45}$$

Plots of b_2 are shown in Figure 6.8. Note that it changes sign at $\alpha \approx 2.65$. As expected, the free theory value $b_2 = s/4$ is approached in both limits $\alpha \to 0$ and $\alpha \to \infty$.

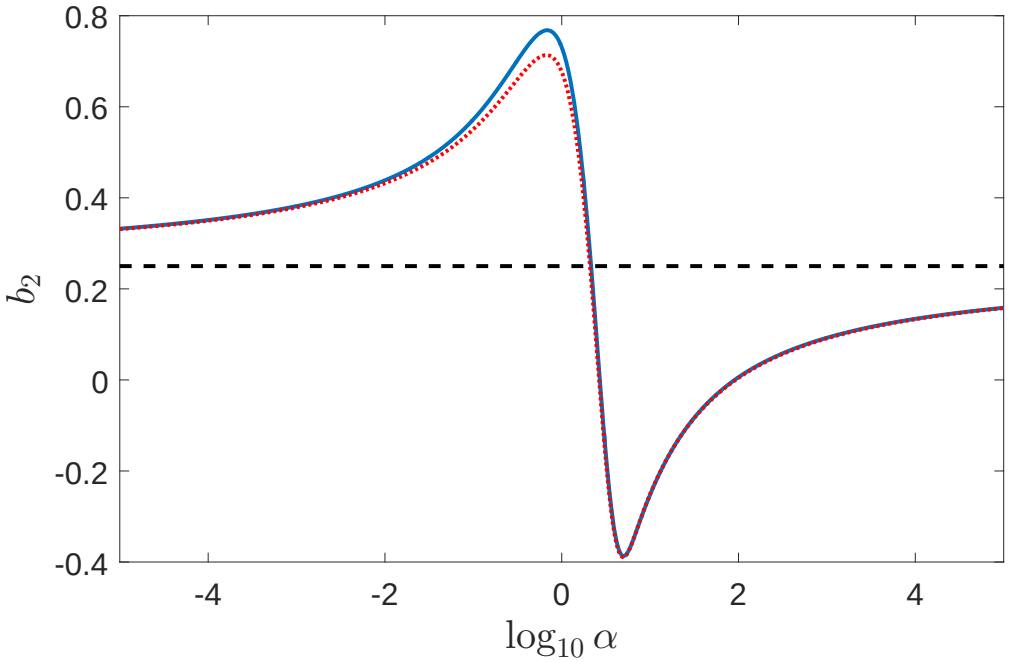

Figure 6.8: The second virial coefficient b_2 as a function of α for bosons (solid blue). The dotted red curve is the approximation (6.45). The non-interacting value $b_2 = 1/4$ (dashed horizontal line) is approached as $\alpha \to 0$ and $\alpha \to \infty$.

CHAPTER 7

METASTABILITY OF BOSE AND FERMI GASES ON THE UPPER BRANCH

This chapter was adapted from "Metastability of Bose and Fermi gases on the upper branch" by André LeClair, Itzhak Roditi, and Joshua Squires, published in Phys. Rev. A 94, 063608 (2016).

7.1 Abstract

We study three dimensional Bose and Fermi gases in the upper branch, a phase defined by the absence of bound states in the repulsive interaction regime, within an approximation that considers only two-body interactions. Employing a formalism based on the S-matrix, we derive useful analytic expressions that hold on the upper branch in the weak coupling limit. We determine upper branch phase diagrams for both bosons and fermions with techniques valid for arbitrary positive scattering length.

7.2 Introduction

It is well known that the two-body interactions of a non-relativistic quantum gas in 3 spatial dimensions can be fully described by the s-wave scattering length, a_s. For $a_s > 0$, interactions are repulsive and the S-matrix has a pole corresponding to a bound state or "molecule". Thus if one starts with a sample consisting of only the fundamental particles, they will start to combine into

molecules, which complicates the thermodynamics. The "upper branch" corresponds to $a_s > 0$ with the assumption that the molecules are absent. This situation has been realized in experiments [95–100] and has also been studied theoretically [101–109]. It is thus natural to inquire under what conditions the upper branch is metastable.

In this paper we will study this question based on the formalism developed in [60]. It provides an expression of the free energy at finite temperature and density built on an integral equation for the pseudo-energy with a kernel based on the logarithm of the two-body S-matrix at zero temperature. This integral equation is reminiscent of the Yang-Yang equations used in the Thermodynamical Bethe Ansatz [61]. The formalism is well suited to studying the upper branch since it is based on the S-matrix and the molecules are easily eliminated from the thermodynamics by simply not including a pseudo-energy for them.

For both bosons and fermions, the limit $a_s \to \pm\infty$ is the so-called unitary limit, where the theory is scale invariant. The unitary limit has been explored extensively within this formulation of statistical mechanics in [110–112], and will therefore not be discussed in this work. Although we will restrict our analysis of the upper branch to $a_s > 0$, it is nevertheless important to mention that for bosons the upper branch phase is believed to extend smoothly across unitarity.

In order to determine the boundary between the stable and unstable regions of the upper branch, we will use the criterion put forward in [105, 107], namely that the compressibility κ vanishes. The phase diagram will be determined as a function of the dimensionless ratios

$$\alpha = \frac{\lambda_T}{a_s}, \qquad x = \frac{\mu}{T} \tag{7.1}$$

where $\lambda_T = \sqrt{2\pi/mT}$ is the de Broglie thermal wave length, μ the chemical po-

tential, and $\hbar = k_B = 1$.

In the following section we give a brief summary of the formalism (for further detail see [60]) and the conventions used in this paper. We then present our results on the stability of the upper branch, and provide an analytic treatment of the integral equation in the weak coupling limit.

7.3 Formalism and Conventions

In this section we review the main result of [60]: consistent resummation of two-body scattering leads to an integral equation for a pseudo-energy, whose solution can be used to calculate thermodynamic quantities of interest. We will analyze the upper branch for both bosons and fermions. The Bose gas will be described by the action

$$S = \int d^3\mathbf{x}dt\left(i\phi^\dagger\partial_t\phi - \frac{|\nabla\phi|^2}{2m} - \frac{g}{2}\left(\phi^\dagger\phi\right)^2\right), \tag{7.2}$$

while for fermions we consider the two-component model defined by:

$$S = \int d^3\mathbf{x}dt\left(\sum_{\alpha=\uparrow,\downarrow} i\psi_\alpha^\dagger\partial_t\psi_\alpha - \frac{|\nabla\psi_\alpha|^2}{2m} - g\psi_\uparrow^\dagger\psi_\uparrow\psi_\downarrow^\dagger\psi_\downarrow\right). \tag{7.3}$$

In order to distinguish between the stable and unstable regions of the upper branch, the isothermal compressibility

$$\kappa = -\frac{1}{V}\left(\frac{\partial V}{\partial p}\right)_T = -n\left(\frac{\partial n^{-1}}{\partial p}\right)_T, \tag{7.4}$$

where V is the volume and p the pressure, will be needed. The second equality above follows since $n = N/V$ with N fixed. The compressibility and particle

density can be more conveniently expressed in terms of a scaling function, q, of the dimensionless ratios x and α:

$$n\,\lambda_T^3 = q(x,\alpha) \tag{7.5}$$

$$\kappa = \frac{1}{nT}\frac{\partial_x q}{q} = \frac{1}{T}\left(\frac{mT}{2\pi}\right)^{3/2}\frac{\partial_x q}{q^2}. \tag{7.6}$$

It will also prove useful to define the Fermi surface wavevector $k_F = (3\pi^2 n)^{1/3}$, where n is the 2-component density, and the Fermi temperature $T_F = k_F^2/2m$ in terms of q:

$$\frac{T}{T_F} = \left(\frac{4}{3\sqrt{\pi}\,q}\right)^{2/3}, \qquad \frac{1}{k_F a_s} = \frac{\lambda_T}{a_s}(6\pi^2 q)^{-1/3} \tag{7.7}$$

Both of the above expressions also hold for bosons [111].

Before moving on to a discussion of our results on the upper branch we will put the integral equation

$$y(\mathbf{k}) = 1 + \beta\int\frac{d^3\mathbf{k}'}{(2\pi)^3}G(\mathbf{k},\mathbf{k}')\frac{z}{e^{\beta\omega_{\mathbf{k}'}} - szy(\mathbf{k}')}, \tag{7.8}$$

and q in more convenient forms. Rotational invariance demands y be a function of $|\mathbf{k}|^2$, thus after rescaling $\mathbf{k} \to \sqrt{2mT}\mathbf{k}$, the angular integrals in the integral equation (7.8) can be performed analytically (see appendix A in [111]). The result is the following:

$$\begin{aligned} y(k) = 1 + \frac{8}{\pi}\int_0^\infty dk'k'\,\frac{z}{e^{k'^2} - szy(k')} \\ \times\left\{\frac{\alpha}{2k\sqrt{\pi}}\log\left[\frac{\alpha^2/\pi + (k+k')^2}{\alpha^2/\pi + (k-k')^2}\right]\right. \\ -\left(\frac{k'}{k}+1\right)\arctan\left(\frac{\sqrt{\pi}}{\alpha}(k+k')\right) \\ \left.-\left(\frac{k'}{k}-1\right)\arctan\left(\frac{\sqrt{\pi}}{\alpha}(k-k')\right)\right\}. \end{aligned} \tag{7.9}$$

Similarly, q can be expressed:

$$q = \frac{4}{\sqrt{\pi}}\int_0^\infty dk\,k^2\,\frac{y(k)z}{e^{k^2} - s\,y(k)z}. \tag{7.10}$$

Finally, note that since the fermion model has two components, in equation (7.5), $q \to 2q$ while equations (7.7) and (7.10) remain valid. Henceforth q will refer to one of the two components.

7.4 Analysis of the Upper Branch

As described in the introduction, the upper branch for Bose and Fermi gases refers to $a_s > 0$ with the exclusion of the formation of bound states. In the S-matrix based formalism considered in this paper, removing these states (and the resultant pole in the S-matrix) amounts to simply not including a bound state pseudo-energy. Below we present both boson and fermion phase diagrams for $a_s > 0$, as well as an analytic expression for y in the weak coupling limit.

7.4.1 Phase Diagrams

To determine the metastable region of the upper branch, we have calculated the compressibility as a function of the dimensionless variables x and α. This has been achieved by solving the integral equation (7.9) and calculating q numerically, from which (7.6) is used to determine the stability of the upper branch phase. The curve where the compressibility vanishes provides the boundary between the stable and unstable phases [105, 107]. Our upper branch phase diagram for fermions (bosons) is shown in Figure 7.1 (Figure 7.2). We emphasize no assumption about the coupling strength has been made in obtaining these phase diagrams.

For fermions we find the phase boundary gradually slopes towards $T/T_F = 0$

as $1/k_F a_s$ increases. This is consistent with the expectation that the upper branch should be stable in the limit of zero coupling. Whereas we find that T/T_F approaches zero asymptotically in the latter limit, in contrast, for the Nozieres-Schmitt-Rink (NSR) based approach employed in [105], it was found that after approximately $1/k_F a_s = 2.5$ the upper branch phase is metastable for all T/T_F (see Figure 7.1). Though our treatments of the upper branch are quite different, it is encouraging that our results generally agree within the range $0.5 < 1/k_F a_s < 2.0$. Yet another contrasting result is given in [113], where it's found that the upper branch is always metastable, even at unitarity.

In order to provide a possible explanation for our weak coupling discrepancy with the excluded molecular pole approximation (EMPA) of Shenoy and Ho, we will consider the limit of very weak coupling, $k_F a_s \to 0$. Much of the following analysis is heavily borrowed from section B and appendix A of [113], where it's shown that the EMPA, which begins with the low-fugacity density expansion

$$n_E(T,\mu) = n_0(T,\mu) + \partial \Delta P^{(2)}/\partial\mu, \tag{7.11}$$

is identical to an approach which starts with the NSR 2-body interaction contribution to the pressure

$$\Delta P^{(2)} = \sum_{\mathbf{q}} \int_{-\infty}^{\infty} \frac{d\omega}{\pi} \frac{\delta(\mathbf{q},\omega)}{e^{\beta\omega} - 1}. \tag{7.12}$$

Note $n_0(T,\mu)$ is the ideal gas density.

The primary obstacle in comparing an NSR-based formalism with our own is that the phase shift $\delta(\mathbf{q},\omega)$ is a complicated function whose definition on the upper branch is not yet agreed upon. In the present limit however, we are concerned only with the leading contribution to the phase shift. Within the EMPA this is simply the vacuum two-body phase shift, $\delta(k) = -\arctan(k a_s)$. Hence

after expanding (7.12) in powers of z^2, changing variables using the relation $k^2/m = \omega + 2\mu - \mathbf{q}^2/4m$, and integrating we obtain

$$\Delta P^{(2)} = \frac{2^{3/2}T}{\lambda_T^3} \sum_{n=1}^{\infty} \frac{z^{2n}}{n^{5/2}} \int_0^{\infty} \frac{dk}{\pi} e^{-\frac{n\beta k^2}{m}} \frac{d\delta(k)}{dk} \tag{7.13}$$

which is Eq. (20) in [113]. Noting $\frac{d}{dk}\delta(k) \approx -a_s$ as $k_F a_s \to 0$ then gives

$$\Delta P^{(2)} = -\frac{2T}{\alpha \lambda_T^3} Li_3(z^2). \tag{7.14}$$

Inserting into (7.11) and multiplying through by λ_T^3 results in the EMPA weak coupling scaling function

$$q_E = q_0 - \frac{4}{\alpha} Li_2(z^2). \tag{7.15}$$

In Figure 7.3 we compare q_E and our result in the identical limit, obtained by inserting (7.19) into (7.10). q and q_E agree well for small x. As x increases, the two results begin to diverge and eventually our q experiences a maximum (where $\kappa = 0$) just before becoming imaginary, signifying an x where the integral equation has no solution. For $\alpha = 10^3$ this maximum occurs around $x \approx 30$, where $T/T_F \approx 0.03$.

The validity of the EMPA at such large fugacities and small temperatures is unclear, as the NSR approximation is rooted in the virial expansion which relies upon $z \ll 1$. We believe this to be a possible explanation for the differences in our phase diagram and that of [105] for fermions at weak coupling: the upper branch phase transition occurs at a very large fugacity, well above the low-fugacity regime where the NSR approximation is most applicable. This also explains why our results are in relative agreement for $1/k_F a_s \in [0.5, 2]$, where the phase transition occurs at much higher temperatures.

In the bosonic case the $\kappa = 0$ curve is approximately linear, approaching the T/T_F axis near $T/T_F = 4.2$. This trend is similar to that calculated in [107],

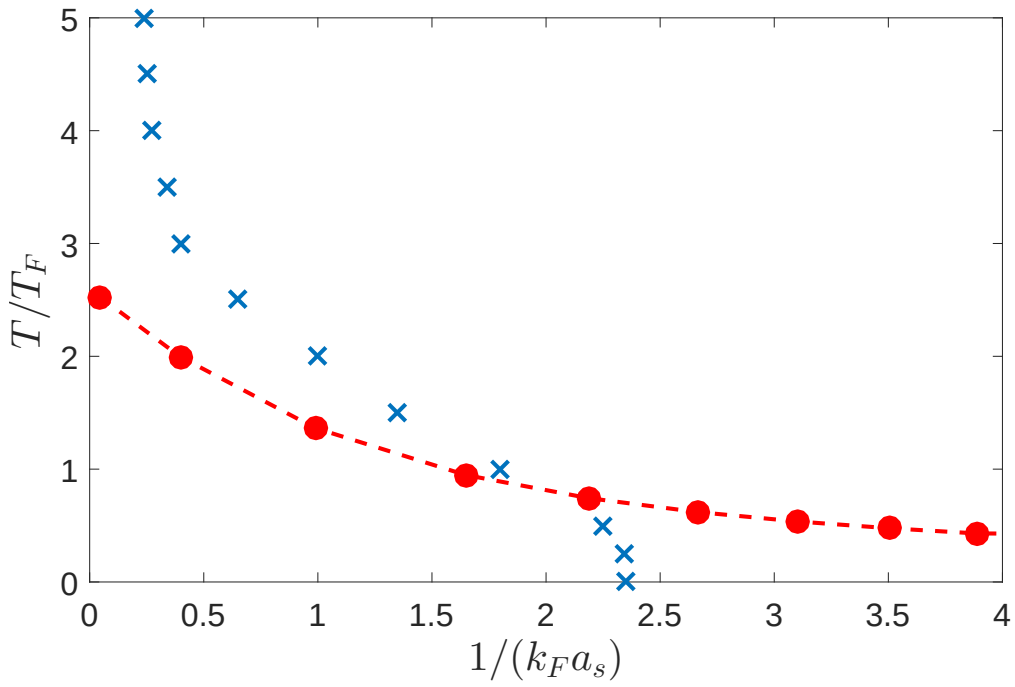

Figure 7.1: Upper branch phase diagram for the Fermi gas. The dashed red curve corresponds to $\kappa = 0$, which defines the boundary between stable and unstable phases. Below this curve the upper branch is unstable. The blue crosses are values of the phase transition estimated from the data presented in [105].

although they are able to extend their results across unitarity, and find the T/T_F intercept to be closer to $T/T_F = 3$.

Both of our phase diagrams take into account only two-body scattering processes. The extent to which many-body interactions alter our findings is presently unknown, but the similarity we see in both the boson and fermion phase diagrams with those of [11,13], which do include many-body effects, suggests the two-body interaction is dominant. For bosons in the unitary limit, the effect of many-body interactions has been estimated to be on the order of a few percent [108]. Unfortunately, experimental and theoretical results alike are limited for the upper branch outside of unitarity.

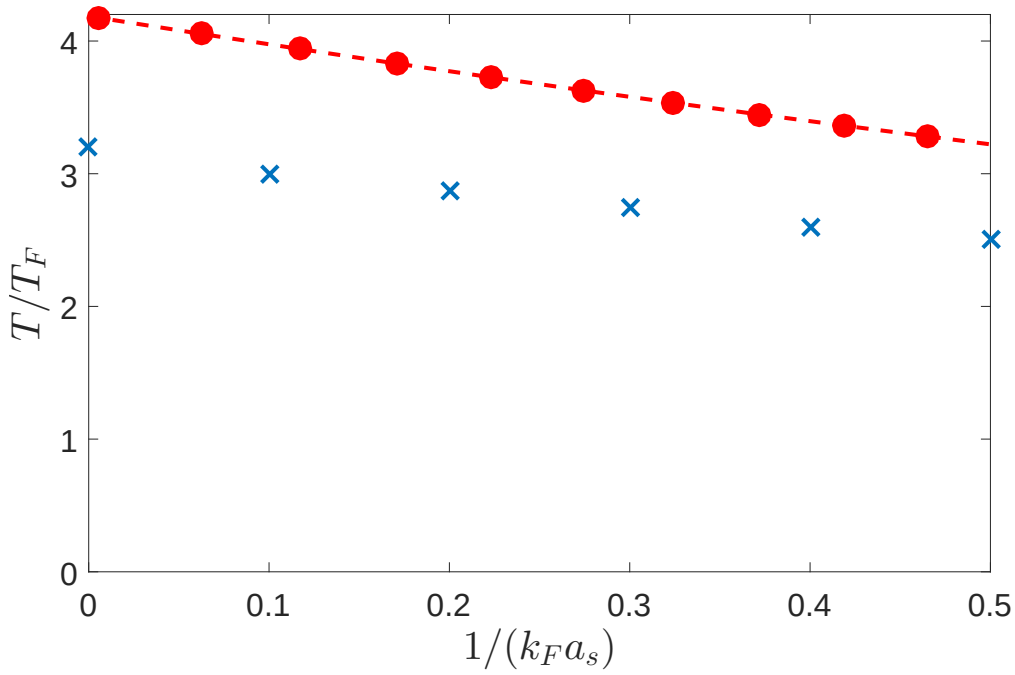

Figure 7.2: Upper branch phase diagram for the Bose gas. The dashed red curve corresponds to $\kappa = 0$, which defines the boundary between stable and unstable phases. Below this curve the upper branch is unstable. The blue crosses are values of the phase transition estimated from the data presented in [107].

7.4.2 Weak Coupling Limit

For repulsive interactions in the weak coupling regime ($a_s \ll 1$, or equivalently $\alpha \gg 1$) the kernel becomes independent of k, k':

$$G(\mathbf{k}, \mathbf{k}') \approx \frac{-8\pi a_s \sigma}{m}. \tag{7.16}$$

Repeating the manipulations described above in going from (7.8) to (7.9) then gives

$$y = 1 - \frac{16\sigma}{\sqrt{\pi}\alpha s} \int_0^\infty dk' \frac{1}{y(k')} \frac{k'^2}{e^{k'^2}/(szy(k')) - 1}.$$

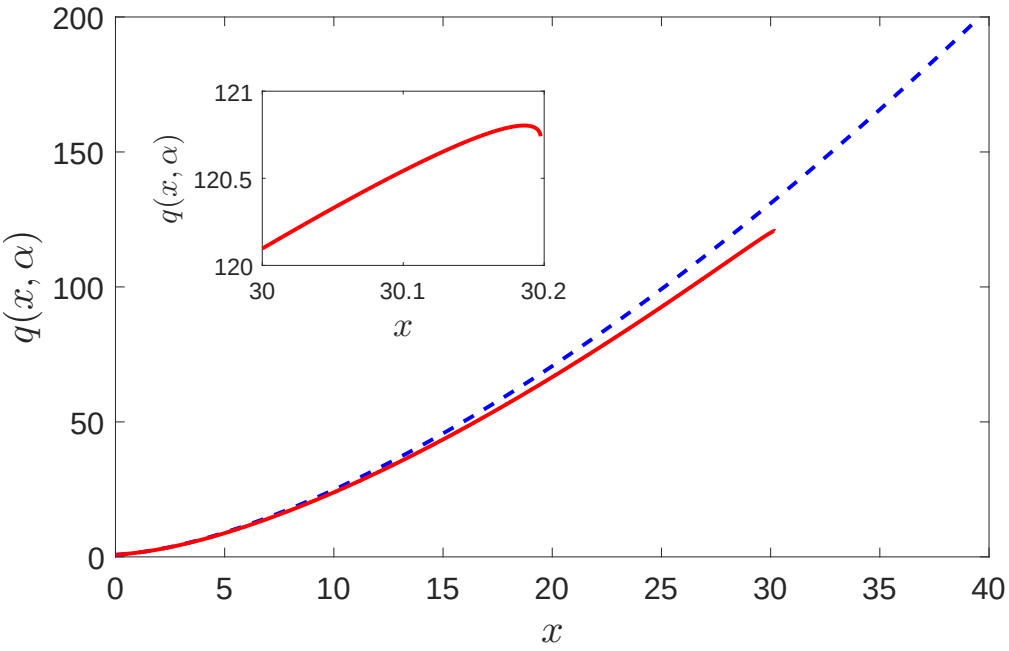

Figure 7.3: Scaling functions vs. x obtained in the $k_F a_s \to 0$ limit within the EMPA (dashed blue) and with our formalism (solid red), for $\alpha = 10^3$. The EMPA scaling function is smooth, corresponding to the upper branch being metastable for all T/T_F at weak coupling. Inset: Our q attains a maximum immediately before becoming imaginary. In other words, a bound state is formed and the integral equation no longer has a solution.

Since the kernel is a constant, so is y and the remaining momentum integral can be expressed in terms of the polylogarithm:

$$y = 1 - \frac{4\sigma}{\alpha s y} Li_{3/2}(szy). \tag{7.17}$$

Thus we have reduced the integral equation to a transcendental equation, in terms of the scattering length and fugacity, valid for small positive a_s. Generally the upper branch phase is stable in the weak coupling limit.

For a free ideal gas $y = 1$, as reflected by the form of (7.17) as $\alpha \to \infty$. Though (7.17) admits no analytic solution for arbitrary μ, an approximate solution can be obtained by setting $y = 1$ in the argument of the polylog. Doing so results in

a quadratic equation with solutions

$$y = \frac{1}{2}\left(1 \pm \sqrt{1 - \frac{16\sigma Li_{3/2}(sz)}{\alpha s}}\right). \tag{7.18}$$

The positive root must be chosen in order to recover the correct ideal gas behavior.

In the fermionic case (7.18) can be written

$$y = \frac{1}{2}\left(1 + \sqrt{\frac{\alpha + 8Li_{3/2}(-z)}{\alpha}}\right), \tag{7.19}$$

which suggests an alternate criterion for the stability of the upper branch at weak coupling. For $\alpha \gg 1$ and a given critical x denoted x_c, if

$$\alpha = |8Li_{3/2}(-e^{x_c})| \equiv \alpha_c \tag{7.20}$$

then the pair (x_c, α_c) lies on the phase boundary. If $\alpha < a_c$, then y is complex and the upper branch will be unstable. In Figure 7.4 the upper branch phase boundary for weakly interacting fermions is computed with this criterion, as well as through the application of (7.6) with numerical solutions of (7.9) and (7.17). All three curves exhibit the same asymptotic behavior as $k_F a_s$ decreases. At weak coupling, critical points obtained through solving (7.17) are nearly indistinguishable from those calculated by solving the full integral equation, while the condition provided by (7.20) becomes more valid as α increases.

A similar analysis for bosons is hindered by the fact that the upper branch becomes metastable for all T/T_F before the weak coupling condition can be sufficiently met. Thus for a weakly coupled bose gas, the primary utility of (7.17) and (7.18) lies in computing arbitrary thermodynamic functions, rather than assessing the stability of the upper branch.

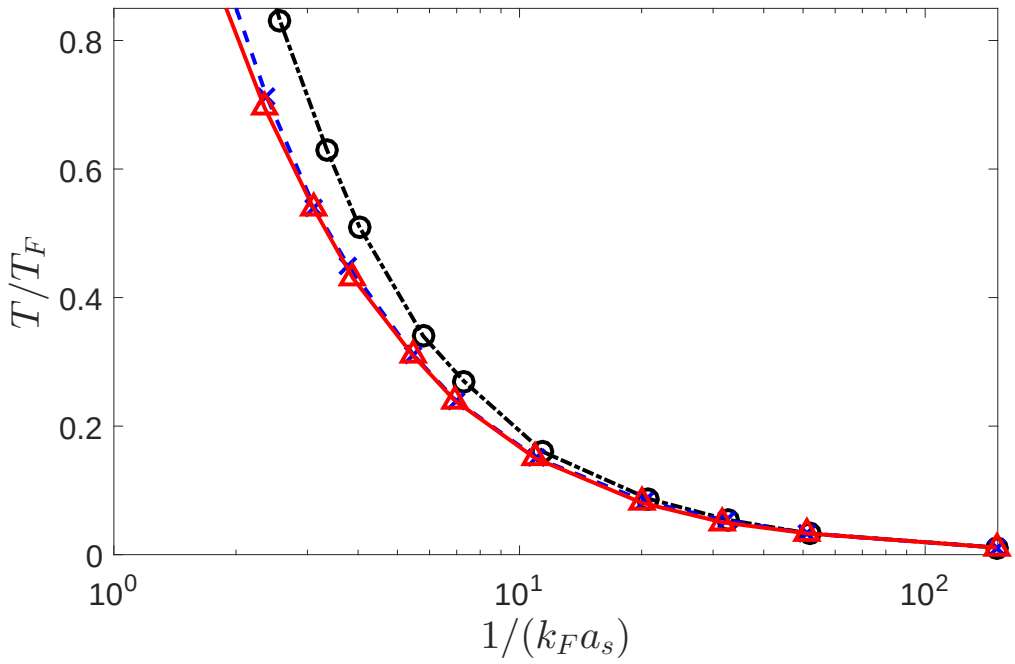

Figure 7.4: Weak coupling behavior of the upper branch phase boundary for fermions. The solid red(dashed blue) curve of zero compressibility was obtained through numerically solving the full integral equation given by (7.9)(transcendental equation given by (7.17)). The black dash-dot curve was calculated by using (7.20) to obtain the critical pair (x_c, α_c) corresponding to the phase boundary.

7.5 Conclusion

The formalism developed in [60] based on the two-body S-matrix, previously applied to quantum gases in the unitary limit and to gases with arbitrary negative scattering length, has been used to study the upper branch. Upper branch phase diagrams for bosons and fermions have been calculated and a simple transcendental equation for the pseudo-energy, valid for repulsive interactions in the weak coupling limit, has been derived. Our findings largely agree with those obtained by other theoretical methods, namely the "excluded molecular pole approximation" of [105, 107].

Our methods are most applicable to systems in which two-body interactions dominate. A key open question concerns the degree to which many-body processes affect the metastability of the upper branch [108, 109]. We believe the results obtained in this work will be useful in guiding future experiments on the upper branch, both in answering this question and others.

BIBLIOGRAPHY

[1] P. de Francesco, P. Mathieu, and D. Sénéchal (Springer-Verlag, 1997).

[2] R. Blumenhagen and E. Plauschinn (Springer-Verlag, 2009).

[3] P. Ginsparg, in *Applied conformal field theory*, edited by E. Brézin and J. Zinn-Justin (1988).

[4] S. Rychkov, arXiv:1601.05000 (2016).

[5] V. Gurarie and A. W. W. Ludwig, in *From fields to strings*, edited by M. Shifman (2005).

[6] J. Cardy, J. Phys. A: Math. Theor. **46**, 494001 (2013).

[7] J. Dubail, J. L. Jacobsen, and H. Saleur, Nucl. Phys. B **834**, 399–422 (2010).

[8] W. M. Koo and H. Saleur, Nucl. Phys. B **426**, 459 (1994).

[9] A. M. Polyakov, JETP Lett. **12**, 381 (1970).

[10] F. A. Dolan and H. Osborn, Nucl. Phys. B **599**, 459–96 (2001).

[11] F. A. Dolan and H. Osborn, Nucl. Phys. B. **578**, 491 (2004).

[12] R. Rattazzi, V. S. Rychkov, E. Tonni, and A. Vichi, J. High Energy Phys. **12**, 031 (2008).

[13] R. Gopakumar, A. Kaviraj, K. Sen, and A. Sinha, J. Phys A: Math. Theor. **118**, 081601 (2017).

[14] H. Shimada and S. Hikami, J. Stat. Phys. **165**, 1006 (2016).

[15] S. El-Showk, M. F. Paulos, D. Poland, S. Rychkov, D. Simmons-Duffin, and A. Vichi, Phys. Rev. D **86**, 025022 (2012).

[16] S. El-Showk, M. F. Paulos, D. Poland, S. Rychkov, D. Smmons-Duffin, and A. Vichi, J. Stat. Phys. **157**, 869 (2014).

[17] S. El-Showk and M. F. Paulos, Phys. Rev. Lett. **111**, 241601 (2013).

[18] F. Kos, D. Poland, D. Simmons-Duffin, and A. Vichi, J. High Energy Phys. **106** (2015).

[19] F. Kos, D. Poland, D. Simmons-Duffin, and A. Vichi, J. High Energy Phys., 36 (2016).

[20] F. Kos, D. Poland, and D. Simmons-Duffin, J. High Energy Phys., 91 (2014).

[21] F. Kos, D. Poland, and D. Simmons-Duffin, J. High Energy Phys., 109 (2014).

[22] R. Rattazzi, S. Rychkov, and A. Vichi, Phys. Rev. D **83**, 046011 (2011).

[23] R. Rattazzi, S. Rychkov, and A. Vichi, J. Phys A: Math. Theor. **44**, 035402 (2011).

[24] L. Iliesiu, F. Kos, D. Poland, S. S. Pufu, D. Simmons-Duffin, and R. Yacoby, J. High Energy Phys., 120 (2016).

[25] L. F. Alday, Phys. Rev. Lett. **119**, 11601 (2017).

[26] L. F. Alday, J. High Energy Phys., 131 (2018).

[27] D. Poland and D. Simmons-Duffin, Nat. Phys. **12**, 535–9 (2016).

[28] D. Pappadopulo, S. Rychkov, J. Espin, and R. Rattazzi, Phys. Rev. D **86**, 105043 (2012).

[29] M. F. Paulos, arXiv:1412.4127 (2014).

[30] D. Simmons-Duffin, J. High Energy Phys. **06**, 174 (2015).

[31] F. Gliozzi, Phys. Rev. Lett. **111**, 161602 (2013).

[32] F. Gliozzi and A. Rago, J. High Energy Phys. **2014**, 42 (2014).

[33] S. Hikami, Prog. of Theor. and Exp. Phys. **2018**, 053I01 (2018).

[34] S. Hikami, Prog. of Theor. and Exp. Phys. **2018**, 123I01 (2018).

[35] W. Li, arXiv:1711.09075v3 (2017).

[36] I. Esterlis, A. L. Fitzpatrick, and D. M. Ramirez, J. High Energy Phys. **2016**, 30 (2016).

[37] M. Hogervorst, H. Osborn, and S. Rychkov, J. High Energy Phys. **2013**, 14 (2013).

[38] D. Poland, S. Rychkov, and A. Vichi, Rev. Mod. Phys. **91**, 15002 (2019).

[39] F. A. Dolan and H. Osborn, Nucl. Phys. B **678**, 491 (2004).

[40] M. Hogervorst, H. Osborn, and S. Rychkov, J. High Energy Phys. **2013**, 14 (2013).

[41] J. Cardy, J. Phys. A: Math. Gen. **25**, L201–6 (1992).

[42] V. S. Dotsenko and V. A. Fateev, Nucl. Phys. B **240**, 312 (1984).

[43] H. Saleur, JJ. Phys. A: Math. Gen. **20**, 455 (1987).

[44] G. Delfino, Ann. Phys. **333**, 1 (2013).

[45] G. Delfino and J. Viti, J. Phys. A: Math. Theor. **44**, 032001 (2011).

[46] V. S. Dotsenko, Nucl. Phys. B **911**, 712–43 (2016).

[47] M. Hogervorst, M. Paulos, and A. Vichi, J. High Energy Phys. **2017**, 201 (2017).

[48] G. Delfino and J. Viti, Nucl. Phys. B **852**, 149–73 (2011).

[49] J. A. Gracey, Phys. Rev. D **92**, 025012 (2015).

[50] M. Flohr and A. Müller-Lohmann, J. Stat. Mech., P12004 (2005).

[51] N. Madras and G. Slade (Birkhäuser, Boston, 1993).

[52] E. Brezin, J. C. Le Guillou, and Z.-J. J., Phys. Rev. D **8**, 2418–2430 (1973).

[53] K. Wilson and M. Fisher, Phys. Rev. Lett. **28**, 240 (1972).

[54] R. Guida and J. Zinn-Justin, J. Phys. A: Math. Gen. **31**, 8103 (1998).

[55] M. Picco, S. Ribault, and R. Santachiara, SciPost Phys. **1**, 009 (2016).

[56] F. Evers and A. D. Mirlin, Rev. Mod. Phys. **80**, 1355 (2008).

[57] E. Perlmutter, J. High Energy Phys. **2015**, 88 (2015).

[58] C. J. Pethick and H. Smith (Cambridge University Press, 2002).

[59] H. T. C. Stoff, K. B. Gubbels, and D. B. M. Dickerscheid (Springer, 2009).

[60] P. T. How and A. LeClair, Nucl. Phys. **B824**, 415 (2010).

[61] C. N. Yang and C. P. Yang, Jour. Math. Phys. **10**, 1115 (1969).

[62] G. Franca, L. A., and J. Squires, J. Stat. Mech. **2017**, 073103.

[63] N. D. Mermin and H. Wagner, Phys. Rev. Lett. **17**, 1133 (1966).

[64] P. C. Hohenberg, Phys. Rev. **158**, 383 (1967).

[65] V. Berezinskii, Sov. Phys. JETP **34**, 610 (1972).

[66] J. Kosterlitz and D. Thouless, J. Phys. C: Solid State Phys. **6**, 1181 (1973).

[67] P. Hadzibabic, M. Krüger, M. Cheneau, B. Battelier, and J. Dalibard, Nature **441**, 1118 (2006).

[68] K. Martiyanov, V. Makhalov, and A. Turlapov, Phys. Rev. Lett. **105**, 030404 (2010).

[69] B. Fröhlich, M. Feld, E. Vogt, M. Koschorreck, M. Kohl, C. Berthod, and T. Giamarchi, Phys. Rev. Lett. **109**, 130403 (2012).

[70] V. Makhalov, K. Martiyanov, and A. Turlapov, Phys. Rev. Lett. **112**, 045301 (2014).

[71] A. T. Sommer, L. W. Cheuk, M. J. H. Ku, W. S. Bakr, and M. W. Zwierlein, Phys. Rev. Lett **108**, 045302 (2012).

[72] S. Tung, G. Lamporesi, D. Lobser, L. Xia, and E. A. Cornell, Phys. Rev. Lett. **105**, 230408 (2010).

[73] L. Ha, C. Hung, Z. Zhang, U. Eismann, S. Tung, and C. Chin, Phys. Rev. Lett. **110**, 145302 (2013).

[74] L. Rammelmüller, W. J. Porter, and J. E. Drut, Phys. Rev. A **93**, 033639 (2016).

[75] I. Boettcher, L. Bayha, D. Kedar, P. A. Murthy, M. Neidig, M. G. Ries, A. N. Wenz, G. Zürn, S. Jochim, and T. Enss, Phys. Rev. Lett. **116**, 045303 (2016).

[76] J. Duan and L. Shieh, Phys. Rev. Lett. **62**, 981 (1989).

[77] M. Randeria, J. Duan, and L. Shieh, Phys. Rev. B **41**, 327 (1990).

[78] J. R. Engelbrecht and M. Randeria, Phys. Rev. B **45**, 12419 (1992).

[79] J. R. Engelbrecht and M. Randeria, Phys. Rev. B **45**, 10135 (1992).

[80] E. R. Anderson and J. E. Drut, Phys. Rev. Lett. **115**, 115301 (2015).

[81] D. S. Petrov, M. A. Baranov, and G. V. Shlyapnikov, Phys. Rev. A **67**, 031601 (2003).

[82] S. S. Botelho and C. A. R. Sá de Melo, Phys. Rev. Lett. **96**, 040404 (2006).

[83] K. Miyake, Prog. Theor. Phys. **69**, 1794 (1983).

[84] D. S. Fisher and P. C. Hohenberg, Phys. Rev. B **37**, 4936 (1988).

[85] M. Holzmann, G. Baym, J. Blaizot, and F. Laloë, Proc. Natl. Acad. Sci. **104**, 1476 (2007).

[86] V. N. Popov (Reidel, Dordrecht, 1983).

[87] N. Prokof'ev, O. Ruebenacker, and B. Svistunov, Phys. Rev. Lett. **87**, 270402 (2001).

[88] N. Prokof'ev and B. Svistunov, Phys. Rev. A. **66**, 043608 (2002).

[89] R. con A. and N. Dupuis, Phys. Rev. **A85**, 063607 (2012).

[90] E. B. Kolomeisky and J. P. Straley, Phys. Rev. **B46**, 11749 (1992).

[91] S. Tan, Ann. Phys. **323**, 2987 (2008).

[92] F. Werner and Y. Castin, Phys. Rev. A **86**, 013626 (2012).

[93] G. Bertaini and S. Giorgini, Phys. Rev. Lett. **106**, 110403 (2011).

[94] E. Marcelino, A. Nicolai, I. Roditi, and A. LeClair, Phys. Rev. A **90**, 053619 (2014).

[95] G. Dieckmann, C. A. Stan, S. Gupta, Z. Hadzibabic, C. H. Schunck, and W. Ketterle, Phys. Rev. Lett. **89**, 203201 (2002).

[96] S. Jochim, M. Bartenstein, A. Altmeyer, G. Hendl, C. Chin, J. H. Denschlag, and R. Grimm, Phys. Rev. Lett. **91**, 240402 (2003).

[97] G. Jo, Y. Lee, J. Choi, C. A. Christensen, T. H. Kim, J. H. Thywissen, D. E. Pritchard, and W. Ketterle, Science **325**, 1521 (2009).

[98] J. P. Gaebler, J. T. Stewart, T. E. Drake, D. S. Jin, A. Perali, P. Pieri, and G. C. Strinati, Nat. Phys. **6**, 569 (2010).

[99] R. J. Wild, P. Makotyn, J. M. Pino, E. A. Cornell, and D. S. Jin, Phys. Rev. Lett. **108**, 145305 (2012).

[100] P. Makotyn, C. E. Klauss, D. L. Golberger, E. A. Cornell, and D. S. Jin, Nat. Phys. **10**, 116 (2014).

[101] R. A. Duine and A. H. MacDonald, Phys. Rev. Lett. **95**, 230403 (2005).

[102] G. J. Conduit, A. G. Green, and B. D. Simons, Phys. Rev. Lett. **103**, 207201 (2009).

[103] S. Tsuchiya, R. Watanabe, and Y. Ohashi, Phys. Rev. A **80**, 033613 (2009).

[104] D. Pekker, M. Babadi, R. Sensarma, N. Zinner, L. Pollet, M. W. Zwierlein, and E. Demler, Phys. Rev. Lett. **106**, 050402 (2011).

[105] V. B. Shenoy and T. Ho, Phys. Rev. Lett. **107**, 210401 (2011).

[106] F. Palestini, P. Pieri, and G. C. Strinati, Phys. Rev. Lett. **108**, 080401 (2012).

[107] W. Li and T. Ho, Phys. Rev. Lett. **108**, 195301 (2012).

[108] D. Borzov, M. S. Mashayekhi, S. Zhang, J. Song, and F. Zhou, Phys. Rev. A **85**, 023620 (2012).

[109] S. Jiang, W. Liu, G. W. Semenoff, and F. Zhou, Phys. Rev. A **89**, 033614 (2014).

[110] P. How and A. LeClair, J. Stat. Mech., P07001 (2010).

[111] A. LeClair, E. Marcelino, A. Nicolai, and I. Roditi, Phys. Rev. A **86**, 023603 (2012).

[112] E. Marcelino, A. Nicolai, I. Roditi, and A. LeClair, Phys. Rev. A **90**, 053619 (2014).

[113] L. He, X. Liu, X. Huang, and H. Hu, Phys. Rev. A **93**, 063629 (2016).